UNIVERSITY OF SOUTHAMPTON

FACULTY OF SCIENCE

Department of Physics

THE DEVELOPMENT OF A DIODE LASER PUMPED MODELOCKED Nd:YAG LASER FOR THE STUDY OF NON-LINEAR EFFECTS IN OPTICAL FIBRE

by Stephen John Keen

A thesis submitted for the Degree of Doctor of Philosophy

September 1990

For Mum and Dad,

'Had Cleopatra's nose been shorter, the whole face of the world would have changed'.

Blaise Pascal

CONTENTS

		Page
Abstract		iv
Acknowledgments		v
	CHAPTER 1: INTRODUCTION	
Section 1.1	Thesis contents-	1
Section 1.2	A brief history of diode laser pumped solid state lasers-	1
Section 1.3	The modelocking of laser diode pumped Nd:YAG lasers-	3
Section 1.4	Diode laser pumped 1.3 μm sources-	4
Section 1.5	Optical solitons and non-linear effects in optical fibre-	5
	References-	8
	CHAPTER 2: DIODE LASER PUMPED SOLID STATE LASERS	
Section 2.1	Introduction-	11
Section 2.2	Diode lasers-	11
2.2.2	Phased array diode lasers-	12
2.2.3	The characteristics of a 1W phased array diode laser-	12
2.2.4	The focusing optics for a 1W diode laser-	18
2.2.5	High powered diode lasers-	20
Section 2.3.1	Diode laser pumped solid state systems-	20
2.3.2	Phased array laser diodes as pump sources for solid state lasers-	21
2.3.3	Diode laser sidepumping of solid state lasers-	22
2.3.4	Single frequency microchip lasers-	24
Section 2.4	A review of the properties of Nd:YAG-	24
	References-	29
	CHAPTER 3: A DIODE LASER PUMPED MODELOCKED AND Q-SWITCHED Nd:YAG LASER OPERATING AT 1.3 μm	
Section 3.1.1	Cavity design requirements-	31
3.1.2	Astigmatic compensation-	32
3.1.3	Wavelength selection-	35

Section 3.2.1	Continuous wave characteristics-	38
3.2.2	The free running bandwidth-	39
Section 3.3.1	Modelocking-	41
3.3.2	Amplitude modulation-	41
3.3.3	Phase modulation-	42
3.3.4	The Kuizenga and Siegman theory-	43
3.3.5	AM modelocking-	47
3.3.6	The self-consistent theory for FM modelocked lasers-	47
3.3.7	FM modelocking in the case of detuning-	48
Section 3.4.1	The amplitude modulator-	50
3.4.2	AM modelocking results-	51
3.4.3	Output power from the modelocked laser-	53
3.4.4	Discussion of AM modelocking-	55
Section 3.5.1	The phase modulator-	56
3.5.2	The FM modelocked laser-	58
3.5.3	FM modelocked performance-	58
3.5.4	Comparison with the Kuizenga and Siegman theory-	61
3.5.5	Discussion of FM modelocking-	62
Section 3.6.1	Simultaneous Q-switching and modelocking of the laser-	63
3.6.2	Q-switching and modelocking of the laser-	65
	References-	68

CHAPTER 4: NON-LINEAR EFFECTS IN OPTICAL FIBRE

Section 4.1	Introduction-	70
Section 4.2	Step index optical fibre-	70
Section 4.3	Dispersion in optical fibre-	74
Section 4.4	Stimulated Raman scattering-	77
Section 4.5	SRS in optical fibres-	80
Section 4.6	Solitons-	85

Section 4.7	The soliton self frequency shift-	91
Section 4.8	Modulational instability-	93
Section 4.9	A review of soliton Raman generation in optical fibre-	94
	References-	98
	CHAPTER 5: A STUDY OF SRS IN OPTICAL FIBRE	
Section 5.1	Introduction-	102
Section 5.2	Experimental procedure-	102
Section 5.3.1	Results-	104
5.3.2	Modulational instability-	109
5.3.3	The SRS process in the absence of MI-	115
Section 5.4	The evolution of soliton Raman pulses-	115
Section 5.5	Conclusion-	122
	References-	124
	CHAPTER 6: CONCLUSION AND FUTURE WORK	
Section 6.1	Introduction-	125
Section 6.2	A summary of the achievements of this thesis-	125
Section 6.3.1	Future work-	127
6.3.2	CW sub-picosecond pulse generation via SRS-	128
6.3.3	The generation of tunable sub-picosecond pulses by the use of additive pulse modelocking-	129
	References-	132
Appendix	Papers published	133

UNIVERSITY OF SOUTHAMPTON

ABSTRACT

FACULTY OF SCIENCE

Doctor of Philosophy

THE DEVELOPMENT OF A DIODE LASER PUMPED MODELOCKED Nd:YAG LASER FOR THE STUDY OF NON-LINEAR EFFECTS IN OPTICAL FIBRE

by Stephen John Keen

This thesis deals primarily with the development of a diode laser pumped modelocked Nd:YAG laser operating at 1.3 μm for the production of ultra-short pulses in optical fibre. The Nd:YAG laser was modelocked using both amplitude and frequency modulation (AM and FM) techniques. An acousto-optic modulator was used to AM modelock the laser, bandwidth limited pulses of a duration of 46 psec and a peak power of 0.46W were obtained from this system. FM modelocking was accomplished with a lithium niobate phase modulator and produced two times bandwidth limited pulses of a duration of 19 psec with a peak power of 4.6W. The Nd:YAG laser was simultaneously FM modelocked and Q-switched resulting in peak powers in excess of 1kW in the Q-switch envelope.

The high peak power from this laser was used to generate wavelengths in the range of 1.34 to 1.55 μm, with high conversion efficiencies, by making use of stimulated Raman scattering (SRS) in optical fibre. The radiation formed by SRS fell in the anomalous dispersion region of the fibre and so could support optical solitons. The generated Stokes radiation was found to contain soliton like pulses of a duration as short as 88 fsec.

The diode laser pumped Nd:YAG laser was used in a study of the processes which determine the formation of optical solitons via SRS. In this study the importance of modulational instability in the non-linear process was discovered. This process was found to act as a seed for SRS with the result that the threshold power was lowered for the generation of Stokes radiation and the output spectrum was modified. In this study modulational instability sidebands as high as 8.94 THz were observed.

The thesis concludes with possible methods for the development of a cw source of sub-picosecond pulses by the use of SRS in optical fibre.

ACKNOWLEDGEMENTS

I would like to thank my supervisor, Professor Allister Ferguson, for all the help and encouragement he has given me during my PhD. I am grateful to Professor D. C. Hanna for his assistance in allowing me to complete my PhD at Southampton University. I would like to thank everybody in the laser group, past and present, who have helped me in the research and compilation of this thesis. I am grateful to the Department of Electronics and Information Technology of Southampton University for the loan of optical fibre and the use of apparatus to characterise that fibre. Finally, I would like to thank Catherine for the invaluable help and support she has given me.

CHAPTER 1

INTRODUCTION

Section 1.1 Thesis contents

This thesis describes the development of a diode laser pumped Nd:YAG laser which has been used to produce ultra-short pulses in optical fibre. The thesis reports on the specific requirements for diode laser pumped systems; the characteristics of diode lasers, the pump optics and the optimum laser cavity design (chapter 2). In chapter 3 the results of actively modelocking a laser diode pumped Nd:YAG laser operating at 1.3 μm are described, in both cases the modelocked pulse duration was measured to be below 50 psec in duration. The chapter also describes how the peak power from the laser was enhanced by simultaneously Q-switching and modelocking so that the lasers peak output power was suitable for studying many non-linear effects in optical fibres. In chapter 4 the theory of light propagation in optical fibre is discussed which includes a description of stimulated Raman scattering in optical fibre and optical solitons. A review is made in this chapter of soliton generation by the use of stimulated Raman scattering. Chapter 5 describes the use of the laser diode pumped system to produce sub-picosecond pulses via stimulated Raman scattering and a study of this effect. In this study pulses as short as 88 fsec in duration were measured and modulational instability sidebands of a modulation frequency of 8.9 THz were observed.

Section 1.2: A brief history of diode laser pumped solid state lasers

In recent years there has been a renaissance in the use of laser diodes as pump sources for solid state lasers. The use of laser diodes offers greater efficiency, reliability and compactness. The use of laser diodes and light emitting diodes (LED's) as pump sources for solid state lasers dates back to the early 1960's when GaAs diode lasers were first demonstrated [Hall et al: 1962]. These early diode pumped systems used the lasers in a sidepump configuration, the pump radiation being incident on the gain medium in a direction perpendicular to the resonator axis [Ochs et al: 1964]. The $CaF_2:Dy^{3+}$ lasing medium and the laser diodes both needed to be cooled to liquid Helium temperature for operation of the diodes and to reduce the lower lasing population level of $CaF_2:D^{3+}$. These early examples of laser diode pumping did not live up to the expected advantages of using semi-conductor sources instead of flashlamps.

In 1968 the first laser diode pumped Nd:YAG laser was demonstrated [Ross: 1968]. Nd^{3+} doped into a yttrium aluminium garnet (YAG) host is an excellent laser gain medium (see chapter 2 section 4), due to both its spectroscopic and mechanical properties. By the early 1970's Nd:YAG had become the most widely used solid state material for flashlamp pumped systems. Nd:YAG has its main laser transitions at 1.06 μm in the near infra-red but also has a weaker transition at 1.3 μm. The material is excellent for laser diode pumping as it has absorption bands in the range of typical GaAlAs diode laser

emissions (760 - 860 nm). Naturally a substantial amount of the laser diode pumped work has involved Nd:YAG as it can be operated at room temperature and is easily obtained. The first demonstration of laser diode pumped Nd:YAG used the material at room temperature but the laser diodes needed to be cooled. The first true continuous wave (cw) operation of a laser diode pumped laser was reported upon by Iwamoto [Iwamoto et al: 1976] but the output powers and quality of these systems were limited by the quality of the laser diodes.

In the early 1980's improvements in diode laser technology were made which increased the output powers and operational lifetimes and allowed the diodes to be operated at room temperature. The new generation of high powered diode lasers were made of GaAlAs with typical emission wavelengths in the range of 760 nm to 860 nm. At the beginning of the 1980's maximum power available from these devices was about 100 mW but by the end of the decade as much as 38 W had been obtained from a single laser diode package [Sakamoto et al: 1988]. The rapid improvement of the diode lasers brought a fresh impetus to research into diode laser pumped systems and their possible applications. Although the improvement in diode laser quality meant that for some applications they could be used alone, using them as pump sources for solid state lasers still holds many advantages. These diode laser pumped systems offer the advantages of improved beam quality and brightness, the possibility of modulating the solid state laser to obtain high peak powers and a diversity of wavelengths depending upon the choice of material. The way that the diode laser is used to pump the solid state laser is dependent on the output power of the diode and the type of diode that is being used. The different ways that laser diodes can be used to pump solid state lasers are discussed in chapter 2. The diode laser is either used in a sidepumped arrangement or a longitudinal pumping arrangement. The use of laser diodes in an end pumped configuration allows the solid state laser to be designed with a small mode spot size without any loss in pump/laser mode overlap. This feature of diode pumping means that longitudinally pumped systems can have very low thresholds. Longitudinal pumping of solid state lasers gives an opportunity to exploit lower gain transitions in the more commonly available lasing media and of pumping new materials such as materials doped with other trivalent rare earth ions or stoichimeterics [Huber: 1980]. For instance the 947 nm transition in Nd:YAG, which is a quasi- 3 level laser, has been successfully diode pumped and frequency doubled to produce a compact source of blue light [Fan et al: 1987]. Rare earth materials that have an absorption at the emission wavelength of GaAlAs diode lasers (760 nm - 860 nm) offer new lasing wavelengths in the near infra-red. The rare earth ions of Ho^{3+}(2.1 μm) and Er^{3+}(2.8 μm) have both been diode laser pumped when doped into YAG and lithium yttrium fluoride (YLF) respectively [Fan et al: 1987], [Kintz et al: 1987]. These wavelengths are useful for eyesafe lasers and medical applications. Due to the efficiency of diode laser pumping the thermo-mechanical properties of the solid state material are not of such importance as with flashlamp pumped systems. This allows the Nd^{3+} ion to

be used in a variety of host materials which offer longer upper state lifetimes for energy storage or a larger gain bandwidth for tunability and for ultra-short pulse production.

The predominant amount of research in the 1980's used Nd:YLF, Nd:YAG and Nd:Glass for the solid state material, owing to their proven quality and availability. Many diverse systems and investigations have used diode laser pumping but the main areas of research have been

(i) The development of single frequency diode pumped Nd:YAG lasers [Zhou et al: 1985], [Kane et al: 1985], [Wallmenth et al: 1988], [Clarkson et al: 1989], [Zhou et al: 1990].

(ii) Frequency doubling of diode laser pumped Nd:YAG.[Dixon et al: 1988], [Kozlovsky et al: 1988], [Maker et al: Sept 1989]

(iii) High powered cw and quasi cw side pumped Nd:YAG.[Burnham et al: 1989], [Hanson: 1989]

(iv) The production of short, high peaked powered pulses through Q-switching and modelocking of diode laser pumped Nd:YAG.

The 10's of milliwatts powers that have been generated at 532 nm through the frequency doubling of Nd:YAG has led to there use as pump sources for optical parametric oscillators (OPO) [Maker et al: April 1990], [Kozlovsky et al: 1989] and for the pumping of Ti: Sapphire lasers [Maker et al: 1990].

Section 1.3: The modelocking of laser diode pumped Nd:YAG lasers

In this thesis the results of research in to the modelocking of a diode laser pumped Nd:YAG laser operating at 1.3 μm will be presented. The process of modelocking of a laser increases the peak power and can produce pulses of the order of the inverse of the gain bandwidth of the laser transition. The process is discussed in chapter 3.3. The first report of a flashlamp pumped modelocked Nd:YAG laser was made in 1967 [DiDemenico et al: 1966] and it is now a common feature available from commercially made Nd:YAG lasers. These lasers are typically acousto-optically modelocked with pulse durations of approximately 60 - 100 psec, this pulse duration is about two order of magnitude larger than the laser bandwidth limit. Attempts have been made to shorten the pulses from these lasers, a pulse duration of 25 psec from an actively modelocked Nd:YAG laser with an intra-cavity etalon to flatten the bandwidth is the best that has been obtained from a flashlamp pumped system [Roshors et al: 1986]. The inherent stability and potential compactness of diode laser pumped lasers has revived interest in the modelocking process in solid state materials. As well as the usefulness of a modelocked diode pumped source the lasers provide an opportunity to study the process of active modelocking in solid state materials and to test the validity of modelocking theories that have been devised for homogeneously broadened lasers.

The first reported modelocking of a miniature Nd:YAG laser was made by Alcock et al [Alcock et al: 1986]. This system used a dye laser operating at 590 nm to pump the Nd:YAG, the laser was amplitude modulated and produced pulses of duration of less than

200 psec. Basu et al [Basu et al: 1988] have used a combination of dye pumping and laser diode pumping to modelock a Nd:Glass laser. The AM modelocked laser produced pulses of a duration of 10 psec, but this pulse duration was obtained by extrapolation and not direct measurement.

The first truly diode laser pumped modelocked solid state laser was reported by Maker et al [Maker et al: 1988]. In this experiment a 100mW phased array diode laser was used to optically pump a Nd:YAG laser operating at 1.06 μm, which was arranged in a three mirror folded mirror arrangement. The laser was amplitude modulated at a repetition rate of 240 MHz and produced 54 psec pulses near bandwidth limited pulses. Initial reports of a similar laser but operating at 1.3 μm and pumped by a dye laser were described in this paper. The first laser diode pumping of a Nd:YAG laser operating at 1.3 μm was reported by Keen et al [Keen et al: April 1989]. This experiment is covered in chapter 3.4, near bandwidth pulses of a duration of 46 psec were obtained at this wavelength. Frequency modulation modelocking of a laser diode pumped Nd:YAG operating at 1.06 μm was reported in 1989 [Maker et al: Aug 1989]. The 12 psec pulse duration measured in this experiment were the shortest pulses reported to have been obtained from an actively modelocked Nd:YAG laser. In a similar experiment 9 psec pulses were obtained in Nd:YLF at 1.047 μm [Maker at al :1989]. The frequency modulation modelocking of a Nd:YAG laser operating at 1.3 μm resulted in 19 psec pulses [Keen et al: Nov 1989] and is described in chapter 3.5.

The pulse durations from AM modelocked lasers have been improved by the use of modulators with very high repetition rates. Keller et al [Keller et al: 1990] have developed a modulator with a repetition rate of 500 MHz and have measured pulses of a duration of 9 psec. The advantage of using high repetition rate modulators is discussed in chapter 3.4.

Section 1.4: Diode laser pumped 1.3 μm sources

In the project described in this thesis, the 1.3 μm transition in Nd:YAG has been diode laser pumped. This wavelength is of great importance to optical fibre communications as this wavelength falls in a transmission widow of silica based optical fibre and is at the point of zero group velocity dispersion (GVD) in this type of fibre. For this reason initial research at this wavelength had the aim of producing stable single frequency sources that could be used in coherent optical fibre communication systems. This has been demonstrated by Kubordera et al [Kubordera et al: 1982] who diode pumped $LiNdP_4O_{12}$ (LNP) at 1.3 μm to produce an optical fibre communication system with a bandwidth of 2.8 GHz. H.R Telle has used NdP_5O_{14} to produce a tunable source around 1.3 μm [Telle: 1984]. A. I. Ferguson demonstrated single frequency operation of a miniature Nd:YAG laser at 1.3 μm but this was pumped with a dye laser [Ferguson: 1985]. A highly stable single frequency has been developed by Trutna et al who have used an out of plane geometry to obtain uni-directional operation in a monolithic Nd:YAG laser [Trutna et al: 1987].

In chapter 3 the modulation of a diode laser pumped Nd:YAG laser operating at 1.3 μm is described. Simultaneously Q-switching and modelocking of the laser created high peak powers at 1.3 μm. This system was developed for two main reasons

(i) To generate ultra-short pulses via soliton Raman generation in optical fibre.

(ii) To make a study of non-linear effects in optical fibre.

Section 1.5: Optical solitons and non-linear effects in optical fibre

The generation of optical solitons has been of great interest since their theoretical prediction in 1973 [Hasagawa et al: 1973] and the first experimental evidence of there existence in 1980 [Mollenauer et al: 1980]. The phenomena of solitons and 'solitary waves' exist in a large area of physics such as plasmas, elementary particle physics and meteorology. The existence of solitary waves was first observed and suggested by John Scott Russell, a Victorian scientist and ship engineer. Whilst watching barges on an Edinburgh canal he noticed, as the barges displaced water, well defined waves were formed which propagated down the channel without distortion or loss of speed. He named these waves as solitary waves mainly because this type of wave motion stands alone and apart from other types of oscillatory wave motion. The equation which models the motion of a wave which propagates along the surface of water is known as the Korteweg- de Vries equation. In 1965 Zabusky et al [1965] applied this equation to the one dimensional non-linear oscillation of a lattice and discovered that solitary waves were formed which had the property that they passed through one another without deformation due to collisions. Consequently, they named these solitary waves 'solitons' since they behaved like particles.

In 1973 Hasagawa showed that the propagation of an optical carrier wave envelope in a non-linear stable dispersive medium with negligible distortion from loss could be described by the non-linear Schrodinger equation (NLSE). The NLSE equation in its dimensionless form is given below

$$i\frac{\delta q}{\delta x} + \frac{1}{2}\frac{\delta^2 q}{\delta t^2} + |q|^2 q = 0 \qquad 1.5.1$$

The name the non-linear Schrodinger equation has been coined precisely because its structure is that of the Schrodinger equation of quantum mechanics with $|q|^2$ as a potential. The equation and its derivation and solutions are discussed in more fully in chapter 4.6. In the equation, x, represents the distance along the direction of propagation and , t, represents the time in the group velocity frame of reference. Zakharov and Shabat [Zakharov et al: 1972] have shown that the solutions describe envelope solitons. The characteristic solution of the NLSE is of a pulse whose shape is described by a sech lineshape so q is given by

$$q = N \operatorname{sech} t \qquad 1.5.2$$

The soliton solutions have the property that they are stable to small perturbations, periodic with x and N and can pass through each other with only a change of phase.

An explanation of the terms of the NLSE gives an intuitive understanding of optical solitons. The second term describes the dispersion of the dielectric i.e the variation of the group velocity with wavelength. The third term describes a non-linearity which is proportional to the intensity of the wave. In optical fibre the cause of the non-linearity is the optical Kerr effect which produces a small change in the refractive index of a material in proportion to the intensity of the wave. If the change in propagation constant due to the Kerr effect and dispersion are equal and opposite then pulses can propagate without distortion. This condition describes the propagation of an N = 1 soliton. The conditions necessary to generate a soliton in optical fibre requires a single mode fibre at the wavelength of interest, this wavelength should be beyond 1.3 μm where the group velocity dispersion is of the correct sign. The source of the radiation should be near bandwidth limited pulses of sufficient intensity to support a soliton. It was not until 1980 that Mollenauer et al [Mollenauer et al: 1980] used a color centre laser, which produced 10 psec pulses at a wavelength of 1.5 μm of a power of a few Watts, to produce pulses which showed soliton like behaviour when passed through 700m of fibre. Since then many studies have confirmed the existence of solitons and the validity of using the NLSE to describe the propagation of a wave envelope in an optical fibre.

Owing to the accuracy to which the parameters which describe an optical fibre can be measured, the propagation of optical pulses in fibre is an excellent way of to study the NLSE. The most exciting use for which properties of optical solitons may be used is in the field of optical fibre communications. The property of solitons to propagate through fibre without distortion and the ability to amplify them using optical techniques means that they offer the chance of developing a high bit rate, all optical, communications network. For instance, at the moment electronic amplifiers are needed about every 20 -100 km to amplify the signals along an optical fibre route. Molleneaur et al [Mollenauer et al: 1986] have demonstrated optical solitons travelling the equivalent of 6000 km with the use of optical amplification.

In this thesis a study of optical solitons and non-linear effects in optical fibre is described in chapter 5. The diode laser pumped modelocked and Q-switched Nd:YAG laser generates high peak powers at 1.3 μm. When this is passed through sufficient length of optical fibre a spectrally broad range of wavelengths can be generated via stimulated Raman scattering (SRS). The effect is explained further in chapter 4. The frequency downshift caused by SRS is 440 cm^{-1} in silica fibre, for a 1.3 μm source this radiation is centred at 1.4 μm. The spectrally broad radiation at 1.4 μm is in the negative dispersion region of silica optical fibre and can support optical solitons. A review of this method of

generating optical solitons is made in chapter 4.9. The beauty of this method of generating solitons is in the simplicity of the experimental arrangement and of the conditions that are required to produce them.

In chapter 5 experiments studying the evolution of solitons in optical fibre generated by SRS are described. The dependence of the solitons and the spectrum obtained is investigated with change in wavelength and for two different dispersion minima straggling the lasing wavelength at 1.318 μm. In this study the importance of modulational instability on the process is described. Modulational instability can be explained by consideration of the NLSE when light of a constant amplitude passes through a fibre. The third term in the NLSE equation represents the equivalent potential which traps the quasi particle described by the Schrodinger equation. The potential depth becomes deeper in proportion to the density of the particle owing to the fact that the potential is proportional to the absolute square of the wave function. If the light is propagating in the anomalous dispersion region then any change in local density of the quasi-particle causes an increase in the trapping potential which enhance the self induced increase of the quasi particle density. This process leads to modulational instability and was first demonstrated by Tai et al [Tai et al: 1986]. This effect has been proposed as a method of producing very high modulation frequencies for optical fibre communications. In chapter 6 some concluding remarks are made about future work in this area.

CHAPTER 1: REFERENCES

Alcock I. P. and Ferguson A. I. , 1986, Opt. Comm. , 58, 417.

Basu S. and Byer R. L. , 1988, Opt. Lett. , 13, 458.

Burnham R. and Hays A. D. , 1989, Opt. Lett. , 14, 27.

Clarkson W. A. and Hanna D. C. , 1989, Opt. Comm. , 73, 469.

DiDomenico M. , Geusic J. E. , Marcos H. M. and Smith R. G. , 1966, Appl. Phys. Lett. , 8, 180.

Dixon G. J. , Zhang Z. M. , Chang R. S. F. and Djeu N. , 1988, Opt. Lett. , 13, 137.

Fan T. Y. , Huber G. , Byer R. L. and Mitzscherlich P. , 1987, Opt. Lett. , 12, 678.

Fan T. Y. and Byer R. L. , 1987, Opt. Lett. , 12, 809.

Ferguson A. I. , 1985, Electron. Lett. , 21, 853.

Hall R. N. , Fenner G. E. , Kinsley J. D. , Soltys T. J. and Carlson R. O. , 1962, Phys. Rev. Lett. , 9, 366.

Hanson F. , 1989, Opt. Lett. , 14, 674.

Hasegawa A. and Tappert F. D. , 1973, Appl. Phys. Lett. , 23, 142.

Huber G. , 1980, Current Topics in Materials Science, Volume 4, North Holland Publishing Company.

Iwamoto K. , Hino I. , Matsumato S. and Inove K. , 1976, Japan. J. Appl. Phys. , 15, 2191.

Kane T. and Byer R. L. , 1985, Opt. Lett. , 10, 65.

Keen S. J. , Maker G. T. and Ferguson A. I. , April 1989, Electron. Lett. , 25, 490.

Keen S. J. and Ferguson A. I. , Nov 1989, Appl. Phys. Lett. , 55, 2164.

Keller U. , Li K. D. , Khuri-Yakub B. T. , Bloom D. M. , Weingarten K. J. and Gerstenberger D. C., 1990, Opt. Letts. , 15, 45.

Kintz, Allen R. and Esterowitz L. , 1987, Appl. Phys. Letts. , 50, 1553.

Kozlovsky W. J. , Nabors N. D. , Eckardt R. C. and Byer R. L. , 1989, Opt. Lett. , 14, 66.

Kozlovsky W. J. , Nabors N. D. and Byer R. L. , 1988, IEEE J. Quant. Electron. , 24, 913.

Kubodera and Norde J. , 1982, Appl. Opt. , 21, 3466.

Maker G. T. , Keen S. J. and Ferguson A. I. , 1988, Appl. Phys. Lett. , 53, 1675.

Maker G. T. and Ferguson A. I. , Aug 1989, Opt. Lett. , 14, 788.

Maker G. T. and Ferguson A. I. , Aug 1989, Electron. Lett. , 25, 1025.

Maker G. T. and Ferguson A. I. , Sept 1989, Appl. Phys. Lett. , 55, 1158.

Maker G. T. and Ferguson A. I. , April 1990, Appl. Phys. Lett. , 56, 1614.

Maker G. T. and Ferguson A. I. , 1990, Opt. Lett. , 15, 375.

Mollenauer L. F. , Stolen R. H. and Gordon G. P. , 1980, Phys. Rev. Lett. , 45, 1095.

Mollenauer L. F. , Gordon J. P. and Islam M. N. , 1986, IEEE J. Quant. Electron. , QE-22, 157.

Ochs S. A. and Pankove J. I. , 1964, Proc. IEEE, 52, 713.

Roshors H. , Rabl T. and Seilmeier A. , 1986, Appl. Phys. B. , 40, 59.

Ross M. , 1968, Proc. IEEE, 56, 196.

Sakamoto M. , Welch D. F. , Hamagel G. L. , Streifer W. , Kung H. and Scrifes D. R. , 1988, Appl. Phys. Lett. , 52, 2220.

Tai K. , Hasagawa A. and Tomita A. , 1986, Phys. Rev. Lett. , 59, 135.

Telle H. R. , 1984, Appl. Phys. B. , 35, 195.

Trutna W. R. , Donald D. K. and Nazarathy M. , 1987, Opt. Lett. , 12, 248.

Wallmenth K. and Peuser P. , 1988, Electron. Lett. , 24, 1086.

Zabusky N. J. and Kruskal M. D. , 1965, Phys. Rev. Lett. , 15, 240.

Zakharov V. E. and Shabat A. B. , 1972, Sov. Phys. JETP, 34, 62.

Zhou B. , Kane T. , Dixon G.J. and Byer R. L. , 1985, Opt. Lett. , 10, 62.

Zhou F. and Ferguson A. I. , 1990, Electron. Letts. , 26, 490.

CHAPTER 2
DIODE LASER PUMPED SOLID STATE LASERS

Section 2.1 Introduction

In this chapter the use of diode lasers as pump sources for solid state lasers is described. The characteristics and varieties of diode lasers are described in section 2.2 with specific reference to the 1W diode laser that was used in the experiments described in this thesis. The focusing optics for this diode are described in section 2.2.4. Section 2.3 reviews how the diode lasers can be used to pump solid state lasers. The lasing medium that was used in the experiments was Nd:YAG which was operated around the 1.3 μm transition, the spectroscopic properties of Nd:YAG are summarised in section 2.4.

Section 2.2 Diode lasers

The first GaAs laser diodes were demonstrated in 1962 [Hall et al: 1962] and it was not long before their potential as pump sources for solid state lasers was realised [Newman et al: 1963]. The laser diode as a pump source promised compact, robust and potentially inexpensive laser systems. The emitting wavelength of laser diodes fabricated from (GaAl)As is between 700 and 900 nm, the emission wavelength being dependent upon the concentration of Ga and Al. This range of wavelengths falls conveniently upon the absorption bands of many solid state materials. The diode laser can be finely tuned into these absorption bands, resulting in high absorption to make efficient laser systems. Thermal loading, a problem which is often found with flashlamp pumped systems is overcome, this eliminates the need for water cooling. The laser diode has the advantage that it has a very long lifetime, typically of the order of over 5000 hours.

The laser diode operates by recombination of electron/hole pairs in a forward biased p-n junction. In modern laser diodes very high gain is achieved by the use of quantum wells, which are very thin, typically 20 nm or less. To lower threshold the laser diode gain region is formed in to a Fabry-Perot cavity with a high reflecting coating (H.R.) on the rear surface and a partially reflecting coating on the output facet. Due to total internal reflection and the high index difference (n = 3.6 for GaAlAs) a reflectivity of about 30 % can be achieved, sometimes in very high gain devices an anti-reflection coating (A.R.) will be used to obtain higher slope efficiencies.

The generated light can be confined by two methods;

(i) index guiding: in the plane parallel and perpendicular to the index plane the gain region is surrounded by a lower refractive index.

(ii) gain guiding: the gain region is confined by the distribution of the drive current.

Whether a laser diode is gain guided or index guided has a great bearing on its characteristics. Index guided lasers tend to operate on a single longitudinal and transverse mode, with typical linewidths of the order of 10 MHz. The spot size at the output facet is typically a few square micrometers, this limits the output power before catastrophic

damage to a few tens of milliwatts. Index guided laser diodes offer near diffraction limited performance up to a power of tens of milliwatts. Spectra Diode Laboratories (SDL) have produced an index guided device which can emit up to 100 mW in a near diffraction limited beam.

Gain guided devices use index guiding perpendicular to the junction plane and gain guiding in the junction plane. The difference in confinement leads to the emitted wavefront from these devices having a different curvature in the two perpendicular directions and differing positions of the waist. In the index guided plane the waist is located on the output facet. Gain guided injection diode lasers usually emit on multiple longitudinal modes, the optical spectrum of these devices range up to 2 nm. This property limits the coherence of the device.

The maximum amount of power that can be emitted by a single facet is limited by the energy density on that facet. If the area of the facet is enlarged to reduce the energy density, an increase in output power can be achieved. This is achieved at the expense of the output beam quality which due to interaction between the optical field and injected charge causes the lasing action to be made up of a multitude of incoherent filaments, making focusing to a tight spot difficult.

2.2.2 Phased array diode lasers

The effective emitting region can be enlarged by the use of multi-striped laser diodes. A review of phased array diodes has been made by Streifer et al [Streifer et al: 1988]. A schematic diagram of a 10-stripe laser diode is shown in fig 2.2.1, this is typical of a phased array diode laser. The diode consists of ten 5 μm wide emitters on 10 μm centres. The overall dimensions of the device is 1 μm by 100 μm. Typically a ten striped diode of this type can emit up to 1.2 W before catastrophic damage. Scaling of the dimensions so that the emitting region consists of 20 elements in a 1 μm by 200 μm facet allows a two fold increase in the cw output power.

2.2.3 The characteristics of a 1W phased array diode laser

The 1W diode laser that was used in the experiments described in this thesis was a 20-element phased array diode laser (SDL-2460-H1). The device is a multiple quantum well device, with the active region as thin as 10 to 30 nm. The optical field which is confined by the cladding is substantially larger and is of the order of 300 nm to 500 nm. The higher concentration of Al in the cladding layers lowers the refractive index of the cladding in comparison to the active region, thus allowing guiding of the mode by internal reflection. Each stripe is in close proximity with its nearest neighbour, the optical mode being gain guided in this direction. Gain guiding does not closely bound the mode and allows the modes between adjacent stripes to couple via evanescent waves.

The far field output pattern of the laser is dependent upon the phase shift between adjacent stripes, for a phase shift of 0 degrees a single lobe would be emitted. However, usually there is a phase shift of π degrees between stripes with the resultant far

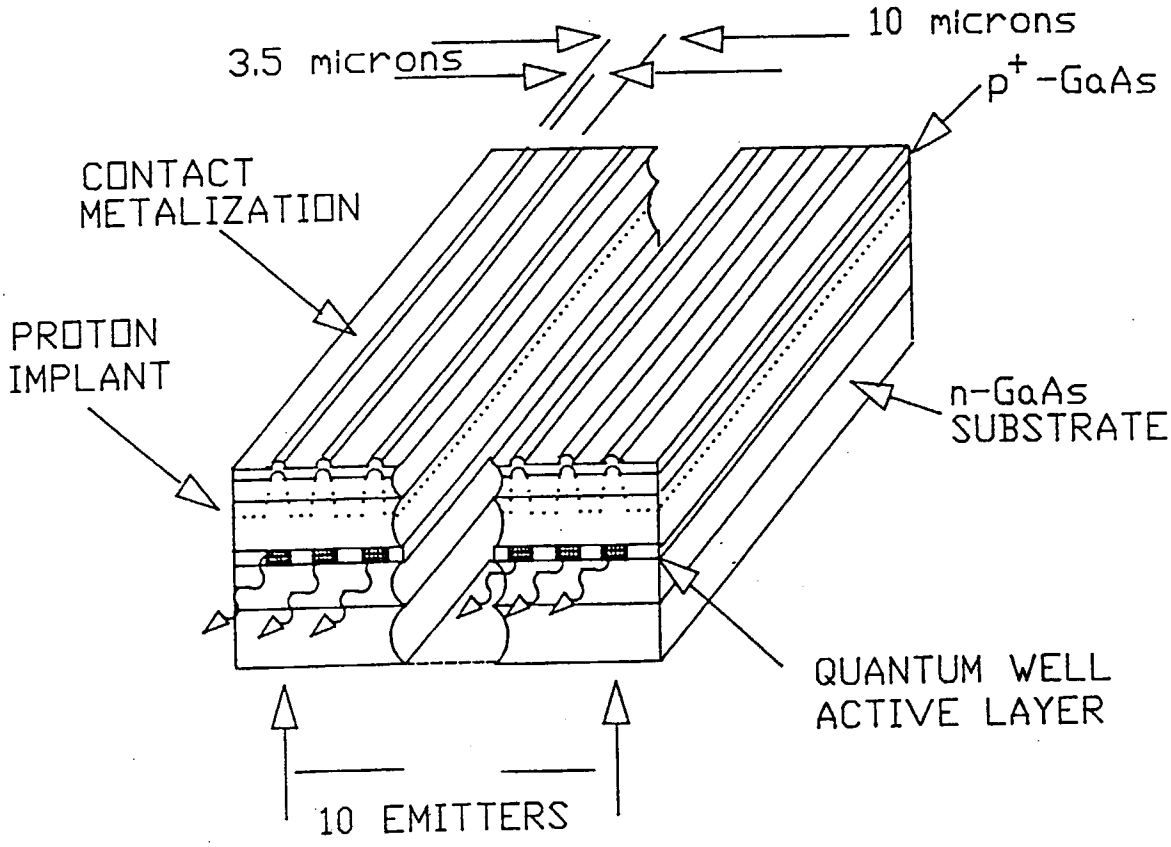

FIG 2.2.1 A SCHEMATIC OF A 10 STRIPE DIODE LASER

FIG 2.2.2

FARFIELD ENERGY DISTRIBUTION IN THE PLANE PARALLEL TO THE p-n JUNCTION

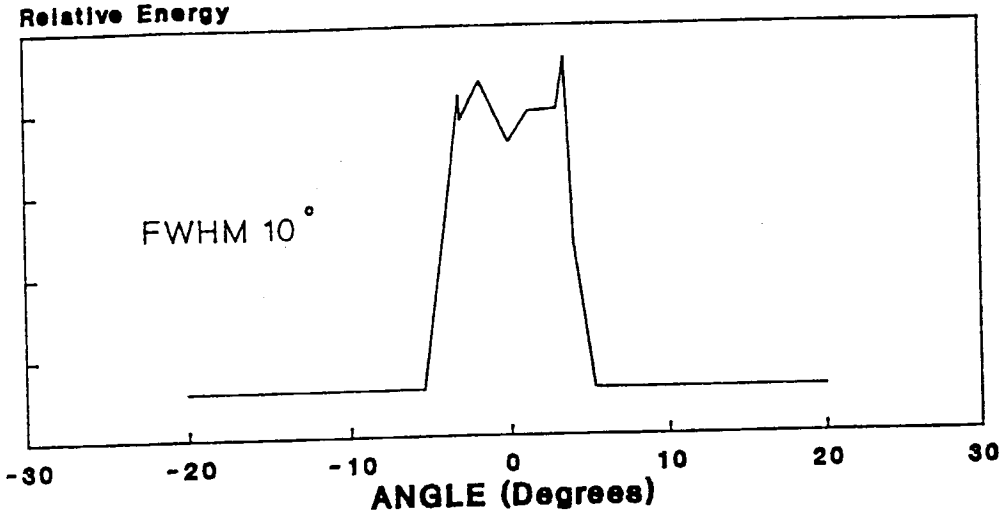

THE FARFIELD IN THE PLANE PERPENDICULAR TO THE p-n JUNCTION

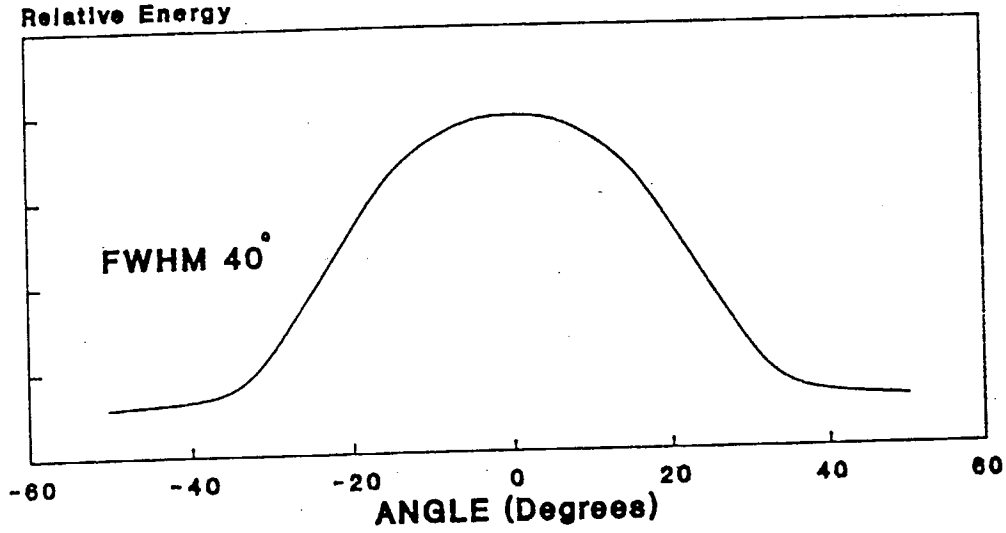

field pattern consisting of two lobes. A typical far field pattern is shown in fig 2.2.2 for a 1 W SDL phased array laser diode. The divergence of the beams is dependent upon whether you are looking parallel or perpendicular to the emitting junction. This is due to diffraction where the smaller the emitting region the greater the divergence. For a 1 W laser diode the divergence is 40 degrees in the plane perpendicular to the junction and 10 degrees in the plane of the junction. The output of the laser is diffraction limited in the plane perpendicular to the junction plane and 25X diffraction limited in the plane parallel to the junction plane [Fan et al: 1989]. The output of the laser is polarised in the plane of the junction. In fig 2.2.3 a diagram is shown of the output spectrum of a 1 W laser diode, the spectral width is about 2 nm, with a coherence length of 0.5 mm. The output spectrum of the diode does not consist of a continuum but of discreet longitudinal modes. For a 2 nm spectral width there will be typically 10 longitudinal modes, these individual modes form 'supermodes' which broaden the individual linewidths of the longitudinal modes. The large spectral width of the laser diodes does not usually present a problem for pumping solid state materials as the absorption band of most solid state materials is spectrally broader.

The electrical characteristics of the 1W diode laser are shown in fig 2.2.4. The diode needs a forward bias of about 2 V to operate, for the 1 W laser diode a typical threshold current is 460 mA, measured at room temperature. The diode has a reverse breakdown voltage of 3 V, hence care is required to protect the diode. In fig 2.2.5 a schematic diagram is shown of a protection circuit that has been used to suppress transients to the laser diode. The output power against current shows that there is spontaneous emission below threshold, this has a wide bandwidth of approximately 25 nm. A red glow can be seen from the laser diode when operated which is the short wavelength component of this. The laser diodes are very efficient with a typical overall efficiency of 25% and a slope efficiency of 0.5 (ouput optical power/input electrical power).

The output wavelength of the 1W diode laser was tuned into the maximum absorption in Nd:YAG by temperature tuning the diode laser, the laser tunes at a rate of 0.3 nm/°C. Temperature tuning was achieved by the use of a Peltier device (built into the laser package) used in a feedback loop designed to keep the temperature at a set constant, the temperature being monitored by a thermistor which was built into the diode laser package. Using this system the temperature could be controlled over a range of 45°C which corresponds to a wavelength range of 13.5 nm. The diode laser used in this experiment operated at 814 nm at 25°C. To tune the diode into the maximum absorption at 807 nm in Nd:YAG required cooling the diode to $\approx$ 5°C. When operated with this level of cooling an efficient heat sink was required to quickly remove the heat away from the diode, about 13 W of power being dissipated by the system. Stable operation of the diode laser was only achieved when using a heat sink with a dissipation constant of 0.25° C/W.

FIG 2.2.3
THE TYPICAL EMMISION CROSS SECTION OF A 1W DIODE LASER

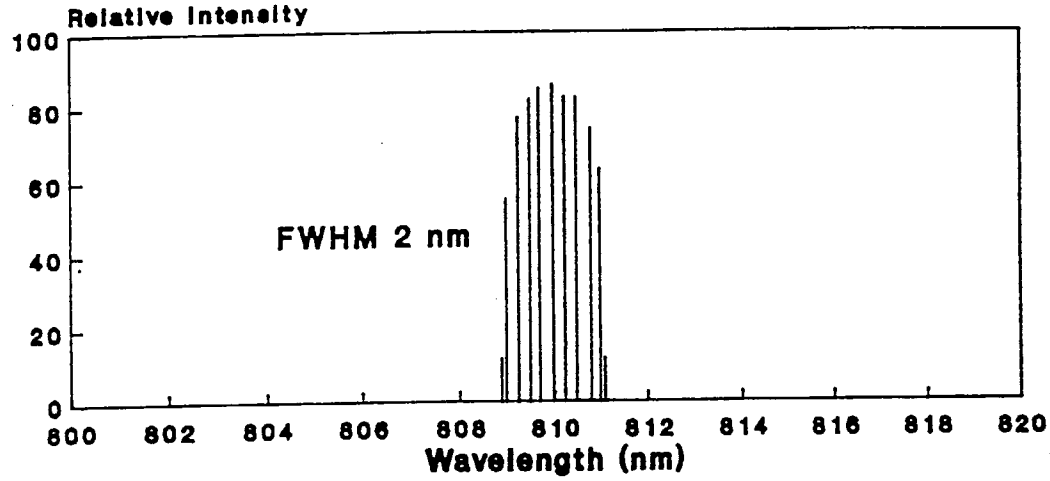

The spectrum is not continuous due to the many longitudinal modes that are running

FIG 2.2.4
THE ELECTRICAL/OPTICAL CHARACTERISTICS OF A 1W DIODE LASER

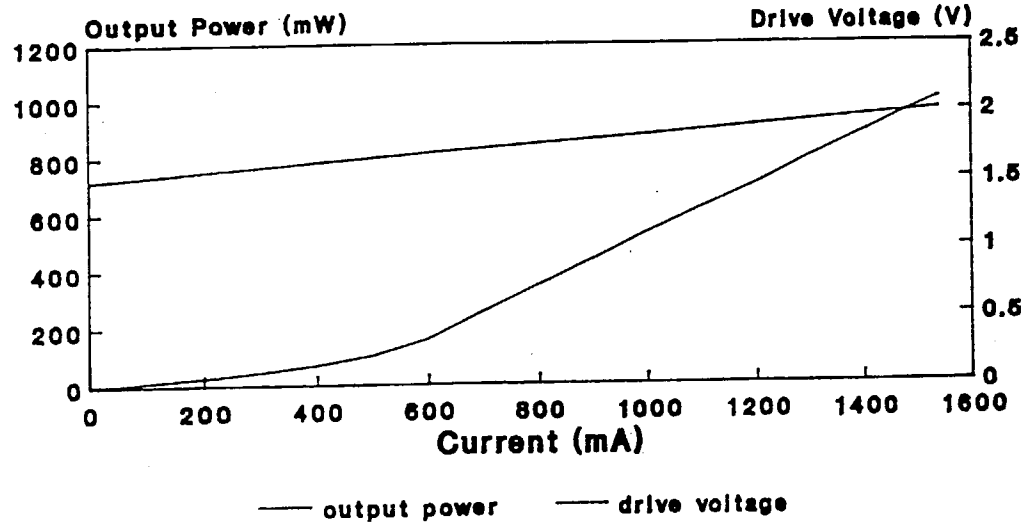

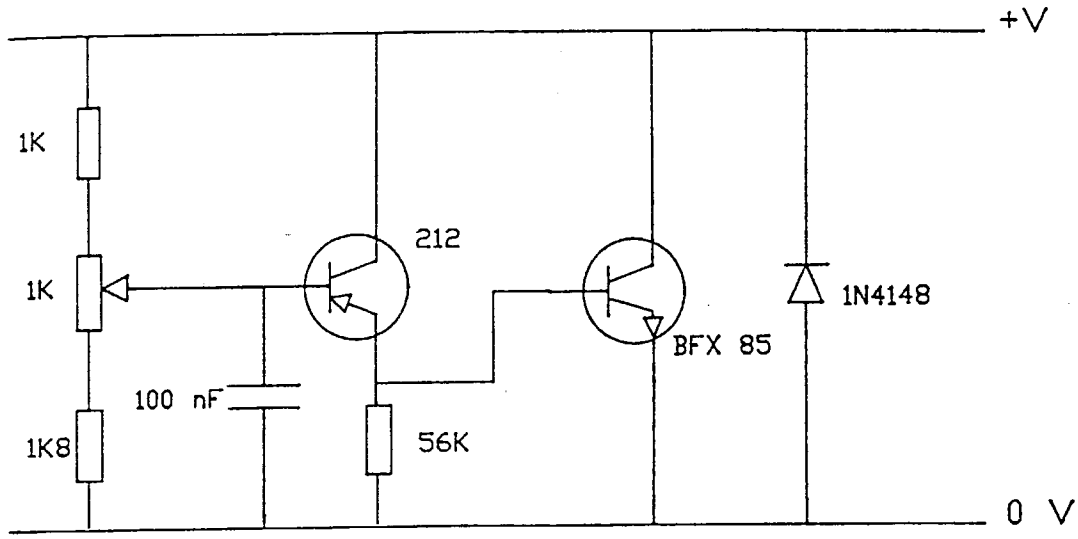

FIG 2.2.5 Diode protection circuit

2.2.4 The focusing optics for a 1W diode laser

The use of phased array laser diodes requires different cavity designs and more elaborate focusing optics. Generally the solid state laser will consist of external mirrors allowing flexibility in the choice of the size of the waists in the cavity and also allows the use of intra-cavity components.

Section 2.2.3 described how the output from phased array laser diodes is highly divergent and astigmatic. This output needs to be focused to a spot size which matches that of the solid state laser, typically this spot size will be in the range of 40 μm to 200 μm so as to achieve efficient longitudinal pumping. In fig 2.2.6 a diagram shows the focusing optics that were used to focus the output from the 1W laser diode used in the experiments. The 1W laser diode has a beam divergence of 40° and 10° FWHM, this implies that the $1/e^2$ guassian profile point is 1.7X greater than these angles so any collimating lens must have a numerical aperture (NA) greater than this angle for efficient energy collection. The collimating lens used in our focusing scheme is a 6.5 mm focal length, 0.615 N.A lens (Melles Griot 06 GLC 001/D). The lens system had a clear aperture of 8 mm and a working distance of 1.2 mm. The 1W laser diode is hermetically sealed with a window thickness of 0.3 mm which is placed about 0.7 mm away from the emitting region, this puts a lower limit on the working distance of any lens system. The collimating lens that has been described compensates for any abberation caused by this window. The collimating lens was found to just collimate the output of the laser diode. The shape of the beam from the collimator was rectangular in shape, with a dimensions ratio of 4:1 reflecting the difference in divergence of the two planes of the laser diode. To make the pump spot more uniform 'circular' for efficient matching to the solid state laser mode, an anamorphic prism pair was used to expand the beam in the plane perpendicular to the index guided plane. The anamorphic prism pair has the advantage over cylindrical optics in that it is compact and transmits the output of the laser parallel to the input beam. The amount of magnification that the prism pair imparts is determined by the angle that they are set relative to the input beam. The magnification of one prism is given by

$$M = H'/H = \cos I'/\cos I \qquad 2.2.1$$

where the parameters H',H,I' and I are defined in fig 2.2.6. The magnification of a prism pair is the square of this value. The prisms are designed so that the angle of incident onto the exit face is near 90°, so all the magnification is imparted by the front face. A wide magnification range can be obtained over a small range of incident angle allowing an anti reflection coating to be used on the prisms which covers this range of wavelengths. In our set up the magnification was set to 4X. In the index guided plane the beam passes unmagnified.

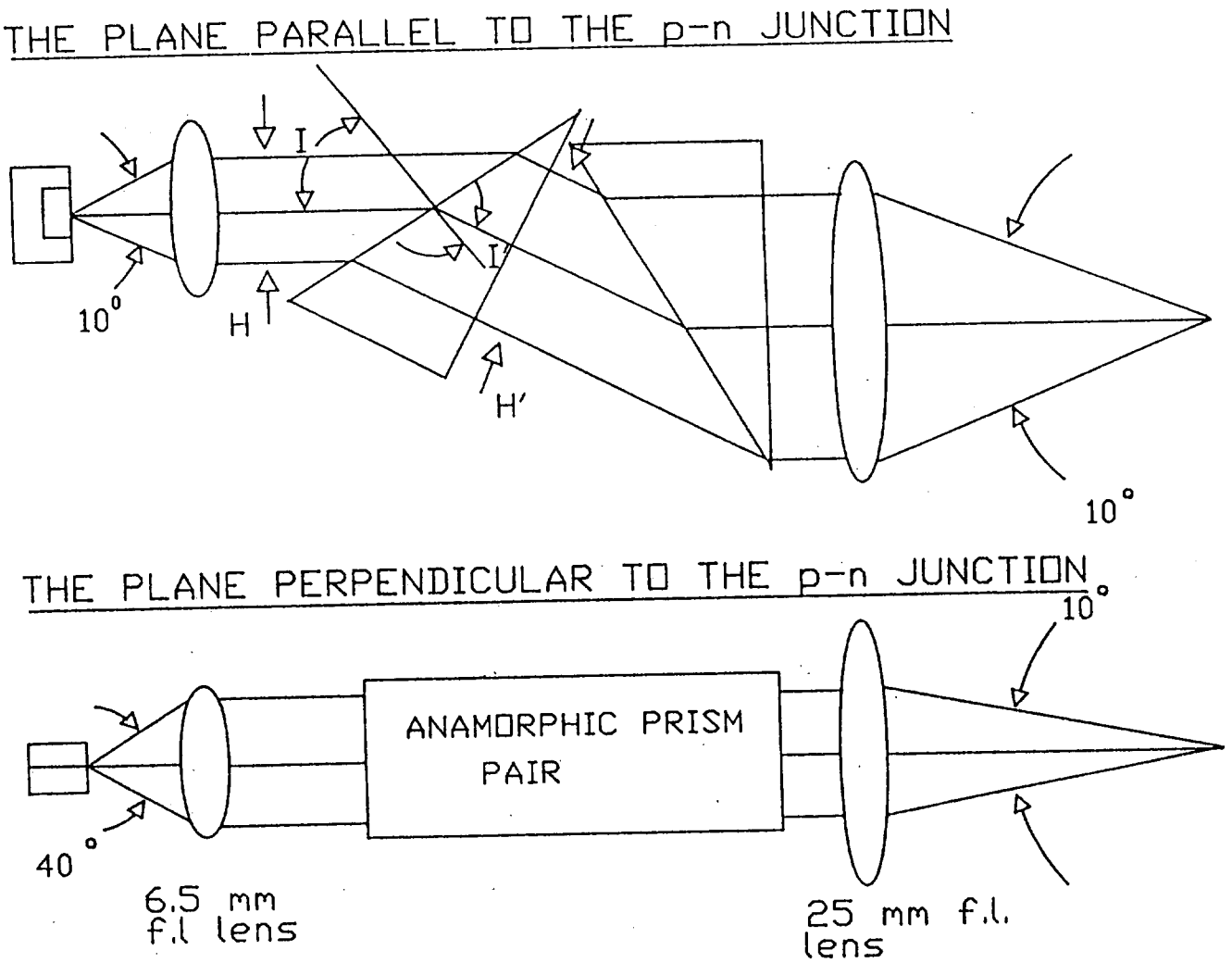
THE PLANE PARALLEL TO THE p-n JUNCTION
I
I'
10°
H
H'
10°
THE PLANE PERPENDICULAR TO THE p-n JUNCTION
10°
ANAMORPHIC PRISM
PAIR
40°
6.5 mm
f.l lens
25 mm f.l.
lens

FIG 2.2.6

The focusing is completed by a 25 mm focal length, 25 mm diameter A.R. coated at 810 nm lens. This focusing system has a 1:1 imaging ratio in the plane parallel to the array junction and has a magnification of 4X in the perpendicular plane. Measurement of the spot sizes from this focusing system by the use of an aperture resulted in the spot size being estimated as 50 μm by 75 μm. In the both planes the focused beam had a divergence of about 6° in the Nd:YAG rod.

2.2.5 High powered diode lasers

It has been discussed in section 2.2.3 how it is important to remove heat away quickly from a diode laser. The problem becomes even more important for high power diode lasers and poses a major problem to the design and use of these diodes. Further increases in output power can be achieved through the use of diode array bars which are a series of phased array diode lasers closely spaced (typically 500 μm). A laser containing 20 phased array diodes in a 1 cm bar has been reported to emit up to 38 W cw at 0°C [Sakamoto et al: 1988]. This design spreads the heat load over a larger area and the intensity on a single facet is reduced at the expense of brightness. The laser can be operated in a pulsed mode which further reduces heating problems, this laser has produced over 100W when modulated at 40 Hz in 150 μsec pulses. The future design and use of high power diode lasers is as much a problem of finding solutions to the thermal problems as it is of the optical design of the diodes. The diode lasers bars can be stacked so that they form a very high powered source which can be used to sidepump solid state lasers. Even though these diodes are very efficient (typically 40%), the waist heat generated by them still poses a major obstacle to their use. For instance, a bar operating at 40 W cw output will generate 65W of heat. This large heat dissipation problem can give rise to frequency drift of the diode laser and frequency chirping of the output when used in a pulsed mode.

Section 2.3.1 Diode laser pumped solid state systems

In section 2.2 it was described how rapidly the power from laser diodes has been increased in recent years. The divergence, beam quality, spectral width and brightness differ widely between these diodes, which is reflected in the way that laser diodes are used as pump sources for solid state lasers. The physical size of the laser diode and the ability to focus them to small spot sizes makes them attractive as pump sources for solid state lasers. Although there is a loss in power in using a laser diode as a pump source for a solid state laser, diode pumped solid state lasers have the advantage of

(i) near diffraction limited sources

(ii) a wide range of lasing wavelengths in the near infra-red

(iii) the possibility of very narrow linewidths sources

(iv) the solid state laser can be modulated, resulting in high peak powers and very short pulses.

Until the development of laser diode bar arrays and stacked bar arrays, a laser diode would be generally used in a longitudinal pump configuration for a solid state laser. Longitudinal pumping is a highly efficient way of pumping a solid state laser, the pump mode can be made to match the single transverse mode of the laser, with the consequence that the inversion profile can be kept to the resonator mode. It is possible using a laser diode pump to reach differential slope efficiencies close to the theoretical limit [Fields et al: 1989]. Also longitudinal pumping allows optimisation of the length of the laser material with respect to crystal lasers and pump light absorption.

One of the most simple forms of longitudinal pumping is shown in fig 2.3.1. This is typical of early pumping schemes which used single faceted gain guided diodes. The output of the laser diode is focused using a graded refractive index (GRIN) lens to a spot size of 40 μm or less. Shown in the diagram is a monolithic Nd:YAG rod, which offered high stability and low scattering losses, making the threshold in these devices very low. Electrical to optical efficiencies of 6% [Zhou et al: 1985] were obtained. The inclusion of a prism between the GRIN lens and focused spots could irradiate the astigmatism caused by the laser diode [Clarkson et al: 1989]

2.3.2 Phased array laser diodes as pump sources for solid state lasers

The focusing scheme described in section 2.2.4 has been used by Berger et al [Berger et al: 1987] to pump a 2 mirror scheme. For a pump power of 1.8 W, 465 mW of TEM_{oo} 1.06 μm was obtained with an overall efficiency of 10.8%. The maximum output power longitudinally pumping a solid state laser is ultimately limited by the pump diode. Scaling of these systems either requires higher powered laser diodes or use of more than one laser diode. One possible method of doing this is by polarisation coupling the output of two laser diodes, this system still only has limited scaleability.

Berger et al [Berger et al: 1988] have developed an end pumped Nd:YAG laser which uses a fibre optic bundle to couple the output of 7 phased array laser diodes into a longitudally pumped system. This fibre bundle transmitted the output of the lasers with an efficiency of 40%. When pumped with 1.9 W of power the system produced a peak power of 660 mW at 1.06 μm with an electrical to optical conversion efficiency of 4.4%. This system has the disadvantage that each diode has to be individually tuned to an absorption and each fibre individually aligned to each diode. In this experiment 100 μm, 1/2 watt phased array laser diodes were used, the output of which could be collected with an efficiency of 42%. The system has the advantage that as well as higher output powers it does not rely on one laser diode, making the system more reliable.

An alternative method of coupling multiple laser diodes into a longitudinally pumped solid state laser takes advantage of the difference in beam divergence in the planes perpendicular and parallel to the junction [Fan et al: 1989]. The arrangement makes use of cylindrical optics to collect and focus the ouput from three 500mW phased array diode lasers. This arrangement produced an output power of 550 mW at 1.06 μm. This method allows an order of magnitude increase in pump power in the same mode volume

as can be obtained with a single array. Again this method suffers from each diode having to be individually temperature tuned and has a focusing system which consists of many components.

The most successful method of longitudally pumping a solid state laser to date has used a laser design which has 'multiple ends' [Watanabe et al: 1989]. The 'multiple ends' design uses a slab type Nd:YAG crystal, the laser beam propagating zig-zag fashion inside the crystal, the laser diode pumping the crystal at each reflection point. The system used by Watanabe et al utilised 20 1W laser diodes whose outputs were fibre coupled and then focused into the slab. In this system the slab needed to be cooled. The lasing system produced 3.5 W at 1.06 μm for an incident pump power of 11.3 W, when pumped with 14 W the laser produced 4.9 W of multimode output.

The system developed by Albars et al [Albers et al: 1990] uses a zig-zag arrangement which allows pumping of the solid state laser at four different sites. The system produced 685 mW output power for 2 W pump at an overall efficiency of 10%. The authors predict that by using higher powered laser diodes (2W) an output of over 3 W could be expected.

The neatest of the zig-zag style of solid state laser has been developed by Baer et al [Baer et al: 1990]. A diagram of the set up is shown in fig 2.3.2. The pump source is a diode bar consisting of ten 1W laser diode arrays placed on 1 mm centres. The output of these lasers are mode matched into the mode of the zig-zag laser by the use of a high numerical aperture optical fibre. For a pump power of 10.9 W from the diode bar an output power of 3.8 W was obtained corresponding to an optical to optical efficiency of 35 %.

2.3.3 Diode laser side pumping of solid state lasers

The laser diode bars and stacks that were described in section 2.2 are generally not suited to longitudinal pumping. The incoherence and large emitting region of the devices make it difficult to efficiently mode match longitudinally in to a solid state laser. These devices have been used to side pump solid state lasers . As well as requiring different cavity and focusing geometries other laser materials under certain circumstances can be better suited to sidepumping by pulsed laser diodes due to a long upper state lifetime and shorter absorption length than Nd:YAG.

The major problem of sidepumping is to match the mode of the laser diode to that of the solid state laser, often there has been a problem in making the laser lase on a single transverse mode. High overall electrical to optical efficiencies has been achieved by Hays et al [1989] achieving an overall efficiency of 18%. The solid state laser pumped by a quasi-CW, 50 mJ/pulse 200 μsec pulse at 810 nm had a multimode output which followed the pump mode. To improve the mode matching and the efficiencies of laser diode pumped systems attempts have been made to focus the laser diodes into the mode of the laser. Using four 5W laser diodes (SDL-3480-L) Burnham et al [Burnham et al: 1989] have coupled into the solid state mode such that there was a 1:1 image magnification. The

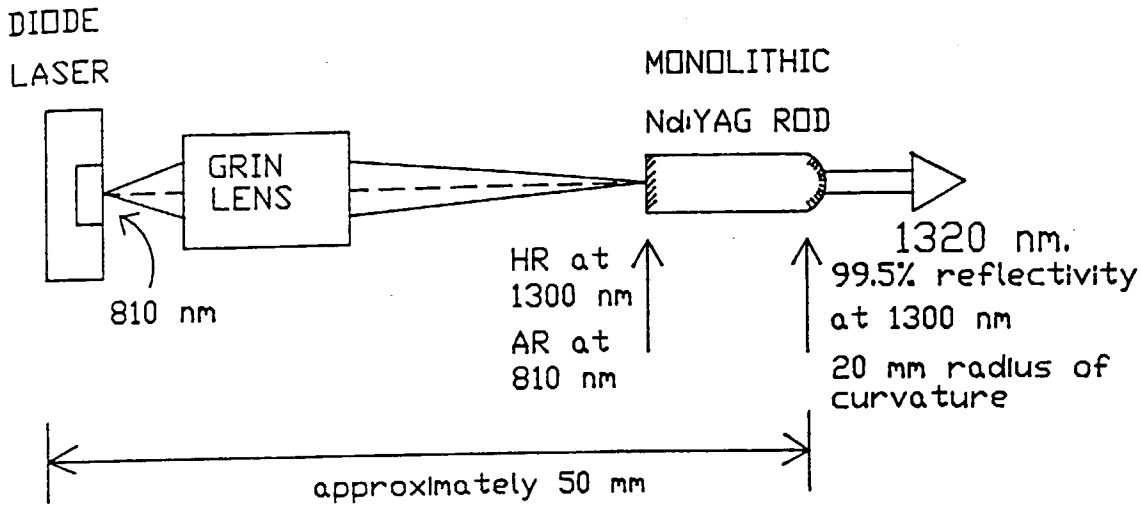

FIG 2.3.1

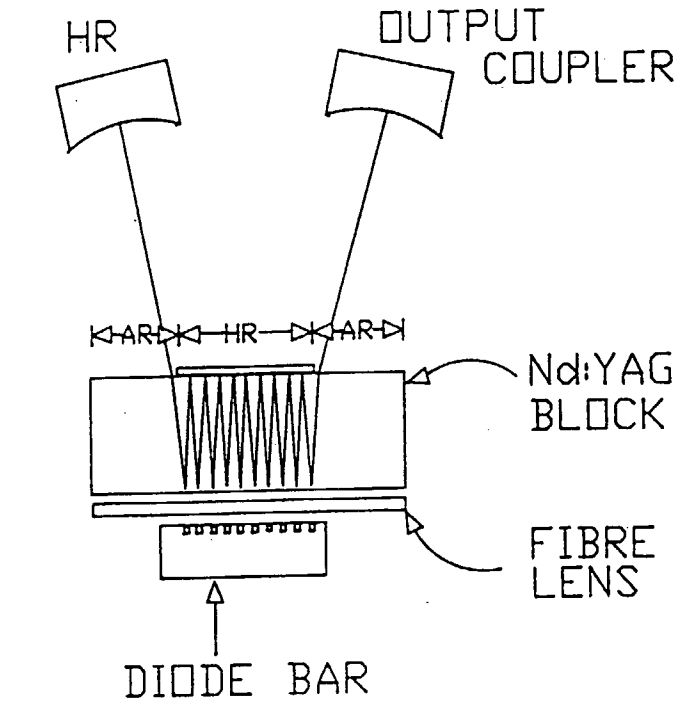

FIG 2.3.2

system produced 3.3 W multimode output and 1.6 W TEM_{oo} output with an overall efficiency of 2%.

A side pumped single longitudinal and transverse mode laser has been developed by Norrie et al [Norrie et al :1989]. The system utilised a 25 W, 200 μsec pulsed diode laser, of dimensions of 1 cm (SDL 32200) which had 1000 emitting stripes. The 1.5 mm diameter Nd:YAG rod acted as a lens for the diode laser radiation, the brass housing for the Nd:YAG rod was finely polished so as to reflect any transmitted light. The laser produced 0.3 mJ, 27 nsec pulses up to 100 MHz with a TEM_{oo} mode profile. The laser ran on multilongitudinal modes but by injection seeding with a single frequency laser, the laser ran on a single longitudinal mode.

The use of Lu^{3+} as a size compensator in the YAG crystal lattice allows a heavier concentration of Nd^{3+} before the florescence lifetime is quenched. The higher concentration of Nd^{3+} gives Nd:Lu:YAG a much shorter absorption length. Nd:Lu:YAG has been used [Allik et al: 1989] in a side pumped configuration resulting in a better optical slope efficiency than that obtained with Nd:YAG. This is attributed to higher pump absorption and lower losses.

2.3.4 Single frequency microchip lasers

An attractive new source of single frequency radiation is the microchip laser [Zayhowski et al: 1989). The solid state material is made very thin, typically 500 μm to 1000 μm. The advantage of using a thin gain medium is that the longitudinal modes of the laser will be spaced such that the next order mode will fall outside the gain bandwidth of the laser. Simply by coating the microchip laser and butting the laser material against a laser diode facet, the microchip laser can be made to lase on a single longitudinal and transverse mode . The mode of the laser is guided by the laser diodes output. The single frequency can be tuned by the use of strain on the microchip laser which can be simply applied with a piezo electric. This method of the use of laser diodes offers the possibility of mass produced laser diode pumped solid state laser operating on a single frequency. Again with this technology materials other than Nd:YAG are of interest due to their higher absorption efficiencies.

Section 2.4 A review of the properties of Nd:YAG

One of the most successful and well established lasing materials is the neodinium ion doped into yttrium aluminium garnet, Nd^{3+}:YAG [Danielymeyer: 1975] For many years it has been used as a lasing source in the near infra-red, principally at 1.06 μm and at 1.32 μm. The yttrium aluminium garnet acts as a host for the Nd^{3+} ion, the Nd^{3+} replacing the yttrium in the crystal lattice. The Nd^{3+} fits into the YAG crystal lattice without change in energy or the need for charge compensation. The sites for the Nd^{3+} are nearly identicle, broadening of the transitions of Nd^{3+} comes as a result of inhomogeneous phonon broadening. As well as the excellent spectroscopic properties that

YAG offers as a host, it has good heat conduction properties, is easy to grow, it is physically hard making it easy to polish and does not solarize at high pump levels.

Other hosts for the Nd^{3+} ion have been found to show excellent lasing characteristics, such as Nd:YLF [Hormer et al: 1969), Nd:CR.GSGG, Nd:BEL [Barnes et al: 1987), and Nd:Lu:YAG [Allik et al: 1989], the choice of the most suitable host is dependent upon the application that it is to be used for and its availability. In cw operation Nd:YAG still has the best performance of the materials listed. The Nd^{3+} ion can be doped into glass [Kozlovsky et al: 1986] where it is inhomogenously broadened and has a large linewidth. This makes it suitable for use as a amplifier and owing to the large linewidth the laser has the potential for supporting very short pulses when modelocked.

An absorption spectrum for Nd:YAG with a doping level of 1% Nd^{3+} is shown in fig 2.4.1, the absorption is shown around 800 nm the region of interest for diode pumping. It is the absorption around this wavelength that makes Nd:YAG such a good material for diode pumping. The peak absorption around 807 nm has a 1/e absorption length of 3 mm^{-1}, with a spectral width of about 4 nm, this is sufficiently wide for most of the spectral width of typical laser diodes to be absorbed. Efficient absorption of the output power from a diode laser can be achieved in 5mm or more of Nd:YAG. The 1/e absorption length is dependent on the percentage dopant of the Nd^{3+} ion, having a higher concentration of Nd^{3+} ions should result in higher absorptions and a more efficient laser system. Unfortunately, Nd:YAG suffers from cross relaxation between adjacent Nd^{3+} which results in a partial transfer of energy between ions. This cross relaxation destroys the $^4F_{3/2}$ excitation, consequently shortening the fluorescence lifetime. This is a limitation of Nd:YAG, if more than 1.5% dopant of Nd^{3+} ions are used then there is a resultant 'quenching' of the florescence lifetime.

The energy levels of Nd:YAG (1% dopant) are shown in fig 2.4.2. The $^4F_{3/2}$ level is in thermal equilibrium with the pump bands. The $^4F_{3/2}$ band does not relax by multiphonon processes and is a metastable state with a florescence lifetime of 240 μsec. The lower laser levels are in thermal equilibrium with the ground state, which is the $^4I_{9/2}$ manifold at room temperature. The energy gap between the ground state and the main lower lasing transitions is 2111 cm^{-1}, so at room temperature the population of the lower lasing level can be neglected. The 946 nm lasing level which is the transition from the $^4F_{3/2}$ to the $^4I_{9/2}$ transition is a quasi-three level laser [Risk: 1988]. The quantum efficiency for the transfer to the $^4F_{3/2}$ state has been measured to vary between 0.65 and 0.95, the error due to uncertainty in measuring the cross section for Nd:YAG, typically a value of 0.7 is used [Fan et al: 1988]. Many of the transitions in Nd:YAG have been made to lase [Marling: 1978) but the main transitions are at 1.064 μm and 1.32 μm. The lower energy level for the 1.32 μm transition is the $^4I_{3/2}$. Due to Stark splitting this line consists of many lines, the two main transitions being at 1.318 μm and 1.338 μm. The emission cross section for these transitions are about equal but are about 1/4 that of the 1.064 μm transition [Birnbaum et al: 1981], making the cross section 0.9 X 10^{-19} cm^2 [Barnes et al: 1987]. The gain bandwidth for the 1.3 μm transition is 180 GHz which is

slightly larger than that of the 1.064 μm transition [Singh et al: 1974]. In table 2.4.1 a summary of the spectroscopic and physical properties of 1% doped Nd:YAG are given.

Table 2.4.1: The spectroscopy of Nd:YAG

For 1% doping of Nd^{3+} by weight.

Refractive index at 1.06 μm	1.818
1/e absorption at 807 nm.	3 cm^{-1}
Upper state lifetime	230 μsec
1.3 μm lasing transition	$^4F_{3/2} \rightarrow {}^4I_{13/2}$
	Two main transitions of equal strength at 1.318 μm and 1.338 μm.
Gain cross section	0.9 X 10^{-19} cm^2.
Gain bandwidth	180 GHz.

Apart from being used as a dopant in specific crystalline hosts, the Nd^{3+} ion can be used so that it is a chemical component of the crystal itself. These class of materials are called Stoichiometric lasers. These materials have reduced concentration quenching compared to Nd:YAG, allowing higher concentrations of Nd^{3+}. This means that efficient absorption can be achieved in as small a volume as possible. For a review of the subject the reader is referred to Huber [Huber: 1980].

FIG 2.4.1

THE ABSORPTION OF 1% DOPED Nd:YAG

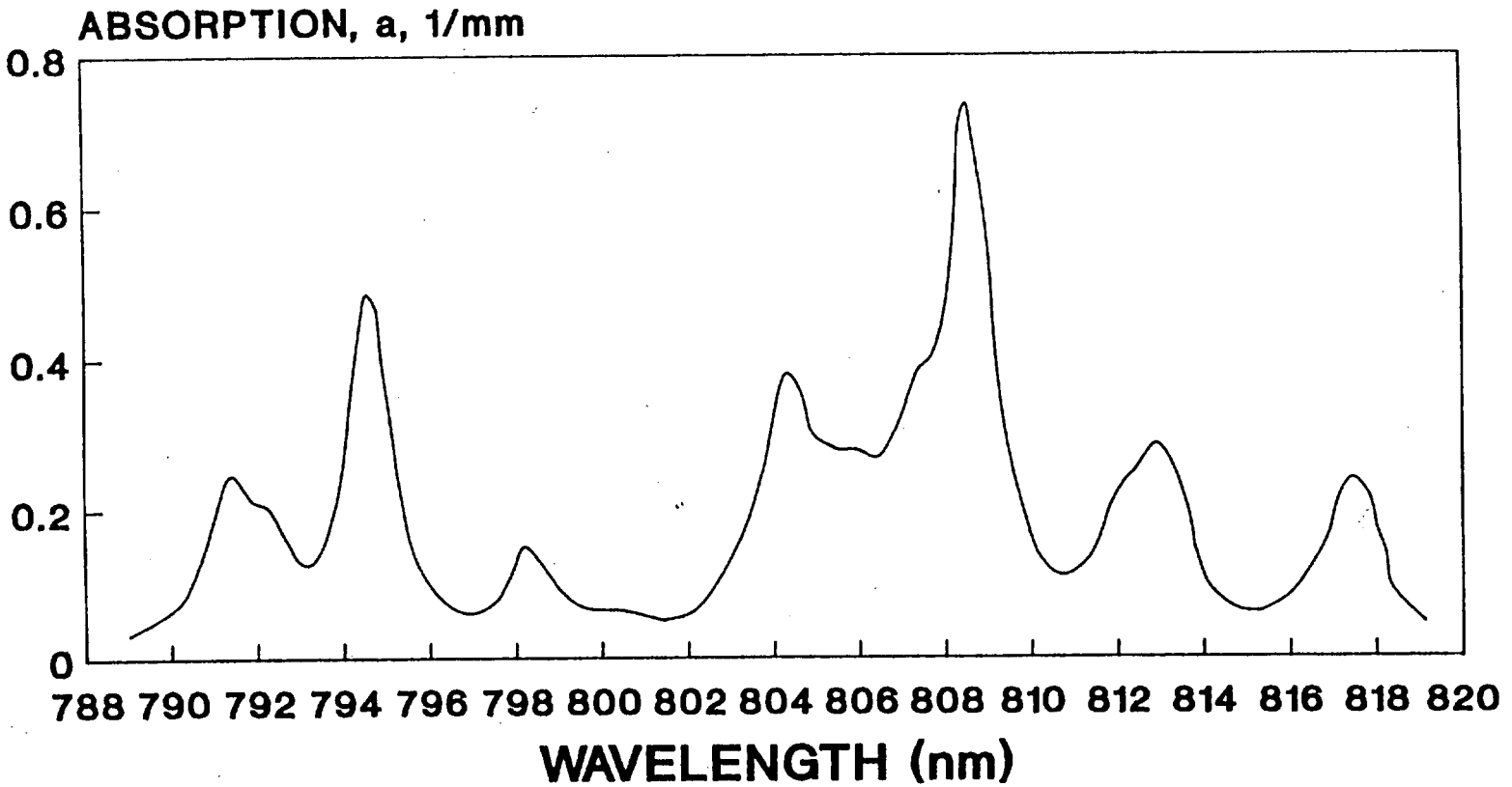

* a defined by I(x) = I(0) exp(-ax) where I(x) is the intensity at a position x.

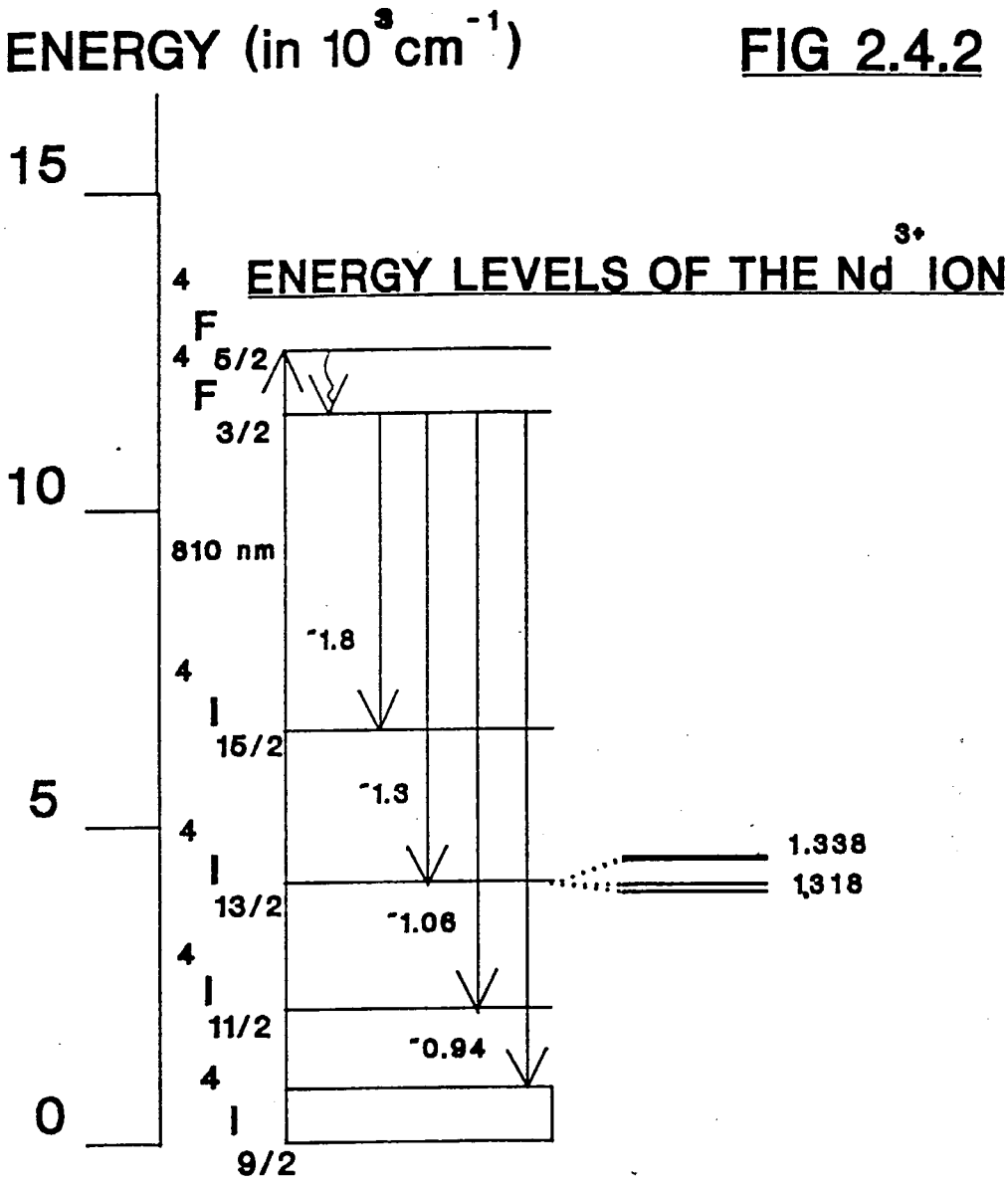

* The wavelengths of the transitions are in microns and are measured about the centre of gravity of the manifold

** The Stark splitting of the 1300 nm transition is shown with the two main transitions indicated.

CHAPTER 2: REFERENCES

Albers P. , Pfistner C.H. and Weber H.P , 1990, Conference on Lasers and Electro-Optics, CMF4.

Allik T. H. , Hovis W. W. , Cuffey D. P. and King V. , 1989, Opt. Lett., 14, 116.

Baer T. M. , Head D. F. and Gooding P. , 1990, Conference on Lasers and Electro-optics O. S. A, Session Tu B1-1.

Barnes N. P. , Gettemy D. J. , Esterowitz L. and Allen R. E. , 1987, IEEE J. Quantum. Electron, QE - 23, 1434.

Berger J. , Welch D. F. , Scrifes D. R. , Streifer W. and Cross P. S. , 1987, Appl. Phys. Lett., 51, 1212.

Berger J. , Welch D. F. , Streifer W. , Hoffman N. J. , Smith J. J. and Rodecki D. , 1988, Opt. Lett., 13, 306.

Birnbaum M. , Tucker A. W. , and Fincher C. L. , 1981, J. Appl. Phys. , 52, 1212.

Burnham R. and Hays A. D. , 1989, Opt. Lett. , 14, 27.

Clarkson W. A. and Hanna D. C. , 1989, J. Modern Opt. , 36, 483.

Danielmeyer H. G. , 1975, in 'Lasers Vol 4', Eds: A. K. Levine and A. DeMarie, Marcel Dekker inc, New York.

Fan T. Y. , Sanchez A. and Defoe W. E. , 1989, Opt. Lett. , 14, 1057.

Fan T. Y and Byer R. L. , 1988, IEEE J. Quantum. Electron. , 24, 895.

Fields R. A. , Rose T. S. , Innocenzi M. E. , Yura H. T. and Fincher C. L. , 1989, Conference on Lasers and Electro-Optics, Session Tu C6-1-Postdeadline.

Hall R. N. , Fenner J. D. , Kingsley J. D. , Seltys T. J. and Carbon R. O. , 1962, Phys. Rev. Lett. , 9, 366.

Harmer A. L. , Linz A. and Gabbe D. R. , 1969, J. Phys. Chem. Solids. , 30, 1483.

Hays A. D. , Burnham R. and Harnagel G. L. , 1989, Conference on Lasers and Electro-Optics, Postdeadline Papers, PD-9.

Huber G. , 1980, 'Miniature Neodymium-lasers', Chapter 1, Current Topics in Materials Science Volume 4, North Holland Publishing Company.

Kozlovsky W. J. , Fan T. Y. and Byer R. L. , 1986, Opt. Lett. , 12, 788.

Marling J. , 1978, IEEE J. Quantum. Electron. , QE-14, 56.

Newman R. , 1963, J. Appl. Phys, 34, 437.

Norrie C. J. , Sinclair B. D. , Gallaher N. , Dunn M. H. and Sibbett W. , 1989, Electron. Lett. , 25, 1115.

Risk W. P. , 1988, J. Opt. Soc. Am B, 5, 1412.

Sakamoto M. , Welch D. F. , Harnard G. L. , Streifer W. , Kung H. and Scrifes D. R. , 1988, Appl. Phys. Letts. , vol, 220.

Singh S. , Smith R. G. and Van Ulbert L. G. , 1974, Phys. Rev. , 10, 2566.

Streifer W. , Scrifes D. R. , Harnagel G. L. , Welch D. F. , Berger J. , Sakamoto M. , 1988, IEEE J. Quantum. Electron. , 24, 883.

Watanabe S. , Kude S. , Yamare T. , and Washio K. , 1989, Conference on Lasers and Electro-Optics, Postdeadline Papers, PD 8-1.

Zayhowski J. J. and Moorudian A. , 1989, Opt. Lett. 14, 24.

Zhou B. , Kane T. J. , Dixon G. J. and Byer R. L. , 1985, Opt. Lett. , 10, 62.

CHAPTER 3

A DIODE LASER PUMPED MODELOCKED AND Q-SWICTHED Nd:YAG LASER OPERATING AT 1.3 μm.

This chapter describes the design and performance of a laser diode pumped Nd:YAG laser that has been modelocked by both amplitude modulation and frequency modulation techniques. Section 1 describes the design of a cavity suitable for diode pumping and the insertion of active devices, section 2 describes the cw performance of this laser. In section 3 a general description of the modelocking process is made with specific reference to the self-consistent theory for homogeneously broadened lasers. The performance of the amplitude modulated and frequency modulated laser is described in section 4 and 5 respectively. The results are compared to the self consistent theory. Simultaneously Q-switching and frequency modulated modelocking is described in section 6, a method which greatly enhances the peak output power from the laser.

Section 3.1.1: Cavity Design Requirements

The design requirements for the modelocked and Q-switched laser cavity are as follows:-

(i) The waist must match that of the pump from the laser diode to achieve maximum pump/laser mode overlap and to minimise threshold.

(ii) A near collimated beam of a few hundred microns is required in the laser cavity for active devices to work efficiently. This must be of sufficient length such that the active modulators can physically be placed in the cavity.

(iii) The waist of the cavity must be positioned so that the pump beam can match the mode of the cavity without pump distortion or a high loss of pump power through transmission through cavity components.

(iv) Losses in the cavity must be minimised so as to achieve maximum conversion efficiency.

(v) An intra-cavity component must be included to differentiate between the two main lasing transitions centred at 1.3 μm, of 1.318 μm and 1.338 μm.

The initial cavity design that was found to meet these requirements is shown in fig 3.1.1 The gain medium is a 10 mm Nd:YAG rod, 4 mm in diameter and doped with 1% Nd^{3+} by weight. One end of the rod was high reflection coated at 1.3 μm (>98%) and anti-reflection coated at 810 nm (<0.5%). The other end of the rod had a 30 minute wedge and was anti-reflection coated at 1.3 μm. An intra-cavity lens of 75 mm focal length and anti-reflection coated at 1.3 μm was used to provide a tight focus in the Nd:YAG rod and a near collimated beam for the insertion of active devices. The cavity was completed with a plane output coupler. The cavity meets all the design requirements but it was found that the any near parallel surfaces formed intra-cavity etalons which modifies the lasing bandwidth when modelocking.

To overcome this problem the cavity shown in fig 3.1.2 was used. The anti-reflection coated end of the Nd:YAG rod has been cut to Brewster's angle at 1.3 μm (60.9°). Light from this laser is horizontally polarised. The intra-cavity lens has been replaced with a high reflecting mirror with a radius of curvature of 150 mm, which is the same effective focal length as the lens. This eradicates the intra-cavity etalon of the lens and decreases losses in the cavity due to better coatings on the mirror.

3.1.2 Astigmatic Compensation

The use of a Brewster angled element in the short focusing arm produces astigmatism in the output laser beam profile. This can be understood by considering the effective distances traversed in passing through the Brewster angled rod in the x and y planes as shown in fig 3.1.3. The use of Snell's law results in the equivalent path lengths given in equation 3.1.1 and 3.1.2 [Hanna: 1969],

$$d_x = t/(n^2 - \sin^2 \theta_1)^{\frac{1}{2}} \qquad 3.1.1$$

$$d_y = tn^2(1 - \sin^2 \theta_1)/(n^2 - \sin^2 \theta_1)^{3/2} \qquad 3.1.2$$

These effective path length are of interest when $\theta_1 = \theta_B$, using $\cos \theta_B = 1/(1 + n^2)^{\frac{1}{2}}$ gives

$$d_x = t(1 + n^2)^{\frac{1}{2}}/n^2 \qquad 3.1.3$$

$$d_y = t(1 + n^2)^{\frac{1}{2}}/n^4 \qquad 3.1.4$$

Here t is the length of the rod and n its refractive index. The beam waist at the plane face of the Nd:YAG rod, in the x and y planes, will be at different effective distances from the rear folding mirror. This has the effect of causing astigmatism in the output beam. This astigmatism can be compensated for by the use of an off axis mirror. The introduction of a 'dog leg' in to the cavity is a common way of correcting for astigmatism in dye lasers and detailed descriptions of the method have been made by Kogelnik et al [1972]. An off axis mirror focuses sagittal (xz) ray bundles at a different location to the tangential (yz) bundles. This results in two effective focal lengths as given below:-

$$f_x = f/\cos \theta \qquad 3.1.5$$

$$f_y = f\cos \theta \qquad 3.1.6$$

where θ is the angle of incidence and f is the actual focal length of the mirror (radius/2). The property that the effective focal length is increased in one plane and reduced in the other can be used to compensate for the two different effective path lengths caused by the Brewster angle. The effective path length, d_x, is longer than that of d_y so a more powerful lens is required in this plane. The angle θ at which compensation takes place can

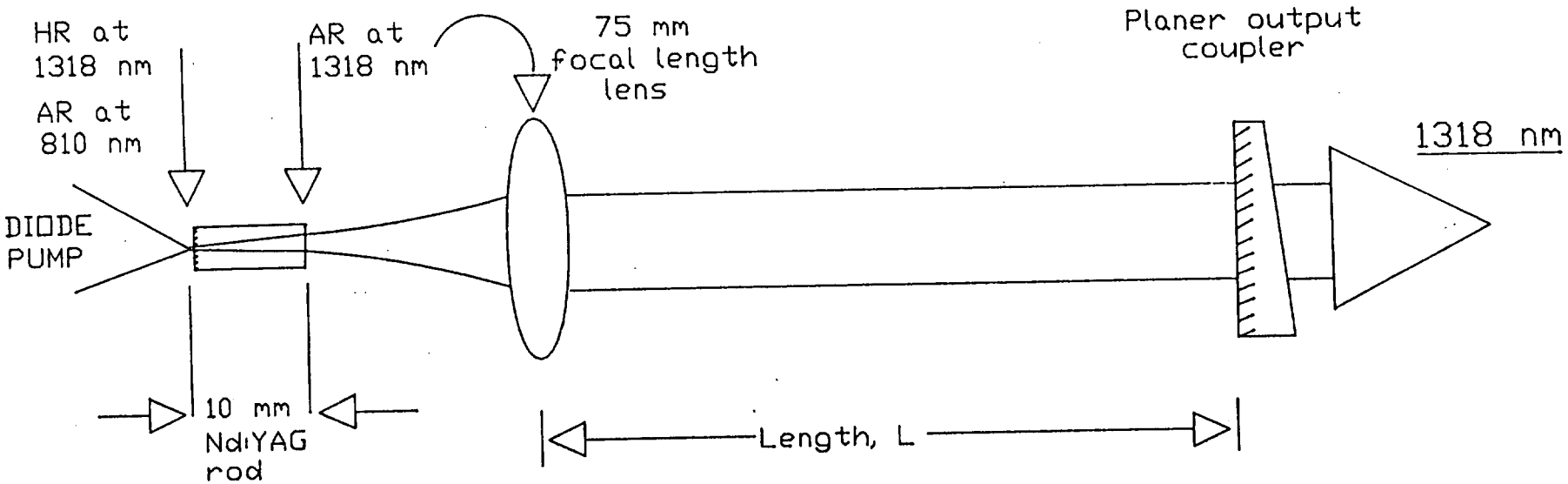
HR at
1318 nm
AR at
810 nm
AR at
1318 nm
75 mm
focal length
lens
Planer output
coupler
1318 nm
DIODE
PUMP
10 mm
Nd:YAG
rod
Length, L

FIG 3.1.1

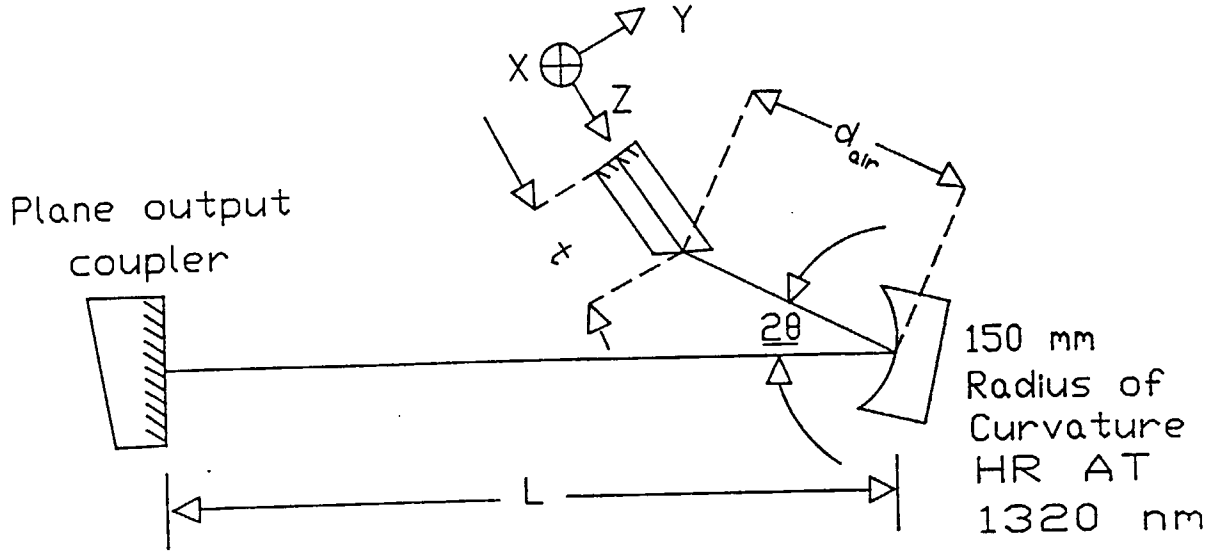

FIG 3.1.2

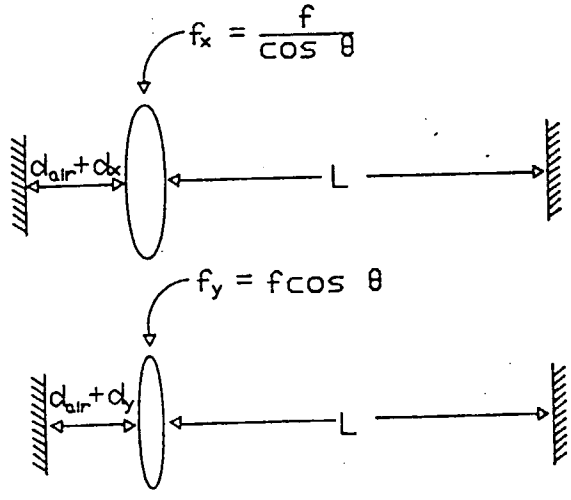

FIG 3.1.3

The equaivalent cavities representing the Brewster angled cavity

be worked out by equating the correction factors, when they are equal the cavity will be corrected for astigmatism. The condition for compensation is:-

$$d_x - f_x = f_y - d_y \qquad 3.1.7$$

implying

$$t(n^2 - 1).(n^2 + 1)^{\frac{1}{2}} / n^4 = f\sin\theta \tan\theta \qquad 3.1.8$$

which can be rewritten in terms of $R = 2f$ and $N = (n^2-1).(n^2+1)^{\frac{1}{2}}/n^4$ to give

$$2Nt = R\sin\theta \tan\theta \qquad 3.1.9$$

The refractive index of Nd:YAG is n = 1.82, the radius of curvature of the mirror is 150 mm and the thickness of the rod is 10 mm. Applying these parameters to equation 3.1.9 results in the compensation angle to be $\theta = 13.77°$. The setting of the angle of incidence of the light on to the backmirror at 13.77° will result in the laser having an output beam profile which is a symmetrical Guassian. This compensation angle implies that the 'dog leg' angle be set to 27.54°.

The beam spot sizes in the cavity can be worked out for this compensation angle for different values of d_{air} as shown in fig 3.1.2. In fig 3.1.4 graphs are shown of how the output beam waist varies with astigmatic compensation angle and how the beam waist in the rod varies with d_{air} at the compensation angle. It can be seen that for this overall cavity length that the cavity is stable from 7.1 to 8.4 mm for d_{air} where at a value of d_{air} = 7.9 mm the cavity is most stable, with an output beam waist of 350 μm. In fig 3.1.5 a graph is shown of how the output beam waist varies with overall cavity length. This is an important factor in the design of the cavity for modelocking as active modelockers of a wide range of frequencies may be used which requires the overall cavity length to be variable without a drastic change in spot sizes and stability in the cavity.

3.1.3 Wavelength Selection

The Nd:YAG crystal has two main lasing transitions at 1.3 μm spaced by 20 nm, these are of equal line strength. To achieve efficient lasing action and stable modelocking the laser is required to operate on just one of these transitions. In both the AM and FM modelocking cases the selection was achieved by the use of an intra-cavity prism. Due to the dispersion of the prism sufficient deviation was present between the two transitions for one transition to lase whilst for the other wavelength the cavity was misaligned. The surpression of the second line could be achieved with an intra-cavity etalon but this could effect the lasing bandwidth so a prism was used in the final system. The Brewster angled prism placed in the near collimated arm of the cavity produces a negligible amount of astigmatism.

FIG 3.1.4(a)
THE OUTPUT WAIST WITH DOG LEG ANGLE

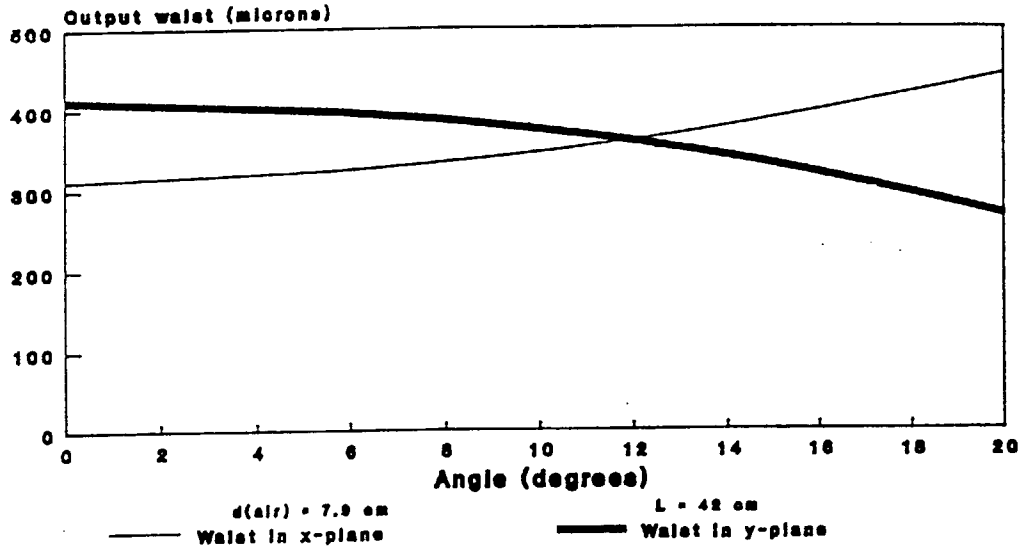

FIG 3.1.4 (b)
THE VARIATION OF THE WAISTS IN THE CAVITY WITH INTRA-CAVITY FOCUS

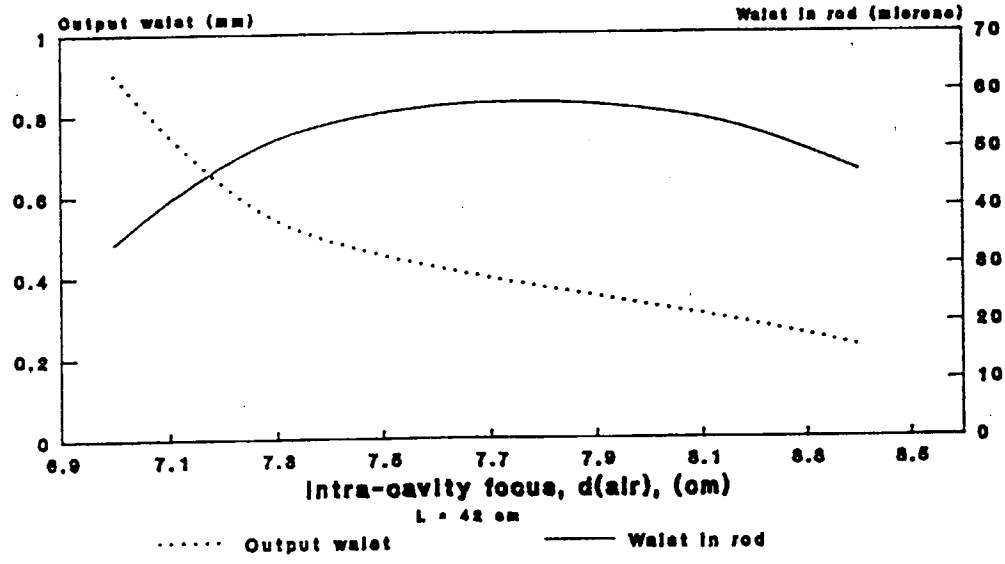

FIG 3.1.5

THE VARIATION OF THE CAVITY'S WAISTS WITH CAVITY LENGTH

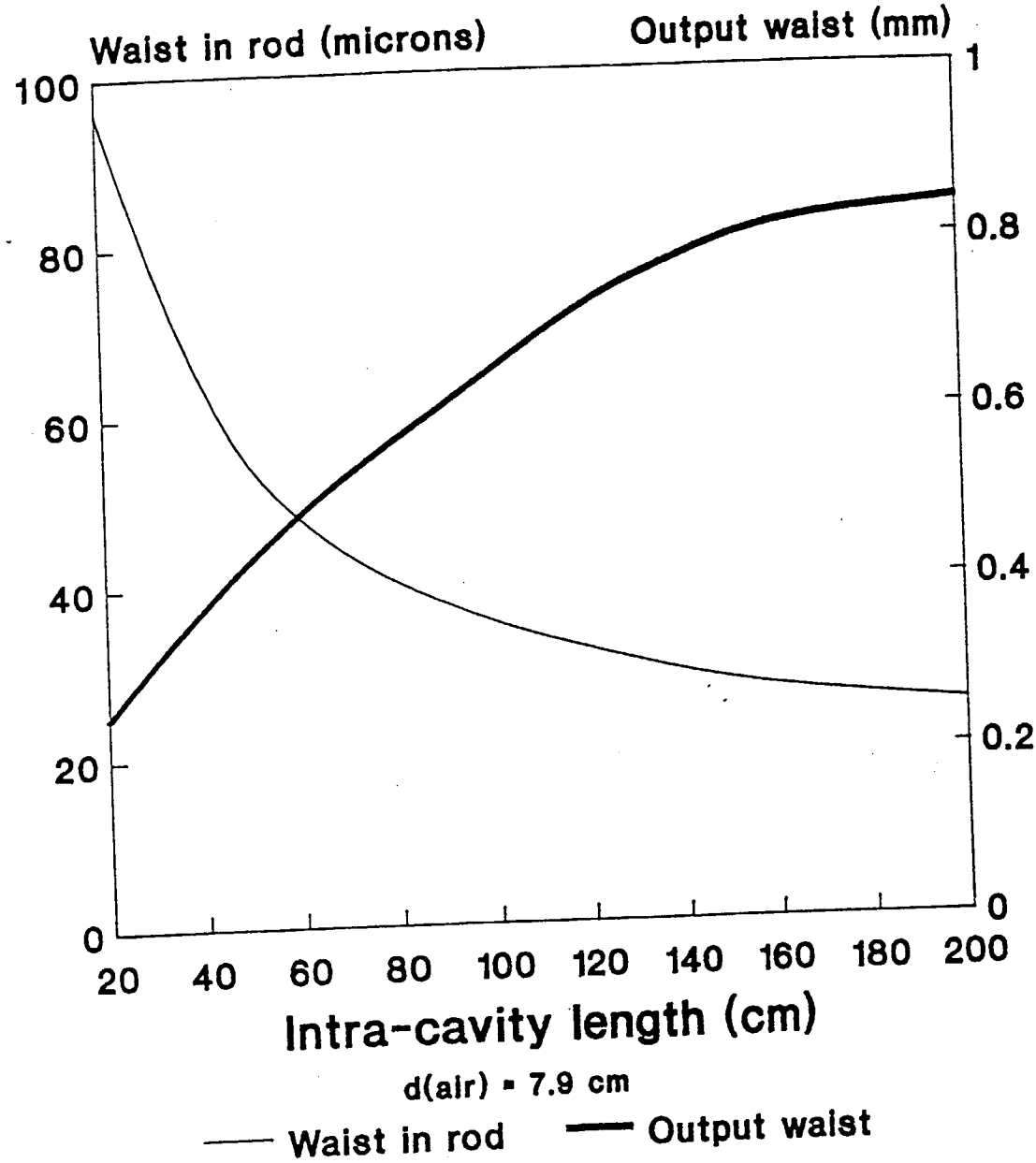

Section 3.2.1: Continuous Wave Characteristics

The final configuration that was used for AM modelocking the Nd:YAG laser is shown in fig 3.2.1. The pump optics and the cavity are as described in section 2.1 and 3.1 respectively. The acousto-optic modulator was in the form of a Brewster angled quartz prism which achieves the necessary wavelength selection and has a low insertion loss. The output power from the laser with a mirror which had 7% output coupling was 9.5 mW for a pump power of 1W, with an incident threshold of 642 mW and a slope efficiency of 6%. When operated with a 0.5% output coupling the laser had an incident threshold of 350 mW and an output power of 10 mW which corresponds to a slope efficiency of 2.2%. The Nd:YAG rod was found to transmit 7% of the incident light, so the amount of energy absorbed at threshold is 325 mW when using a 0.5% output coupling. The angle of incidence on to the mirror was set at the astigmatic compensation angle of 13.3°, at this angle a circular TEM_{00} mode was obtained.

The efficiency of the laser is relatively low, implying that there is a large intrinsic loss in the cavity. An expression for the threshold and slope efficiency for four level lasers has been derived by Fan et al [1988]. Following an analysis of the rate equations describing the population of the upper lasing level the expression below describes the threshold pump power

$$P_{th} = \pi h\nu_p/2\sigma_e\eta_p\tau\,(\omega_o^2 + \omega_p^2)\,\delta \qquad 3.2.1$$

ν_p is the frequency of the pump wavelength, η_p is the quantum efficiency, σ_e the stimulated emission cross section, τ is the upper state lifetime and δ accounts for all the round trip loss. The 1/e electric field amplitude of the laser cavity mode and the Guassian beam pump are given by ω_0 and ω_p respectively. In deriving 3.2.1 it has been assumed that both the pump and cavity modes are TEM_{00} Guassian beams with negligible diffraction in the gain medium. This is an approximate solution to the integral and does not account for different pump distributions, high order transverse modes, non-collinear pump beam and cavity modes, or diffraction of the beams within the gain medium. As long as the pump power can be described such that it is within some pump radius $r = \omega_p$ then the exact form of the distribution of the pump mode is unimportant. The loss in the cavity comes as a result of many factors including impurity absorption in the gain medium and intra cavity components, bulk scattering, absorption at the laser wavelength due to lower laser level population, loss due to non-perfect coatings and the loss due to the output coupler. To make the threshold low requires a small pump and laser spot size and a low loss in the cavity. Equation 3.2.1 implies that reducing the value of the pump and laser mode spot sizes to zero will result in the threshold approaching zero, this does not take in to account diffraction effects, which for very small spot sizes will become a significant effect. Diffraction effects can be taken into account by taking the average

of the spot sizes along the length of the gain medium, this results in an optimum pump and cavity mode spot size for a given length of rod. [Diggonet: 1985]

The slope efficiency of the laser can be calculated by considering the rate equations for the upper laser level with stimulated emission being included, and the circulating intensity in the cavity. The simplified expression for the slope efficiency which assumes the optimum condition for the pump spot sizes ($\omega_0 = \omega_p$) [Huber: 1980] is given by

$$\eta \approx \eta_p \, (h\nu/h\nu_p).(T/\delta) \qquad 3.2.2$$

This expression is an approximation, a more accurate expression for the slope efficiency must take into account the spatial distribution of the pump beam and laser mode in the lasing medium and on the laser power [Clarkson et al: 1989]. The expression shows that to obtain a good slope efficiency a high output coupling with a small intra-cavity loss is required.

The round trip loss in the cavity was estimated by measuring the thresholds for different output couplers and by using equation 3.2.1 which states that the threshold is proportional to the loss in the cavity. The overall round trip loss with a 7% output coupler was calculated to be 12.5%, the acousto-optic modulator having a round trip loss of 2.7% and the loss due to other intra-cavity components 2.5%. Using this value of loss in the cavity and the known spectroscopic values as given in chapter 2 section 2, equation 3.2.1 predicts that the threshold should be 230 mW, which is considerably lower than that obtained. There is a large degree of uncertainty in calculating the thresholds owing to the uncertainty in the quantum efficiency which can range from .95 - .65.

In working out the threshold it has been assumed that there is perfect overlap between the pump and the laser mode. This will not be the case due to imperfections in the laser diodes output, such as astigmatism and non-diffraction limited performance. Imperfections in the laser diode pump will cause a further increase in the threshold.

The highest slope efficiency of 6% was obtained with the 7% output coupling, but using such a large output coupler increases the threshold so that total output power is not optimised. To find the optimum output coupling for the cavity a thin plate was placed in the cavity, at approximately Brewsters angle. The power was measured off this loss plate to determine the maximum power that was available from the laser. Using this technique it was found that an output coupling of 2% was optimum.

3.2.2 The Free Running Bandwidth

The free running bandwidth of the laser was monitored using a plane-plane Fabry-Perot interferometer of free spectral range of 100 GHz, a typical spectrum is shown in fig 3.2.2. It can be seen that the spectrum is heavily modulated with a distance between strongly oscillating modes of 15 GHz. This frequency corresponds to the free spectral range of an etalon of about 1 cm, in the cavity this corresponds to the length of

FIG 3.2.1

SCHEMATIC OF THE AM MODELOCKED CAVITY

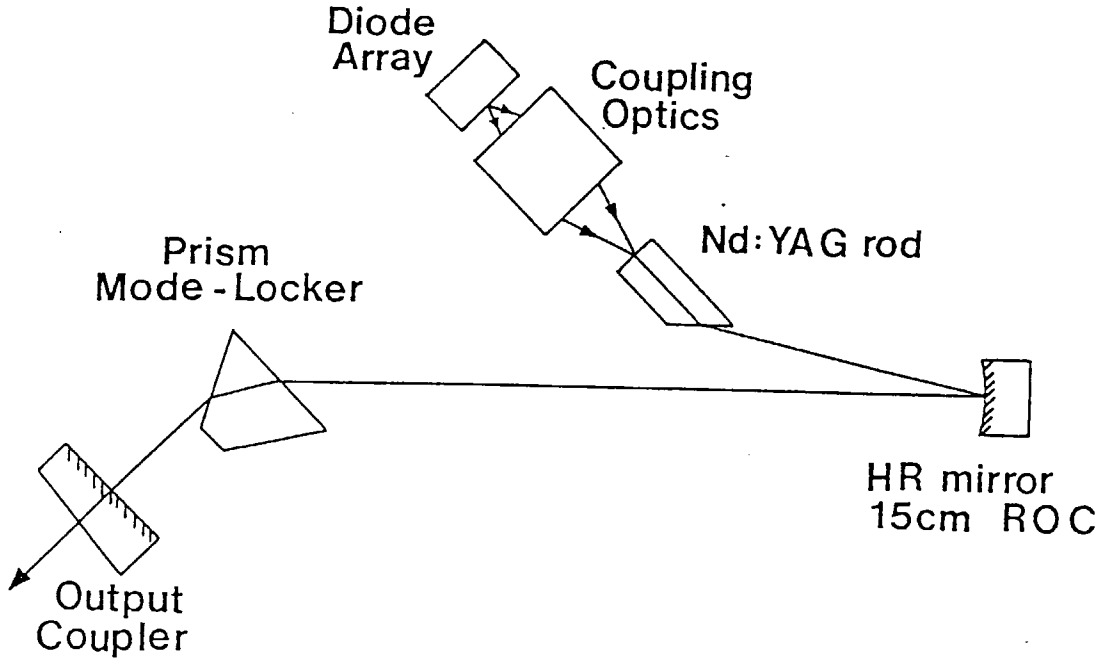

FIG 3.2.2

THE FREE RUNNING SPECTRUM OF THE LASER

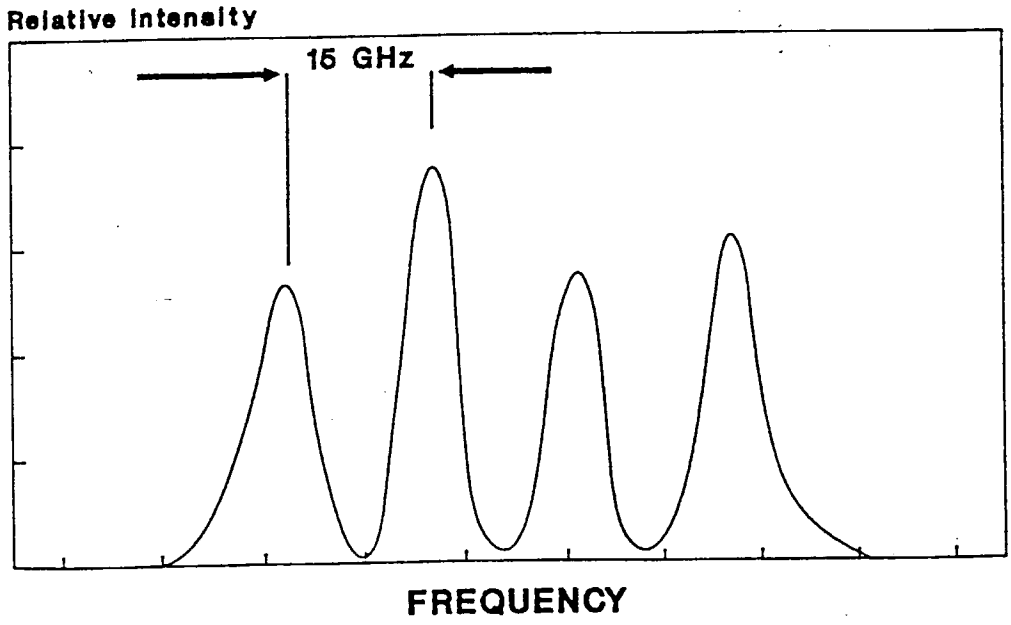

the Nd:YAG rod. It is thought that this effect is due to spatial hole burning in the rod or a loss mechanism on the Brewster angle of the rod. This free running bandwidth is much larger than would be expected for a homogeneously broadened laser.

Section 3.3.1: Modelocking

In this section the modelocking of lasers will be discussed including a description of the Kuizenga theory for homogeneously broadened modelocked lasers. A typical free running laser will oscillate on many longitudinal modes, each of these modes being independent to the next and separated by $\Delta\lambda = c/2l$ where l is the length of the cavity. As a result of the laser running on many incoherent modes the intensity of the laser fluctuates due to random interference between modes. This random fluctuation in intensity reduces the temporal coherence of the laser which is detrimental for some laser applications. The coherence of the laser can be increased by forcing the laser to run on a single longitudinal mode or by inducing the multi-longitudinal modes of the laser to be in phase, this is known as modelocking the laser. Through the process of modelocking it is possible to

(i) Produce high peaked powered pulses

(ii) To produce ultra-short pulses with a duration approaching that of the inverse of the lasing linewidth.

The first report of active modelocking of a laser came in 1964 [Hargrove et al: 1964] with the modelocking of a Helium Neon laser. Since then much work has taken place on the active modelocking of lasers and theoretical understanding of the process. Reviews of the process have been made by Siegman et al [1974]) and New [1983]. The commonest way of modelocking a laser is to by actively modelocking using either amplitude modulation (AM) or frequency modulation (FM). In our study of modelocking active modulators have been used to modelock the laser, both AM modulators and FM modulators.

3.3.2 Amplitude Modulation

Amplitude modulated modelocking of a laser uses an active device which modulates the loss of the laser with a period which is equal to or an integral number of the cavity round trip time c/2L. A simple explanation of the modelocking process is of the modulator imparting sidebands on the cavity modes equal to the cavity mode spacing. This process gives a definite phase between the modes and so 'locks' them.

AM modelocking is usually achieved with an acousto-optic amplitude modulator although other amplitude modulating devices have been used to modelock lasers, such as an electro-optic amplitude modulator [Morimoto et al: 1988] and a piezo-electric modulator [Krausz et al: 1990]. The action of an acousto-optic modulator is in some ways analogous to that of x-rays interaction with matter, as with this effect there is a critical angle, called the Bragg angle where the acousto-optic device will optimally diffract the light beam. Typically a modulator will consist of an acousto-optic crystal substrate and

a transducer which launches an acoustic wave in to the substrate. The laser light is diffracted in passing through the device and is loss modulated at twice the rf drive frequency due to the acoustic standing wave in the modulator substrate. The modulator transmission function for a simple AM modulator can be written as

$$t_{AM}(t) = \cos(\theta_m \sin \omega_m t) \qquad 3.3.1$$

where θ_m is the modulation index. In the Kuizenga and Siegman theory which will be discussed in the preceding section, the transmission function is written as

$$t_{AM}(t) = \exp[-2\delta_t \sin^2 \omega_m t] \qquad 3.3.2$$

These two forms of the transmission functions are similar at the peaks if $\theta_m^2 = 2\delta_m$. In both cases the net amplitude or voltage transmission passing through the modulator can be written as

$$E''(t) = t_{AM}(t)E'(t) \qquad 3.3.3$$

The expression in equation 3.3.2 can be approximated by its quadratic variation about the transmission peak and by assuming that the optical pulse will be short compared to the modulation period, which is the usual condition. In this case the transmission can be approximated by

$$t_{AM}(t) = \exp[-2\delta_t(\omega_m t)^2] \qquad 3.3.4$$

3.3.3 Phase Modulation

The phase modulation of light can be achieved by the use of the electrooptic effect. The application of an electric field along one of the birefigent axis of an electrooptic material results in a change in phase of the electric field but does not change the state of polarisation. The result of passing an optical field through a phase modulator which is sinusoidally modulated will be a set of sidebands around the main signal frequency.

The expression which formerly describes the effect of the phase modulator on an electric field is given below

$$t_{FM}(t) = \exp[j\ 2\delta_c \cos \omega_m t] \qquad 3.3.5$$

where δ_c is the effective single pass phase retardation of the modulator. The single pass phase retardation for an ordinary Fabry-Perot laser cavity is modified depending upon the position of the modulator relative to a mirror. The modified effective phase retardation is then given by [Harris et al: 1965]

$$\delta_c = \left[\frac{2L}{a\pi} \sin \frac{a\pi}{2L} \right] \left[\cos \frac{Zn\pi}{L} \right] \delta_m \qquad 3.3.6$$

where L is the length of the cavity, a the length of the modulator crystal, z_0 the distance of the modulator to a mirror and δ_c the peak phase retardation through the crystal. Assuming a/L << 1 then to achieve the maximum possible phase retardation the phase modulator must be as close as possible to the output coupler.

The expression of equation 3.3.5 reveals some important features of the process of FM modelocking. Applying the approximation that the Guassian pulse duration is much smaller than the modulation frequency then the transmission function can now be written as

$$t_{FM}(t) = \exp[\pm j\, 2\delta_c(1 - \omega_m^2 t^2)] \qquad 3.3.7$$

The equation shows that there are two possible solutions for the FM case corresponding to the two phase extremes of the phase variation. These two modes are referred to as the positive and negative modes, the positive mode corresponds to the positive phase retardation. The second term implies a linear chirp is imparted upon on the pulse on each round trip. Another important feature of a phase modulator is that when a pulse passes through at an angle away from the extremes of phase modulation, a Doppler frequency shift is imparted upon the pulse.

3.3.4 The Kuizenga and Siegman Theory

The Kuizenga and Siegman theory [1970] for the modelocking of homogeneously broadened lasers analyses the roundtrip progress of a Guassian pulse around the intra-cavity components as shown in figure 3.3.1. The effect of the gain medium and of the active modulator on the pulse are evaluated and a self consistent solution is sort i.e one where there is no net change in the pulse after one roundtrip. The analysis has proven to be quite accurate in predicting the performance of homogeneously broadened modelocked lasers, also it provides a useful insight into the modelocking process.

The analysis considers the propagation of a general Guassian pulse given by

$$E(t) = \tfrac{1}{2} E_0 \exp(-\alpha t^2) \exp[j(\omega_p t + \beta t^2)] \qquad 3.3.8$$

Here α describes the Guassian envelope of the pulse and ω_p is the carrier frequency. A non-zero value of β means that the pulse has a linear frequency chirp on it, the sign of β determines whether the leading edge of the pulse is downshifted in frequency or upshifted as shown in fig 3.3.2.

FIG 3.3.1 THE PROGRESS OF THE ELECTRIC FIELD IN A MODE-LOCKED LASER

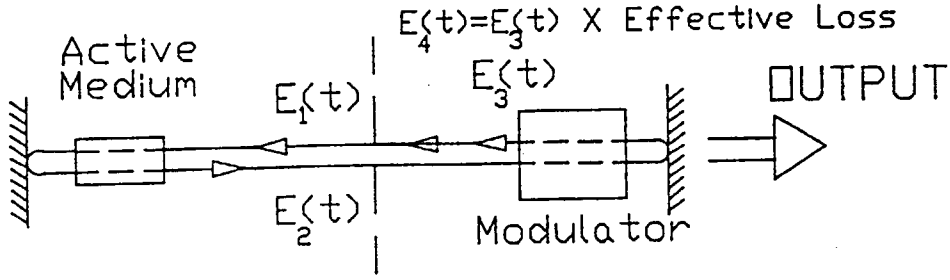

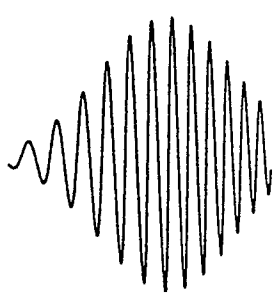

Positive Frequency chirp

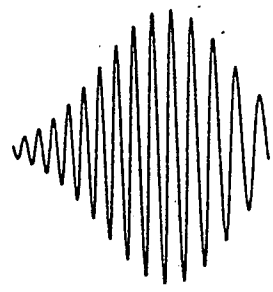

Negative frequency chirp

FREQUENCY CHIRPED GUASSIANS

FIG 3.3.2

The Fourier transform of this pulse is given by

$$E(\omega) = (E_0/2).(\pi/(\alpha - j\beta))^{\frac{1}{2}} \exp[-(\omega - \omega_p)^2/4(\alpha - j\beta)] \qquad 3.3.9$$

The pulse duration which is defined by the half-intensity point is given by

$$\tau_p = \sqrt{(2\ell n2/\alpha)} \qquad 3.3.10$$

The bandwidth of a Guassian pulse is defined as the half power point of the pulse spectrum and is given by

$$\Delta f_p = (1/\pi)\,[(2\ell n2)\,(\alpha^2 + \beta^2)/\alpha]^{\frac{1}{2}} \qquad 3.3.11$$

Combining these two equations the time-bandwidth product of the Guassian pulse can be calculated and is given by

$$\tau_p.\Delta f_p = (2\ell n2/\pi)\,\sqrt{[1 + (\beta/\alpha)^2]} \qquad 3.3.12$$

This equation shows that a bandwidth limited Guassian pulse will have a time-bandwidth product of 0.44, a time-bandwidth larger than this implies that there is a frequency chirp on the pulse.

In their analysis Kuizenga and Siegman show that the gain of the active medium can be approximated by a Guassian lineshape when the pulse bandwidth is much smaller than the linewidth of the gain. This approximation allows a self consistent solution to be sought as a Guassian pulse passing through an active medium with a Guassain lineshape will remain a Guassian. An important factor in the process of FM modelocking is the dispersion of the atomic propagation constant, β_{AT}, which should be added to the host dispersion to fully describe a complex wave propagating through an active medium. The atomic propagation constant is determined by the real part of the atomic susceptibility, $\chi(\upsilon)$[Yariv: 1985], this in turn is determined by the population inversion in the active medium. The atomic propagation constant becomes significant around the atomic line centre ,υ_0, around this frequency the total dispersion is dominated by the atomic dispersion. It has been shown that the atomic dispersion can be written as [Phillips: Thesis 1989]

$$\beta_{AT}(\upsilon) = [\Delta\upsilon_a\gamma_0/4].(\upsilon - \upsilon_0)/[(\upsilon - \upsilon_0)^2 + (\Delta\upsilon_a/2)^2] \qquad 3.3.13$$

where γ_0 is the peak gain of a Lorentzian lineshape with a bandwidth of $\Delta\upsilon_a$. In fig 3.3.3 a plot of the atomic group velocity dispersion (GVD) is shown, this is given by $\delta\beta^2{}_{AT}/\delta\upsilon^2$.

FIG 3.3.3

THE ATOMIC DISPERSION

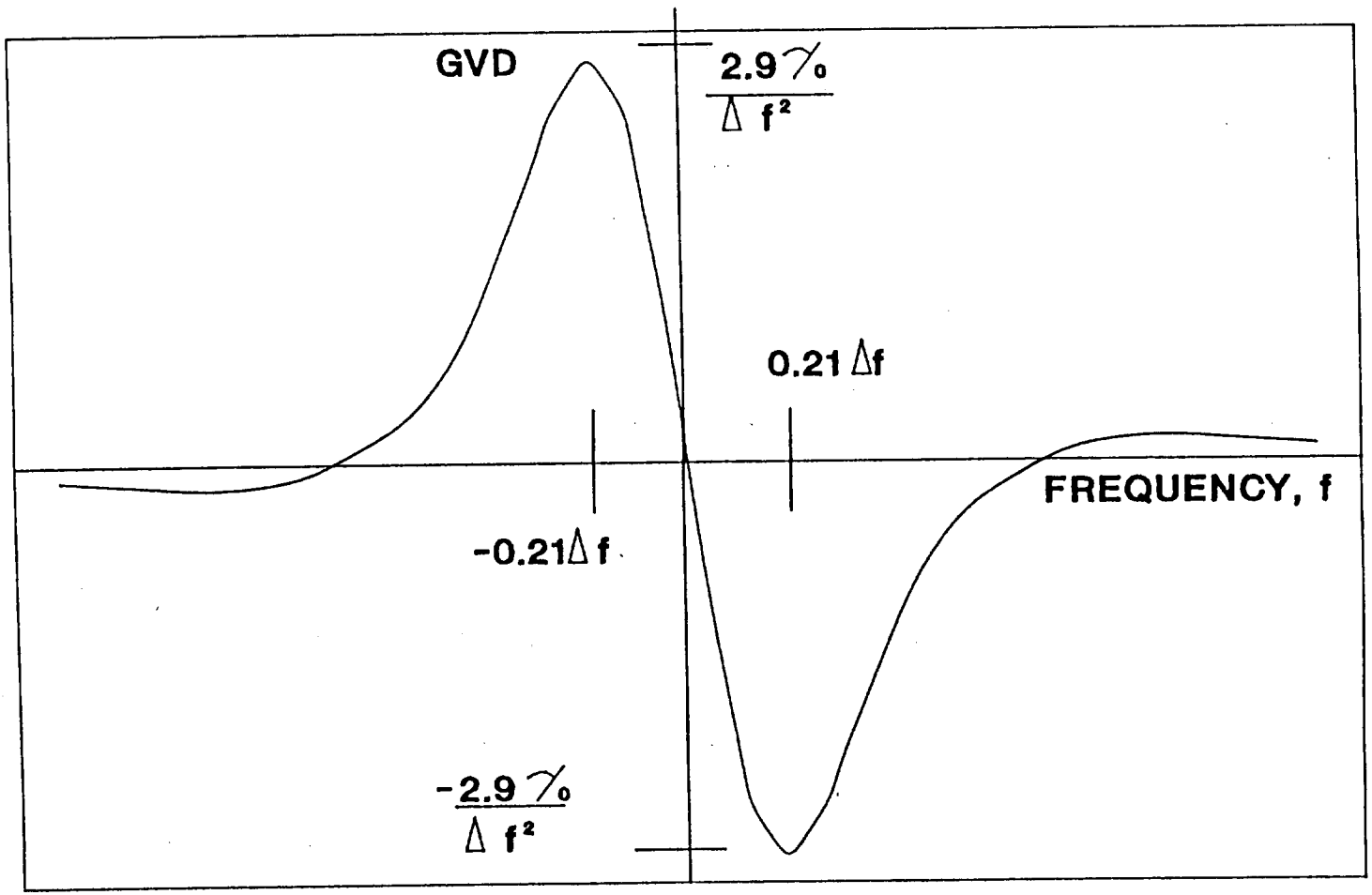

The graph shows that off line centre dispersion rapidly increases, this is of significance for the FM modelocked laser where the phase modulator can take a pulse off linecenter.

3.3.5 AM Modelocking

To derive an expression for τ_p and Δf_p Kuizenga and Siegman apply the self consistency requirement that

$$E_1(t - T_m)e^{-j\phi} = E_4(t) \qquad 3.3.14$$

here ϕ allows for a possible phase shift, T_m is the total round trip time and E_1 and E_4 are defined in fig 3.3.1. E_4 is equated by consideration of the modification to a Guassian pulse through each of the intra-cavity components. The pulse and bandwidth for an AM modelocked laser are then predicted to be

$$\tau_p = (\sqrt{2}\ell n2)^{\frac{1}{2}}/\pi\ (g_0/\delta_t)^{\frac{1}{2}}\ (1/f_m\Delta f)^{\frac{1}{2}} \qquad 3.3.15$$

$$\Delta f_p = (2\sqrt{2}\ell n2)^{\frac{1}{2}}\ (\delta_t/g_0)^{\frac{1}{2}}\ (f_m\Delta f)^{\frac{1}{2}} \qquad 3.3.16$$

where f_m is the frequency of modulation, θ_m is the modulation index, and Δf is the atomic linewidth. The round trip gain in the cavity is described by g_0 and can be approximated by

$$g_0 = \tfrac{1}{2}\ell n(1/R) \qquad 3.3.17$$

where R is an effective reflectivity that accounts for the total round trip loss. The equations predict that for an ideally AM modelocked laser the time-bandwidth product is 0.44 which implies that a bandwidth limited Guassian pulse will be produced. The simple interpretation that can be given to the AM modelocking process is of an equilibrium being established between the pulse shortening due to the amplitude modulator and the pulse broadening of the active medium.

3.3.6 The Self Consistent Theory For FM modelocked lasers

The self-consistent theory for FM modelocked lasers follows a very similar analysis to that for the AM case but with the response of a phase modulator replacing that of an amplitude modulator. For the case where the pulse passes through the phase modulator at the extremes of its phase modulation i.e when the pulse remains on the gain mediums line centre, the pulse duration and bandwidth are predicted to be

$$\tau_p = (2\sqrt{2}\ell n2)^{\frac{1}{2}}/\pi\ (g_0/\delta_c)^{\frac{1}{2}}\ (1/f_m\Delta f)^{\frac{1}{2}} \qquad 3.3.18$$

$$\Delta f_p = (2\sqrt{2}\ell n2)^{\frac{1}{2}}\ (\delta_c/g_c)^{\frac{1}{2}}\ (f_m\Delta f)^{\frac{1}{2}} \qquad 3.3.19$$

where δ_c gives the phase retardation of the phase modulator. The time-bandwidth product for this case is 0.626, the pulses are formed with a linear frequency chirp equal to the spectral width of the pulse which is imparted by the phase modulator. The exact frequency of modulation is given by

$$f_{mo} = [1/(2L/c + 2g_0/\Delta\omega \pm 2\delta_c\lambda/\pi c)] \qquad 3.3.20$$

The second term in this equation allows for the delay of the pulse in passing through the gain medium. The third term shows that there are two possible frequencies of modulation corresponding to the two extremes of the phase retardation, these two frequencies correspond to the positive and negative modes. The equations predict that the pulses will be identicle in pulse duration and bandwidth but will be separated by a small frequency, $(4\delta_c\lambda/\pi c)\, f_{mo}^2$ Hz, and will have frequency chirps of equal magnitude but opposite signs. The positive mode having a positive frequency chirp, likewise the negative mode a negative chirp. The picture that emerges from this analysis of FM modelocking is of an equilibrium being formed between the spectral broadening of the phase modulator and the spectral narrowing of the gain medium.

3.3.7 FM Modelocking In The Case Of Detuning

The behaviour of the FM modelocked laser is significantly changed when the frequency of modulation is changed from that of the ideal frequency given in equation 3.3.20, detuning is defined as the frequency shift away from f_{mo}. When detuned the pulse experiences a Doppler shift each time they pass through the phase modulator. The optical frequency of the pulses is shifted until some equilibrium is reached when the Doppler shift of the modulator is cancelled out by an equal and opposite frequency shift from the gain medium. With the pulse off line-centre the atomic dispersion will become significant as shown in fig 3.3.3. When a linearly frequency chirped pulse is passed through a dispersive medium the pulse can be compressed if the chirp and the GVD have opposite signs. This is the case when the frequency is slightly negatively detuned, the situation for a positively chirped pulse is shown in fig 3.3.4. In the case of the positive mode slight negative detuning puts the pulse in the negative GVD region implying that low frequencies travel with a lower group velocity than high frequencies hence the positively chirped pulse is compressed, the optimum pulse duration is obtained when the pulse has been dechirped so $\beta = 0$. Exactly the same process happens for the negative mode but the chirp and GVD are in the opposite sense. In the context of this theory the positive and negative modes both have a minimum at the same detuning but at different frequencies given by equation 3.3.20. Kuizenga and Siegman show that the pulse durations and bandwidth are governed by the following equations

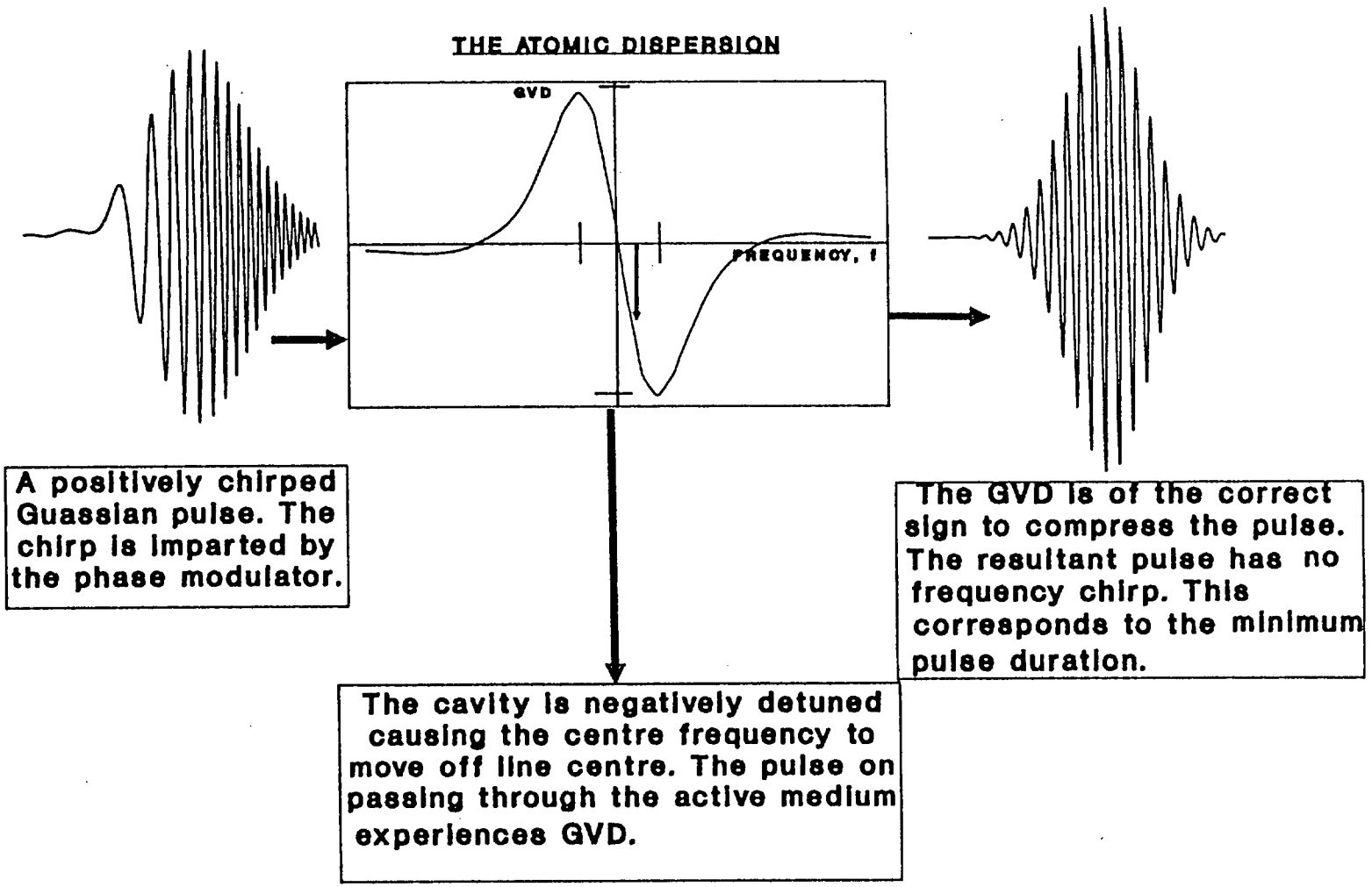

FIG 3.3.4 THE FM MODELOCKING PROCESS

$$\tau_p = \frac{(2\ell n2)^{\frac{1}{2}}}{\pi} \cdot \left[\frac{g}{\delta\cos\theta}\right]^{\frac{1}{2}} \cdot \left[\frac{1}{1+4\eta^2}\right]^{3/8} \cdot \left[\frac{1}{f_m \Delta f \cos\psi}\right]^{\frac{1}{2}} \quad 3.3.21$$

$$\Delta f_p = (2\ell n2)^{\frac{1}{2}} \cdot \left[\frac{\delta_c \cos\theta}{g}\right]^{\frac{1}{2}} \cdot (1+4\eta^2)^{3/8} \cdot \left[\frac{f_m \Delta f}{\cos\psi}\right]^{\frac{1}{2}} \quad 3.3.22$$

the time-bandwidth product is now

$$\tau_p . \Delta f_p = 2\ell n2/\pi \cos\psi \quad 3.3.23$$

$$\psi = \pm \pi/4 + 3/2 \tan^{-1}(2\eta) \quad 3.3.24$$

$$\eta = \upsilon/\Delta\omega \quad 3.3.25$$

where η describes the shift of the pulse centre frequency, ω_p, normalised to the atomic linewidth $\Delta\omega$ and γ describes the phase angle of the pulse to the extreme of the phase retardation.

When the laser is positively detuned the dispersion of the gain medium broadens the pulses. Large detunings in either direction causes the modelocking process to breakdown as the active medium cannot counteract the frequency shift imparted by the phase modulator. The laser can then operate in an FM laser mode where the frequency spectrum is modulated at repetition rate of the modulator.

Section 3.4.1: The Amplitude Modulator

The Kuizenga and Siegman theory described in section 3.3 has shown the dependence of the pulse duration on the modulation index θ_m and the modulation frequency f_m. To produce short pulses an ideal amplitude modulator should have as high a modulation index as possible without adversely affecting the modulation index. In arriving at the final arrangement for the AM modelocked laser a wide range of modulators were tried. Typically these had fundamental resonant frequencies at around 40 MHz corresponding to a modulation frequency of 80 MHz, these modulators are typical of those used to modelock argon ion lasers and Nd:YAG lasers. The inherent problem with these modulators is that they do not provide a significantly large diffraction efficiency at 1.3 μm to stably modelock the laser. Typically the modulators had a θ_m of approximately 0.4 which when inserted into equation 3.3.15 with typical parameters of the laser predicts a pulse duration of the order of around 100 psec. In practice using these modulators pulsewidths of this duration were obtained. Improvement upon the pulse duration at this frequency required increasing the modulation depth, θ_m, by increasing

the rf power to the modulator . This has the tendency to cause heating in the crystal and as the devices have a high Q factor, the modulator drifts off its resonant frequency with a loss of diffraction efficiency. To overcome this problem a feedback arrangement as shown in fig 3.4.1 was used [Klen et al: 1981]. This system uses small changes in the applied rf power to slightly change the amount that the crystal is heated which keeps the modulator at resonance. The resonance is detected by monitoring the reflected rf power. This was used in conjunction with a temperature control unit on the modulator. A marginal improvement in the pulse duration was achieved but large improvements could not be obtained mainly due to the limitation of the method as $\tau_p \propto 1/P^{\frac{1}{4}}$ (θ_m is proportional to $P^{\frac{1}{4}}$).

Operation of the modulators at their third harmonic has proven to be a successful method of improving the pulse duration [Maker et al: 1988]. The loss in the modulation index is compensated for by the modulation frequency being increased by a factor of 3, it also has the advantage of making the laser more compact. When this method was tried with a 1.3 μm laser diode pumped system stable modelocking was only achieved when the bandwidth was limited using an intra-cavity etalon, with this system pulses of 140 psec were obtained. The very low diffraction efficiency at this frequency (< 4%) meant that excess bandwidth in the laser caused instability, hence there was the need for an etalon.

The modulator that successfully AM modelocked the laser was a custom made amplitude modulator made by ISLE Optics. The modulator was made out of high quality fused silica glass and was in the form of a Brewster angled prism so that the crystal would supply the necessary dispersion to select between the 1.318 μm and 1.338 μm transitions. The modulator was 2.5 cm in length with a fundamental resonance centred at 120 MHz. A cw laser beam at 1.3 μm was passed through the modulator and the average power of the zero-order beam was monitored with a large area photodiode. Using this method it was found that a diffraction efficiency of 8% could be obtained with this modelocker at a drive frequency of 120.3 MHz and an applied rf power of 2 W (the rf signal was supplied by a Marconi 2022A frequency synthesizer and a Wessex Electronics RC601-5 power amplifier). The modulator had a low enough Q so that it stayed on resonance without the need for feedback electronics or temperature control.

3.4.2 AM Modelocking Results

The final cavity configuration for the AM mode locked laser is shown in fig 3.2.1. The modulator was placed on a mount that allowed tilt and translation of the modulator to maximise the diffraction efficiency through optimisation of the Bragg angle and adjustment of the laser mode relative to the sweet spot of the modulator. The modulator was placed as close as possible to the output coupler to maximise the modulation. The laser was operated with an output coupling of 7%. The substrate of the mirror had a 10° wedge so as to prevent feedback into the laser and to remove any possibilities of etalon effects. It was found that a wedge of 2° or over was needed to prevent feedback into the

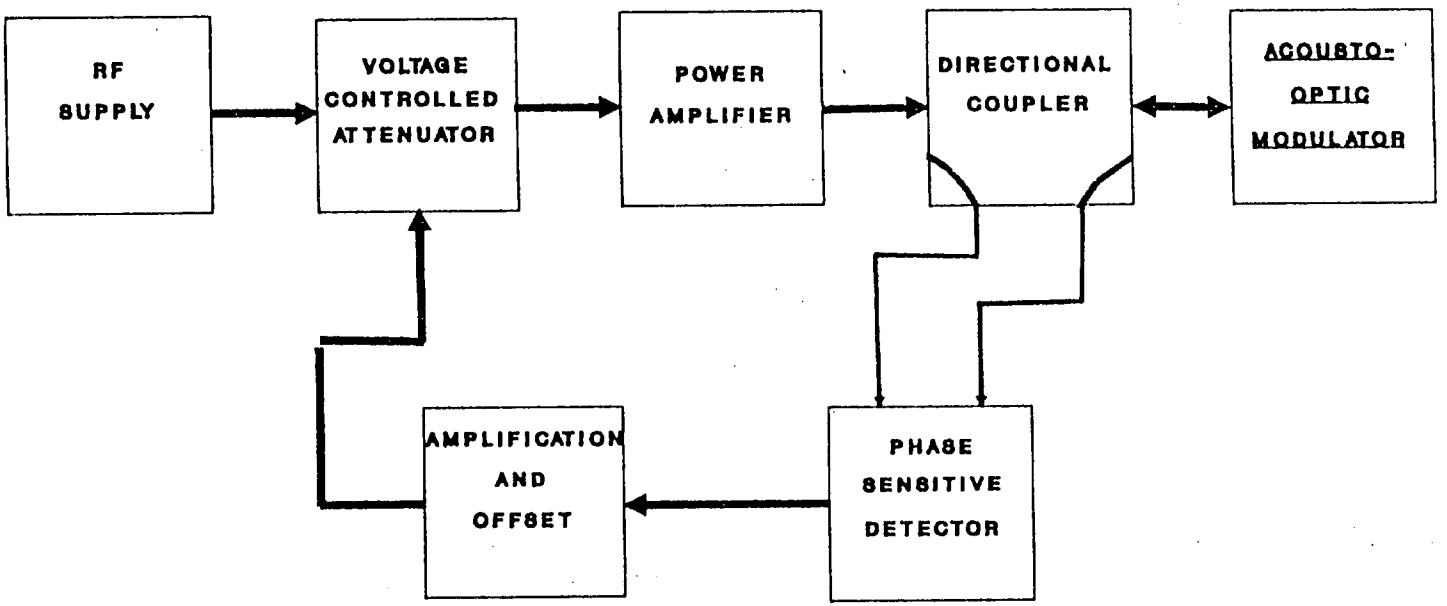

FIG 3.4.1

ACTIVE FEEDBACK TO STABALISE AM MODELOCKING

laser causing instability in the modelocking process. The overall cavity length was 62.5 cm to match the modulation frequency of 240 MHz.

The modelocked pulses from the laser were optimised by the use of a sampling oscilloscope and a fast photodiode, the output from the rear folding mirror was utilised. The other output from the rear mirror was passed through a plane-plane Fabry-Perot interferometer to simultaneously measure the bandwidth of the laser. An accurate measurement of the pulse duration from the laser was taken by using a second order background free autocorrelation technique. The autocorrelator used a $LiIO_3$ crystal as the second harmonic crystal.

It was found that the pulses generated were very sensitive to the adjustment of the Bragg angle and cavity length. By careful adjustment of these parameters, stable modelocking was achieved. A typical second order background free autocorrelation of the pulses is shown in fig 3.4.2. The full width half maximum (FWHM) of the autocorrelation was measured to be 65 psec. The autocorrelaton closely approximated that of a Guassian pulse. Applying the correction factor for an autocorrelation of a Guassian pulse gives the pulse duration to be 46 psec. The corresponding bandwidth was measured to be 9 GHz, giving a time bandwidth product of .42. This is in close agrement to the bandwidth limit for Guassian pulse of 0.44, implying that there is no excess bandwidth in the pulses.

The value of 46 psec pulse duration can be compared with the value predicted by the Kuizenga and Siegman theory for τ_p given in equation 3.3.15. The relevant parameters for the laser system are $\theta_m = 0.4$, $f_m = 240$ MHz, $\Delta f = 180$ GHz. Equation 3.3.17 can be used to obtain an approximate value for the gain in the cavity which for an output coupling of 7% and including other intra-cavity losses is $g \approx 0.065$. Using these parameters theory predicts a pulse duration of 45 psec which is in good agreement with the measured pulse duration.

3.4.3 Output Power From The Modelocked Laser

The laser always operated on the TEM_{00} mode and on the 1.318 μm transition as was found with the cw operation of the laser. The output power of the laser, when pumped with a 1W laser diode and optimally mode locked was 5.5 mW, with an incident threshold of 680 mW corresponding to a slope efficiency of 4.3%. The energy in a single modelocked pulse is equal to 23 pJ which corresponds to a peak power of 0.46 W. This represents a drop in the efficiency of the laser and a rise in threshold in comparison to the cw system. The Kuizenga and Siegman theory predicts that for an ideal modelocked laser there will be no drop in output power when the laser is optimally modelocked in comparison to the free-running laser. In practice there are small intra-cavity etalon effects which for the free-running laser cause axial mode selection to optimise the output power, for this reason the loss in a modelocked system will be greater than for a free-running laser. This effect is more pronounced when the laser is operating close to threshold and when θ_m is small. It was found that when optimally modelocked the laser output power was at its peak. It is likely that the modulator is lossy when operating at

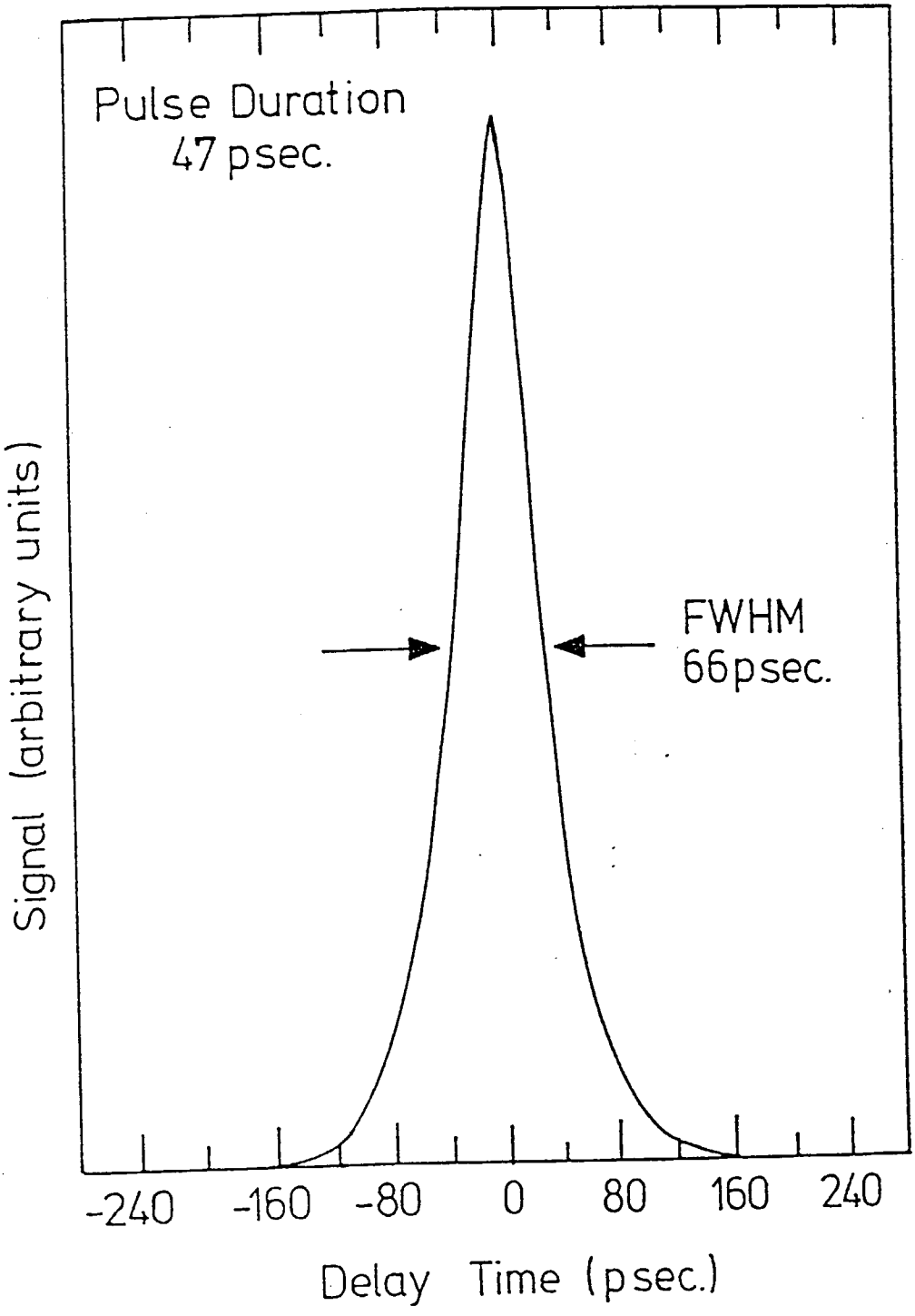

FIG 3.4.2 AN AUTOCORRELATION OF A TYPICAL AM MODELOCKED PULSE

high diffraction efficiencies. Detuning of the laser results in a rapid drop in output power due to the additional loss of the modulator.

3.4.4 Discussion of AM Modelocking

The performance of the laser diode pumped modelocked Nd:YAG laser operating at 1.3 μm compares favourably with the larger flashlamped pumped systems operating at 1.3 μm. The best pulse duration previously reported from a 1.3 μm system was 53 psec [Keller et al: 1988], this system used harmonic modelocking to increase the modulation frequency and hence reduce the pulse duration.

The pulse duration obtained from a similar system operating at 1.06 μm [Maker et al: 1988] was 55 psec, the slightly larger pulse duration can be explained by the larger linewidth of the 1.3 μm to the 1.06 μm transition (180GHz cf 120GHz). The near bandwidth limited pulses produced by both lasers were in close agreement with the pulse durations predicted by the Kuizenga and Siegman theory. The reason for the better performance of these lasers over flashlamp pumped systems can be attributed to the higher modulation frequencies used and the improved stability of the diode pumped system.

Pulse shortening of AM modelocked flashlamp pumped systems has been achieved by the use of intra-cavity etalons [Graener et al: 1981]. The broadening of the lasing bandwidth allowed pulses as short as 12 psec to be produced. The pulses from high powered systems have been further shortened by the use of fibre/grating compressors [Gomes et al: 1988]. These systems are capable of producing 1.5 psec pulses at 1.06 μm and 33 fsec pulses at 1.3 μm, but reduce the average power from the laser and require elaborate alignment.

The most efficient way of shortening the pulses from an AM modelocked system is to increase the modulation frequency or the modulation index, both of these parameters have an inverse to the power of a half dependence. The depth of modulation is proportional to the square root of the power applied to the modulator implying that τ_p is proportional to $P^{\frac{1}{2}}$. Increasing the power to the modulator will produce a modest shortening of the pulse duration and the maximum amount of power that can be applied to the modulator is limited by thermal problems unless water cooling is used. Increasing of the modulation frequency is the easiest way of producing shorter pulses. Typically fused silica is used as the substrate for acousto-optic devices offering low insertion loss and high acousto-optic efficiencies up to drive frequencies of ~150 MHz. At higher frequencies than this fused silica has a high acoustic attenuation rate which limits its performance. This problem can be overcome by using other materials for the modulators substrate. Keller et al [1990] have overcome this problem by the use of sapphire as the substrate. The modulator they built had a repetition rate of 500 MHz and was used to AM modelock a laser diode pumped Nd:YLF laser. They report 10 psec pulses from this system. It would be expected that using such a modulator on a Nd:YAG laser would result in modelocked pulses of a similar duration.

Section 3.5.1: The Phase Modulator

The phase modulation of light can be achieved by making use of the electrooptic effect. The electrooptic effect occurs in crystals that do not have inversion symmetry. The effect describes the change in the indices of the ordinary and extraordinary rays that is caused by and is proportional to an applied electric field. Depending upon the exact arrangement of the interaction, devices using this effect can be used as variable wave plates for beam deflection, and as amplitude and phase modulators. Lithium niobate ($LiNbO_3$) was used in the experiment for the phase modulator. $LiNbO_3$ offers a relatively high electrooptic coefficient, it is not hydroscopic and can be grown and polished to good optical quality with little absorption at the lasing wavelength (1.3 μm). The crystal has the drawback that its optical quality can be impaired when exposed to modest powers of visible light due to the photorefractive effect [Ashkin: 1966].

The $LiNbO_3$ crystal was a Brewster angled device of length 25 mm with an aperture of 6mm X 6mm. The electric field was applied transverse to the modulator so as to make use of the r_{33} electrooptic coefficient as shown in fig 3.5.1. Gold coatings were evaporated on to the $LiNbO_3$ so that good electrical contact could be made to the crystal. To maximise the electric field on the crystal, the crystal was used in a LC parallel resonant circuit as shown in fig 3.5.2, the modulator itself was used to form the capacitance. This method is one that has been used by Bramwell [1988] and Phillips et al [1989] to FM modelock dye lasers and Nd doped fibre lasers. Silver paint was used to make a good electrical contact between the brass housing for the crystal and the gold coatings. The resonant frequency of a simple LC circuit is given by

$$f_0 = 1/2\pi.\ 1/(LC)^{\frac{1}{2}} \qquad 3.5.1$$

The capacitance formed by the crystal is of the order of a few pF, making it important to reduce any stray capacitance due to connections and the wire in the LC circuit. The small inductance required (10's of mH) to form resonances of a few hundred MHz was formed by using a few turns of wire. This was attached to the brass housing so that it was close to the capacitance of the crystal, thus minimising stray capacitance and inductance. The resonant frequency of the circuit was finely tuned by measuring the resonant frequency with a grid dip meter. The resonant frequency could be changed by adjusting the windings of the inductor. Power was applied to the circuit by way of a search coil which was interleaved with the inductor so as to achieve maximum coupling. The source of the rf power was a Marconi signal generator and a Wessex electronics rf amplifier. The LC circuit was chosen to have a resonance at 295 MHz with a bandwidth of about 3 MHz.

The single pass phase retardation of the modulator was estimated by the use of a single frequency Helium-Neon laser and a confocal Fabry-Perot interferometer, the arrangement is shown in fig 3.5.3. A single frequency source when passing through a

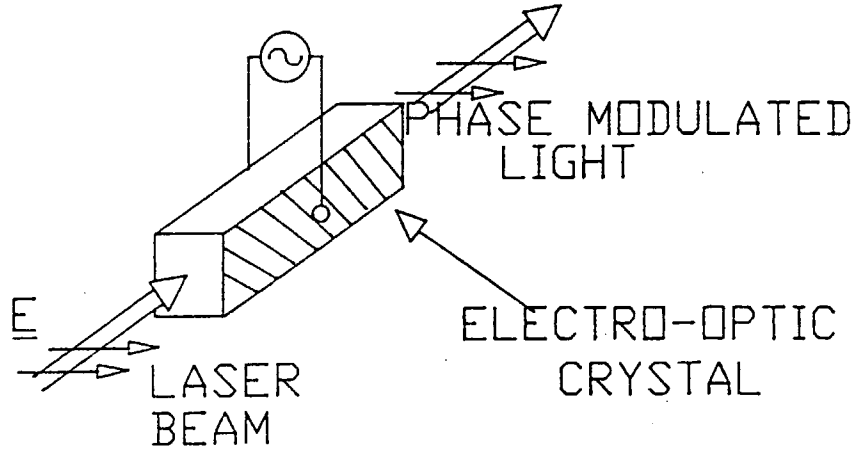

FIG 3.5.1 THE PHASE MODULATION OF LIGHT

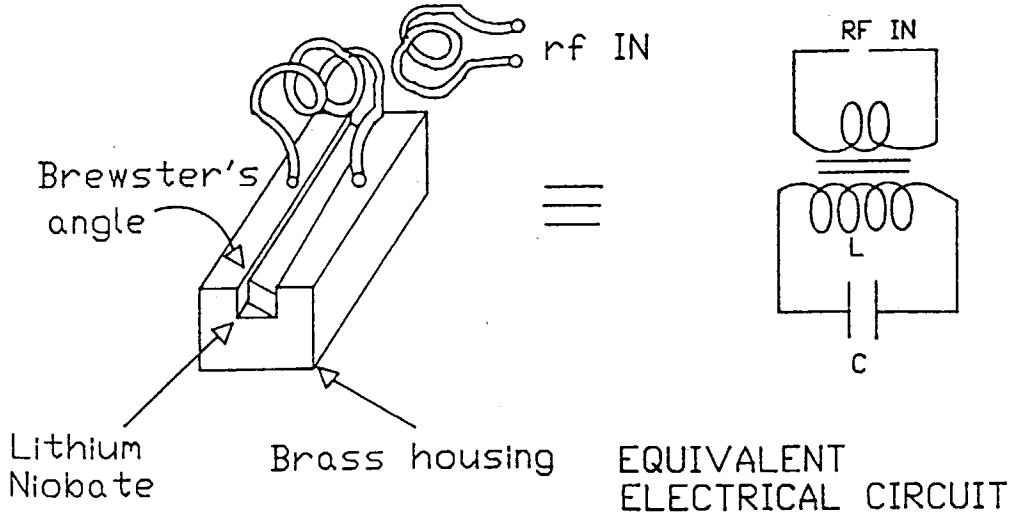

FIG 3.5.2 THE PHASE MODULATOR

phase modulator with a sinusoidal drive signal is transmitted with an infinite set of Bessel function amplitude sidebands as described in 3.5.2.

$$E_{out}(t) = E_0 \sum_n J_n(\delta_f) \exp[i(\omega_0 + n\omega_m)t] \qquad 3.5.2$$

this implies that

$$J_0^2(\delta)/J_n^2(\delta) = I_c/I_n \qquad 3.5.3$$

where $J_n(\delta)$ is the Bessel function of the n^{th} sideband. J_0 refers to the carrier frequency, I_c the carrier frequency intensity. The modulator was estimated to have a phase retardation of 1 radian at 295.3 MHz for 1W of applied power.

3.5.2 The FM Modelocked Laser

The cavity configuration for the FM modelocked laser is shown in fig 3.5.4. This arrangement is similar to the cavity used for the AM modelocked laser except that the cavity now includes an intra-cavity prism made of high optical quality fused silica. The overall length of the cavity has changed to match the phase modulators resonant frequency of 295 MHz. The phase modulator was placed as close as possible to the output coupler so as to maximise the phase retardation.

It was found that the best FM modelocked pulse duration was obtained when using a 0.5% output coupling. In this case the laser had an incident threshold of 320 mW and a maximum power output of 15 mW, this corresponds to a slope efficiency of 3.2%. Maximum power from the laser was achieved with a 2% output coupling. The laser had an incident threshold of 420 mW and a maximum power output of 35 mW at 1.318 μm and with a TEM_{00} profile. This corresponds to a slope efficiency of 9.2 %. The insertion loss of the prism and the $LiNbO_3$ was calculated to be 1% and 0.5% single pass respectively.

3.5.3 FM Modelocked Performance

The performance of the FM modelocked laser was monitored using similar diagnostics as those used in the AM modelocking experiment (Section 3.4.2). The phase modulator was driven at 295.3 MHz with an applied power of 1W. The cavity length was matched to the drive frequency by way of a precision translator and by finetuning of the drive frequency to the modulator. It was found that two different set of stable pulses existed which could be selected by a small change in the cavity length of the order of 20 kHz. These two pulse sets correspond to the extreme of the phase retardation of the phase modulator. It was evident by viewing of the pulses on the fast oscilloscope, that one set of pulses was significantly shorter, this was later confirmed when autocorrelating, the longer pulses having a pulse duration of about 70 psec. The pulse duration was measured using a standard second order background free autocorrelation technique. It was found

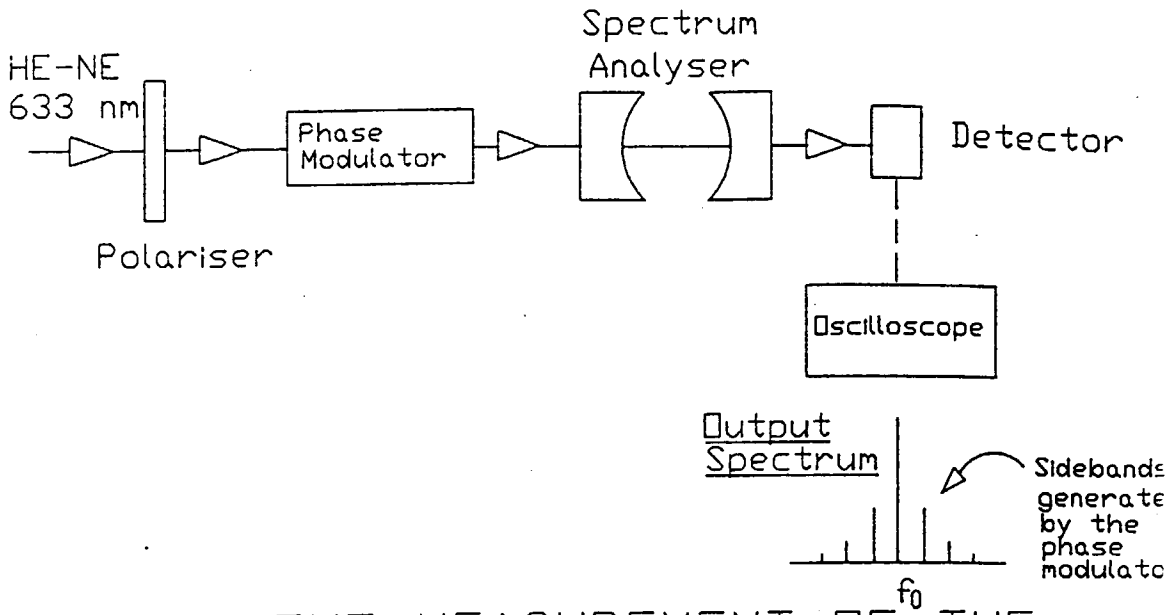

FIG 3.5.3 THE MEASUREMENT OF THE SINGLE PASS PHASE RETARDATION

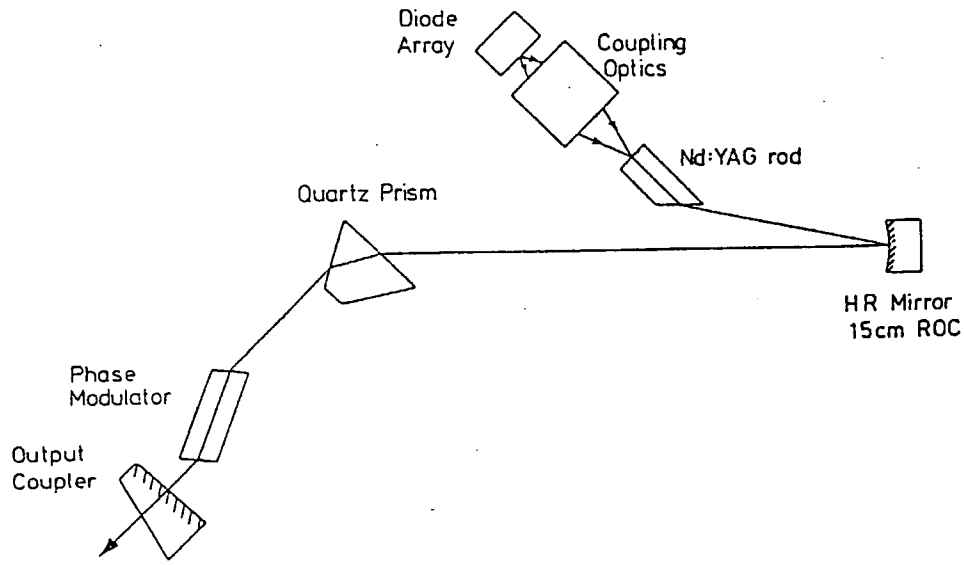

FIG 3.5.4

SCHEMATIC DIAGRAM OF THE FM MODELOCKED CAVITY

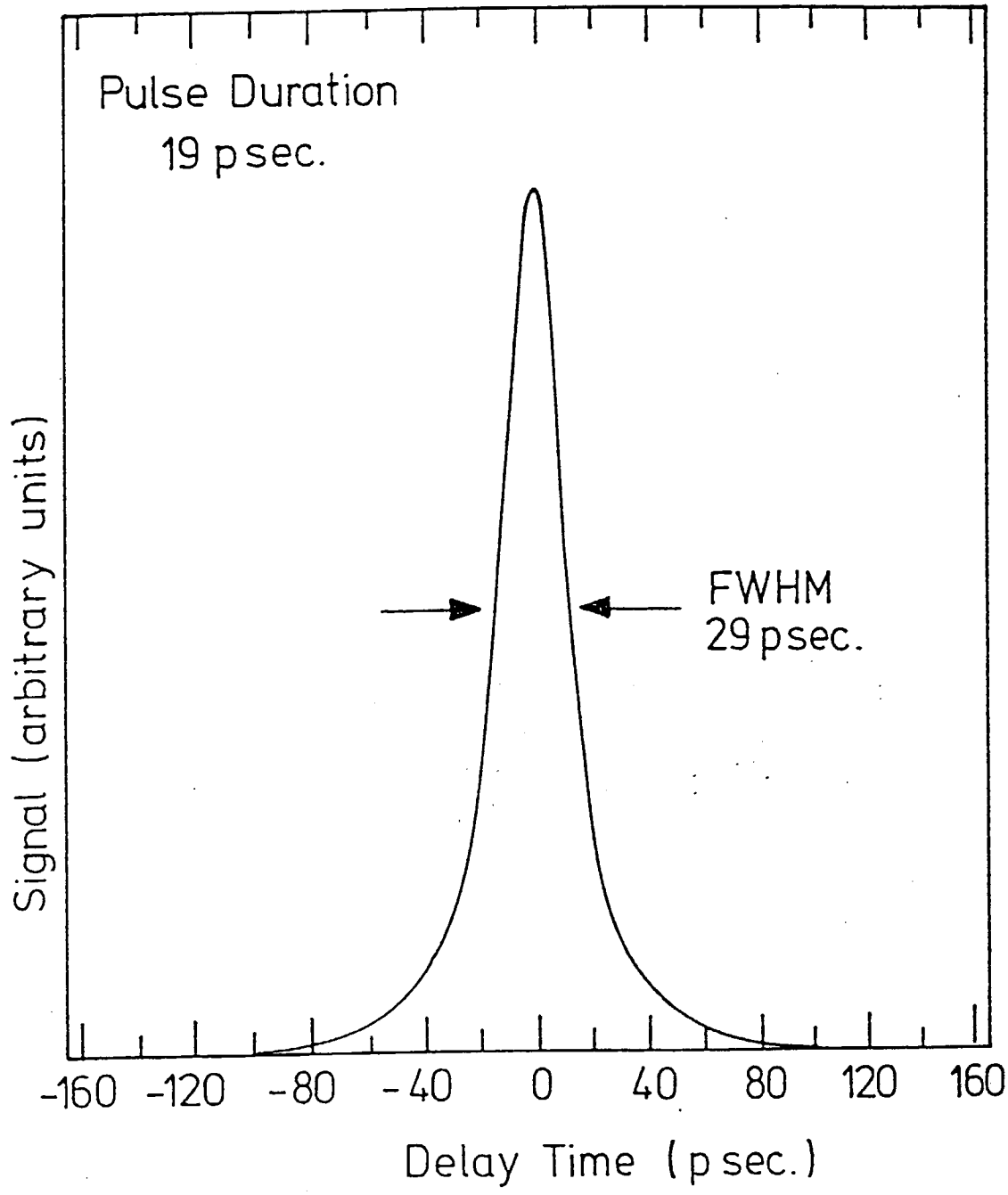

FIG 3.5.5 A TYPICAL AUTOCORRELATION OF A FM MODELOCKED PULSE

that the most stable and shortest pulses were obtained when an output coupling of 0.5% was used. In fig 3.5.5 a typical background free autocorrelation of the modelocked pulses is shown. The pulse shape of the autocorrelation was checked by digitising the autocorrelation using a Thurbly DSA 524 digital storage scope and then down loading this to an IBM computer. A curve fitting routine then compared the waveform with common pulse shapes, the autocorrelation was found to best fit a sech pulse shape. The FWHM of the autocorrelation was 29 psec so the actual pulse duration was 19 psec. The pulse duration obtained was found to be insensitive to both the power applied to the modulator and to the position of the laser mode through the modulator. Owing to the very short pulse durations and the existence of two closely spaced set of modelocked pulses, the quality of the modelocking was sensitive to any small changes in the cavity length making good vibration isolation of the experiment essential.

The bandwidth of the laser was simultaneously measured using a plane-plane Fabry Perot interferometer with a 100 GHz free spectral range. As found with the AM modelocked laser the free running bandwidth was found to be much larger than expected due to the effect of the Brewster angled rod causing mode selection. The free running bandwidth of the laser was about 37 GHz and when optimally modelocked the bandwidth reduced to 35 GHz. The average power of the laser, using a 0.5% output coupling, dropped from 15 mW to 13 mW when optimally modelocked. There was no detectable difference between the average power of the two modelocked pulses. This corresponds to an energy per pulse of 44 pJ implying that there is a peak power of 2.2 W in a modelocked pulse. Maximum energy and peak power were obtained when using a 2% output coupling. The output when optimally modelocked was 31 mW corresponding to an energy per pulse of 105 pJ. The pulse duration changed to 22 psec due to the change in output coupling so the peak power in a pulse is 4.8 W.

3.5.4 Comparison With The Kuizenga And Siegman Theory

The parameters of the system can be applied to the Kuizenga and Siegman theory. To do this equation 3.3.21 should be used which predicts the FM modelocked pulse duration when the laser cavity is detuned. In estimating the pulse duration using these equations a value of $\eta = \pm 0.288$ should be used which corresponds to the condition when the frequency chirp on the pulse due to the phase modulator is compressed by the anomalous dispersion of the gain medium. The other necessary laser parameters are $g = 0.04$, $\cos\theta \sim 1$, $\cos\Psi \rightarrow 1$, $f_m = 295.3$ MHz and $\Delta f = 180$ GHz. Applying these values equation 3.3.21 gives the pulse duration as 21 psec. This pulse duration is in good agreement with the experimental pulse duration of 19 psec.

The time-bandwidth product for the modelocked laser is 0.66 which is 2X bandwidth limited for a sech pulse shape. Neither the time-bandwidth product or the pulse shape are in agreement with the Kuizenga and Siegman theory. The active modulator does not appear to be having much effect on the bandwidth of the laser, the free running bandwidth of the laser was 37 GHz compared to the FM modelocked

bandwidth of 35 GHz. The large free running bandwidth of the laser could explain the large time bandwidth product as the modulator does not appear to be the dominant factor in determining the modelocked bandwidth which is assumed in theory.

The spatial hole burning which is found in this laser system also effects the FM operation of the laser. When the laser was sufficiently detuned FM operation of the laser took place with a bandwidth as large as 65 GHz being excited. A recent study by Adams et al [1990] has shown that ideal FM operation of a longitudinally pumped laser is only achieved when the Nd:YAG laser is operated in a uni-directional configuration, eliminating any spatial hole burning effects. The free running laser runs on a single longitudinal mode with a narrow linewidth but when used in the FM laser mode a bandwidth of 120 GHz can be obtained, which is close to the fall linewidth of the 1.06 μm transition. It can be concluded that to fully describe the standing wave laser the Kuizenga and Siegman theory would need to be modified to allow for the effect of the spatial hole burning.

3.5.5 Discussion Of FM Modelocking

The FM technique of modelocking a laser has proven to be a superior technique to that of AM modelocking. The pulses from the FM modelocked systems are shorter, more stable, less sensitive to the modulators efficiency and position, and causes a smaller drop in output power when optimally modelocked. The Kuizenga and Siegman theory has shown that for both the AM and FM modelocking techniques that the controlling of the modulation frequency is the most efficient way of shortening the pulse duration. Repetition rates of three to four hundred MHz are easily obtainable when building phase modulators without any serious loss in phase retardation, whilst repetition rates of this order of magnitude are difficult to obtain in common amplitude modulators without a serious degradation in efficiency. The use of even higher modulation frequencies in the case of FM modelocking should shorten the pulse duration even further but a possible limiting factor will be the length of the phase modulator crystal which for picosecond pulses will start to limit the bandwidth [Harris et al: 1969]

FM modelocking has proven to be a successful way of modelocking other laser systems. Maker et al have used the FM modelocking technique to obtain 9 psec pulses from a laser diode pumped Nd:YLF system [Maker et al: 1989 Aug] and 12 psec from a similar Nd:YAG system operating at 1.06 μm [Maker et al: 1989]. For both these systems the pulse duration was about twice as short as that predicted by theory. This anomaly has also been found by Phillips [Thesis:1989] in the modelocking of Nd: fibre lasers. The authors have attributed this to the non-linear index of the active medium, which through self phase modulation (SPM, see section 4.6) causes a chirping of the pulse. The effect of SPM can be allowed for in the self-consistent theory by a modification of the modulation index, adding to the complex portion of the modulation index [Krausz et al: 1989]. The physical explanation for this is that the frequency chirp imparted by the central portion of the pulse will in the FM modelocked laser either enhance or partially compensate for

the chirp imposed by the modulator. For the 1.3 μm system the pulse durations obtained agreed well with theory. The pulse durations were measured at various pump powers, which varied the intra-cavity power, but no significant change in the pulse duration was observed.

Section 3.6.1: Simultaneous Q-Switching And Modelocking Of The Laser

Many laser applications involve the study of non-linear effects in crystals and optical fibre. Generally these non-linear effects are intensity dependent and for this reason the peak power of the laser is the most important factor when observing these phenomena. The FM modelocked laser at 1.3 μm had a peak power output of 4.8W, this is below the threshold for most non-linear effects in optical fibre. The peak power from the laser can be enhanced by factors of hundreds by simultaneously Q-switching the laser. Q-switching of a laser refers to the process of allowing the population inversion of the laser to build up to a value much greater than usual and then restoring the high Q factor of the cavity so that the stored energy is released in a short intense pulse. The artificially low Q results in high gain in the cavity and high energy storage. The energy storage is a function of the upper state lifetime, for this reason it is preferable to Q-switch with lasing materials with a long upper state lifetime. In fig 3.6.1 the diagram shows the general Q-switching action. When the high Q factor is restored to the cavity the gain is much larger than the loss so lasing operation rapidly builds up from spontaneous emission. The characteristic Q-switch pulse which is emitted from the laser represents the dynamics of the rapid build up from noise of the lasing action, the rapid depletion of the inversion due to the large circulating intensity and the loss of power due to losses in the cavity, given by R. A short pulse is omitted from the laser which decays approximately in the time of the cavity photon lifetime given by

$$t_c = nl/c(1-R) \qquad 3.6.1$$

Thus the pulse durations from typical Q-switched laser are of the order of 10's of nanoseconds. Detailed analysis of the rate equations [Siegman: 1986] reveal that the build up time (the time between the Q-switch opening and the pulse emerging), the pulse duration and pulse shape are all functions of the ratio of the inversion before the Q-switch is opened to the threshold inversion and the cavity photon lifetime. Shortest Q-switch pulses are achieved through operating the laser well above threshold and with as short a cavity photon lifetime as possible. When the laser is repetitively Q-switched the pulse duration and energy also becomes a function of the repetition rate and the upper state lifetime of the laser. This leads to an optimum repetition frequency to optimise the peak power in the Q-switch pulses. The optimum frequency for Nd:YAG has been shown to be 1 kHz [Chester et al: 1970].

Simultaneously Q-switching and modelocking of the laser imposes further restrictions on the Q-switch operation. Consideration of the transient build up time of the

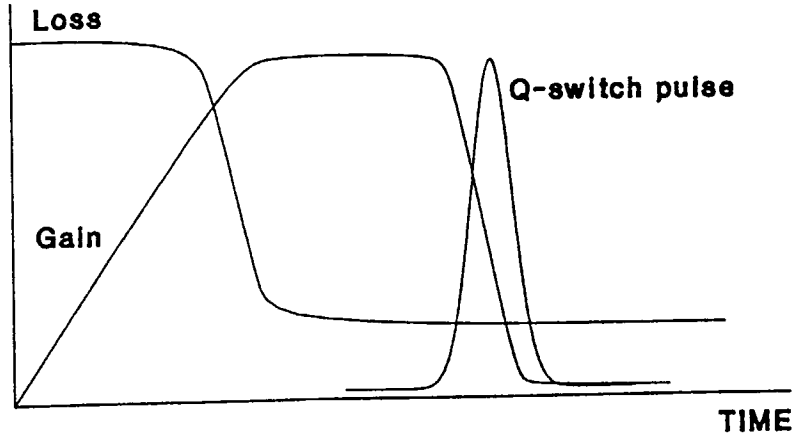

FIG 3.6.1 LASER Q-SWITCHING

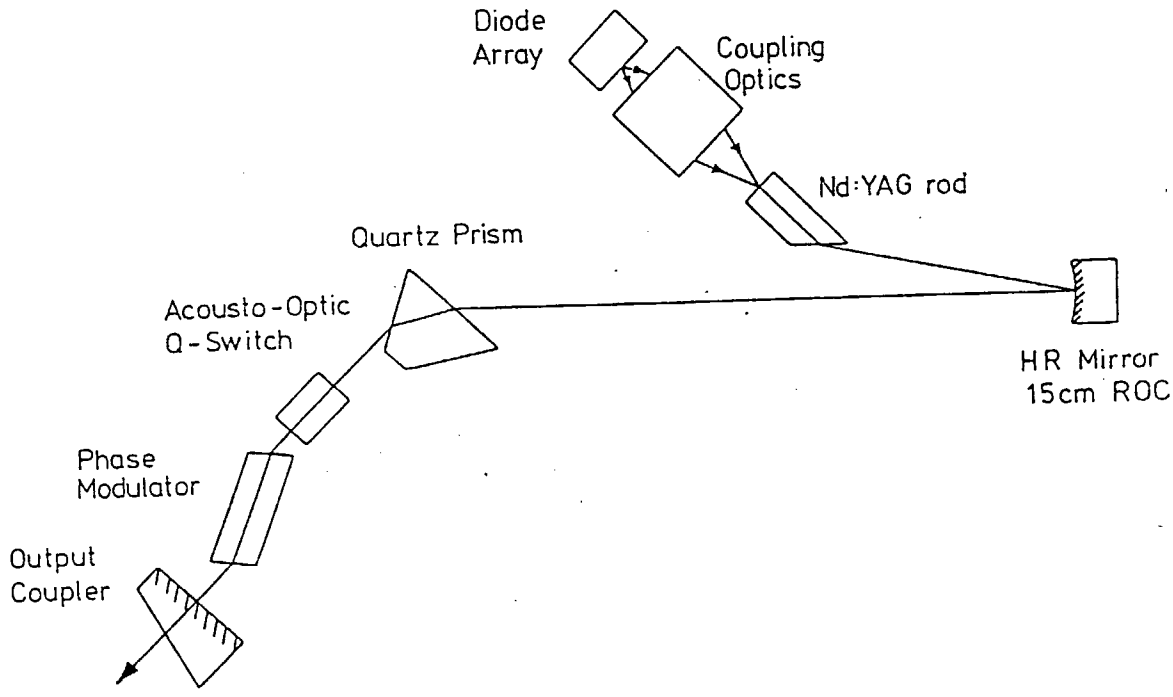

FIG 3.6.2 SCHEMATIC DIAGRAM OF THE FM MODELOCKED /Q-SWITCHED CAVITY

AM modelocking process has shown that typically the pulsewidth will not be in a steady state until about 1000 roundtrips of the cavity [Kuizenga et al : 1973]. Enough roundtrips can be made of the cavity in the build up time of the Q-switch for modelocked pulses to be formed but optimum modelocking can only be achieved when there is a small amount of lasing action between Q-switched pulses, this is called pre-lase. This small amount of pre-lase allows the modelocking to be in a steady state when the Q-switch is opened.

Q-switched operation of a laser can be achieved by a variety of means, from simple mechanical choppers to electrooptic modulators. An acousto-optic Q-switch was used in this experiment. The acousto-optic Q-switch operates in a similar way to that of the amplitude modulator described in section 3.4. Applying an rf signal to the acousto-optic device results in an index grating that diffracts the light out of the laser cavity which spoils lasing. Acousto-optic Q-switches are limited by the diffraction efficiency they can achieve, so they are usually only used on low gain systems. The relatively simple supply for the Q-switch, low insertion loss and the ease of using the devices repetitively make acousto-optic devices ideal for diode pumped systems.

3.6.2 Q-switching And Modelocking Of The Laser

The acousto-optic modulator used in the experiment was made of lead molybdate (ISLE Optics) and was anti-reflection coated at 1.3 μm for low insertion loss, The crystal was 2.3 cm in length. The modulator was driven at 80 MHz at a power level of 1W which gave an estimated diffraction efficiency of 26% at 1.3 μm. The Q-switch had a passive switch on time of 0.5 μsec.

The Q-switch was inserted in to the cavity as shown in 3.6.2. Insertion of the Q-switch dropped the cw output power to 32 mW when the cavity was operated with a 2% output coupling, it is estimated that the Q-switch accounts for less than 0.5% single pass loss. The Q-switch being an acousto-optic device, required angular adjustment to optimise the Bragg angle and translation to optimise the 'sweet spot' of the device. The Q-switch was controlled, by way of its power supply, which required a TTL logic level '1' signal to apply rf to the Q-switch and logic level '0' to turn it off. Fig 3.6.3 shows the control signals to the Q-switch and the resulting rf signal. The Q-switch was operated at the repetition rate of 1 kHz, the Q-switch was turned off for 1 μsec which was sufficient time for the Q-switching process to have finished. The Q-switch could hold off lasing, but by adjusting the rf power to the Q-switch and the Bragg angle allowed the laser to be operated with about 100 μW of pre-lase.

Stable Q-switched operation of the laser was achieved when using a 0.5% and 2% output coupler, unstable Q-switched operation was obtained when a 7% output coupling was used due to the laser only being just above threshold (~ X1.2). It was found that stable Q-switching and FM modelocking operation could only be obtained when pre-lase was used, only random noise was seen in the absence of pre-lase. The Q-switched modelocked pulses were optimised by viewing the Q-switch envelope on a fast Ge detector, the average power from the laser was monitored using a calorimeter (Laser

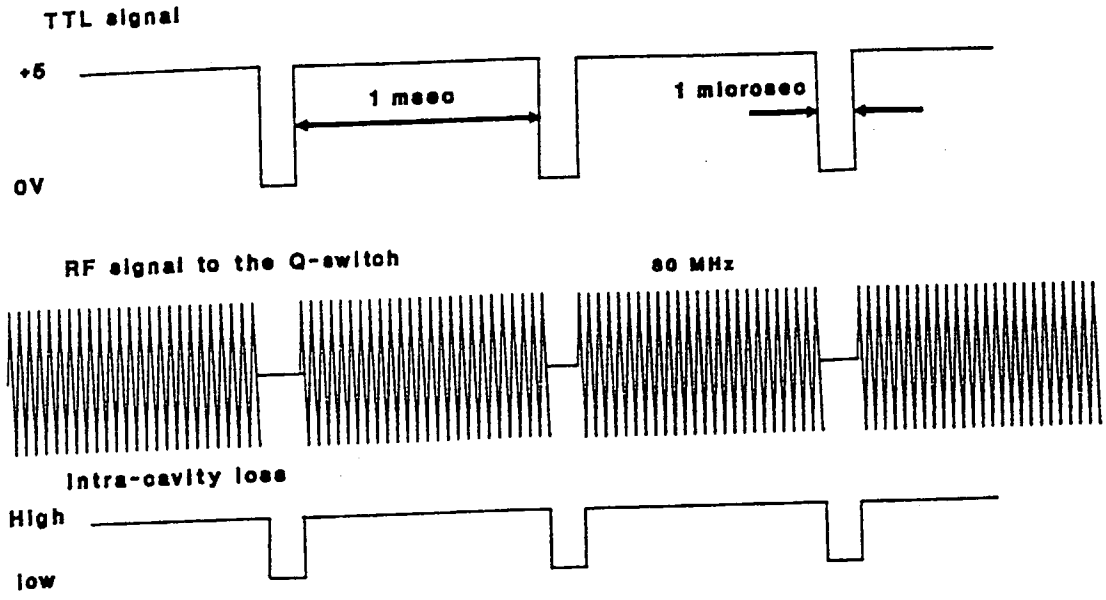

FIG 3.6.3 THE CONTROL SIGNALS TO THE Q-SWITCH

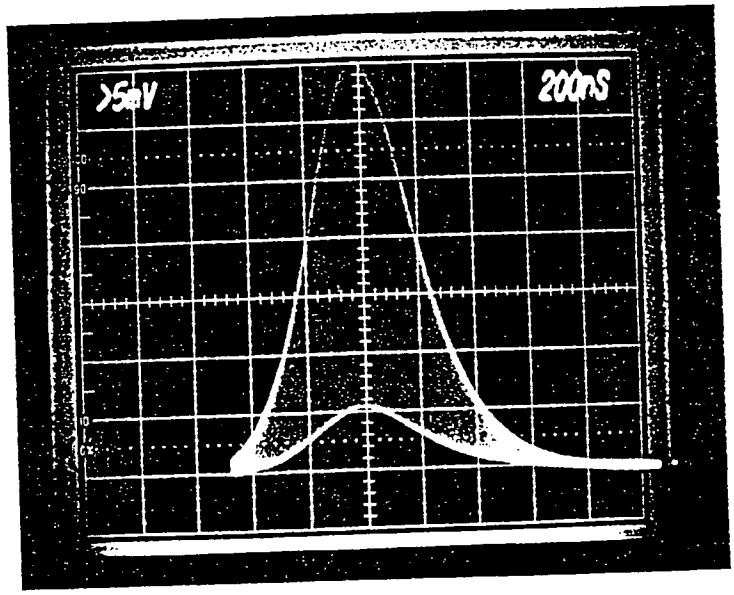

FIG 3.6.4
A TYPICAL Q-SWITCHED/MODELOCKED PULSE ENVELOPE

Instrumentation M5100). Fig 3.6.4 shows a typical modelocked and Q-switched pulse envelope, the Q-switch envelope had a duration of 350 nsec and an energy of 2.1 μJ for a 0.5% output coupling. When a 2% output coupling was used the average power was 4 μJ with a pulse envelope duration of 400 nsec. It was found that the removal of the drive frequency to the phase modulator made little difference to the average power from the laser when optimally modelocked.

The average pulse duration of the modelocked pulses in the Q-switch envelope was measured using a standard background free autocorrelation technique. The pulsed signal from the photomultiplier tube was averaged using a boxcar integrator which was triggered by the TTL signal to the Q-switch. The integration time of the boxcar integrator was minimised so as to avoid any distortion of the autocorrelation pulse shape. The average pulse duration of the modelocked pulses was found to be 30 psec again the pulse shape best fitting a sech pulse shape. The degradation of the modelocked pulse duration when the laser is Q-switched can be attributed to the instability that the Q-switching action has on the laser.

The Q-switching enhances the peak power from the laser, for a 0.5% output coupling the power has been enhanced by a factor of X376 and for the 2% output coupling by X284. Relating these factors to the peak power that were obtained when the laser was cw modelocked implies that there is a peak power of in excess of 700 W and 1 kW in the Q-switch/modelocked pulse envelope for the 0.5% and 2% output coupling respectively. The enhancement in the average powers from the laser were modest compared to some Nd:YAG Q-switch systems [Maker et al: 1988]. The laser was operated only 2 to 3 X above threshold which adversely effected the quality of the Q-switching and was the dominant factor in determing the quality of the Q-switching. Improvement in the Q-switching would require either lowering the threshold of the laser or increasing the power of the pump source which could be achieved by polarisation coupling of two 1W laser diodes (see section 2.1).

Summary

A laser diode pumped Nd:YAG laser operating at 1.3 μm has been modelocked using both AM and FM techniques. AM modelocking achieved pulse durations of 46 psec, whilst when FM modelocking a pulse duration of 19 psec was observed. For both these methods the experimental pulse durations agreed with the pulse durations predicted by the self-consistent theory of Kuizenga and Siegman. Both systems offered stable, picosecond pulses that are shorter than those that are typically obtained from flashlamp Nd:YAG lasers. Simultaneously Q-switching and FM modelocking of the laser resulted in the peak power from the modelocked laser being enhanced by a factor of X376 and peak powers of over 1kW.

REFERENCES: CHAPTER 3

Adams C. S. , Maker G. T. and Ferguson A. I. , 1990, Opt. Comm. , 76, 127.

Ashkin A. , 1966, Appl. Phys. Letts. , 9, 72.

Bramwell S. R. , 1988, PhD Thesis, Univ. Soton. , 'Frequency Modulation of Dye Lasers', Chapter 5.

Chester R. B. , Korr M. A. and Geusie J. E. , 1970, Proc. IEEE, 58, 1899.

Clarkson W. A. and Hanna D. C. , 1989, J. Mod. Opt. , 36, 483.

Digonnet M. and Gaete C. J. , 1985, Appl. Opt. , 24, 333.

Gomes A. S. L. , Gouveia-Neto A. S. and Taylor J. R. , 1988, Opt. Quant. Electron. , 20, 95.

Graener H. and Laubereau A. , 1981, Opt. Comm. , 37, 138.

Hanna D. C. , 1969, IEEE J. Quant. Electron. , QE-5, 483.

Harris S. E and Wallace R. W. , 1969, J. Opt. Soc. Am. , 59, 744.

Harris S. E. and McDuff O. P. , 1965, IEEE J. Quant. Electron. , QE-1, 355.

Hargrove L. E. , Fork R. L. and Pollack M. A. , 1964, Appl. Phys. Letts. , 5, 4.

Huber G. , 1980, 'Miniature Nd: lasers', chapter 1, Current Topics in Material Science, Vol 4, North Holland Publishing Company.

Keller U. , Weingarter K. J. , Li K. D. , Gerstenberger D. C. , Khuri-Yakub P. T. and Bloom D. M. , 1990, Opt. Letts. , 15, 45.

Keller U. , Valdmones J. A. , Niss M. C. and Johnson A. M. , 1988, IEEE J. Quant. Electron. , 24, 427.

Klenn H. , Kuhl J. and Van Der Lind V. , 1981, Opt. Comm. , 38, 390.

Kogelnik H. W. , Ippen E. P. , Dienes A. and Shank C. V. , 1972, IEEE J. Quant. Electron. , QE-8, 373.

Krausz F. , Brabec T. , Winter E. and Schmidt A. J. , 1989, Appl. Phys. Letts. , 55, 2386.

Krausz F. , Turi L. , Kuti C. and Schmidt A. J. , 1990, Appl. Phys. Letts. , 56, 1415.

Kuizenga D. J. and Siegman A. E. , 1970, IEEE J. Quant. Electron. , QE-6, 694.

Kuizenga D. J. , Phillian D. W. , Lund T. and Siegman A. E. , 1973, Opt. Comm. , 9, 221.

Maker G. T. , Keen S. J. and Ferguson A. I. , 1988, Appl. Phys. Letts. , 53, 1675.

Maker G. T. and Ferguson A. I. , 1989, Opt. Letts. , 14, 788.

Maker G. T. and Ferguson A. I. , Aug 1989, Electron. Letts. , 25, 1025.

Morimoto A. , Kabayaski T. and Sueta T. , 1988, IEEE J. Quant. Electron. , QE-24, 94.

New G. H. C. , 1983, Rep. Prog. Phys. , 46, 877.

Phillips M. W. , Ferguson A. I. and Hanna D. C. , 1989, Opt. Letts. , 14, 219.

Phillips M. W. , 1989, PhD Thesis, Soton Univ, Chapters V + VI.

Siegman A. E and Kuizenga D. J. , 1974, Opt. Electon. , 6, 43.

Siegman A. E. , 1986, 'Lasers', Chapter 26, Oxford University Press.

Yariv A. , 1985, 'Optical Electronics', Third Edition, Chapter 9, Holts-Saunders, New York.

CHAPTER 4
NON-LINEAR EFFECTS IN OPTICAL FIBRE

Section 4.1 Introduction

In this chapter a theoretical description of soliton Raman generation in optical fibre is presented. In section 4.2 a description of the properties of single mode optical fibre is reviewed. Section 4.3 describes the sources of dispersion in fibre and how this dispersion can be manipulated by careful choice of the fibre parameters. A general theoretical interpretation of stimulated Raman scattering is made in section 4.4 and in section 4.5 it is shown how the effect is modified in optical fibre. In sections 4.6 and 4.7 the existence and the properties of optical solitons are described. Section 4.8 introduces the concept of modulational instability in optical fibre. Section 4.9 reviews research into the generation of optical solitons by the use of stimulated Raman scattering.

Section 4.2 Step index optical fibre

A simple model of light propagating in optical fibres is that of light being reflected back and forth from the core-cladding boundary and thereby travelling zig-zag fashion along the core of the fibre. This is an adequate model for multimode fibres but a more rigorous analysis must take into account that light is an electromagnetic wave phenomenon and that there will be modes of guided wave propagation.

A complete analysis of the bound modes using Maxwell's equations can be found in Synder and Love [Synder et al: 1983]. In this summary of optical fibre properties the characteristics of step index fibres will be described. Specifically the waveguide properties of these optical fibres when the wavelength of the incident is the order of the core radius of the fibre. The typical geometry of a step index fibre is shown in fig 4.2.1. the fibre has a core of radius, a (typically a few microns), and a refractive index n_1 surrounded by the cladding of refractive index n_2 and a typical diameter of 125 μm. The fibre is usually made out of pure silica with dopants added, such as GeO_2 or P_2O_5 to raise or lower the index of the core or cladding so that $n_1 > n_2$ allowing the fibre to guide light. This index difference has an important effect on the characteristics of an optical fibre. Typically, single mode optical fibres are made with $n_1 - n_2 << n_1$, in this case the fibres are referred to as being 'weakly guiding'. Within the weakly guiding limit ($n_1 - n_2/n_1 \rightarrow 0$) these fibres have the characteristic of supporting modes which are sets of linearly polarised waves in which the transverse electric and magnetic fields are each parallel and mutually orthogonal over the whole fibre cross section. These fibres have the additional advantage of requiring only low dopant levels which minimises losses due to scattering.

The bound modes of the waveguide can be computed by applying Maxwell's equations and suitable boundary conditions which apply for the cylindrical waveguide. The analysis was first presented by Gloge [Gloge: 1971] for the case of weakly guiding step index fibres. Detailed descriptions can be found in Yariv [Yariv: 1985] and Synder

and Love [Synder et al: 1983] but in this thesis just the main relevant results will be presented.

The analysis finds that for a bound mode to exist the propagation constant, β, obeys the following condition

$$n_c k_0 > \beta > n_{cl} k_0 \qquad 4.2.1$$

Thus the propagation constant for the guided mode lies between the value of that of the core and the cladding. The almost plane-parallel, transverse electromagnetic wave solutions are known as linearly polarised LP_{km} modes, with eigenvalues labelled as β_{km} with both k,m = 0, 1, 2, 3, ... It is usual when analyzing the modes in optical fibre to work with a normalised frequency parameter, V, and a normalised propagation constant b_{km} as defined in equations 4.2.2 and 4.2.3 respectively

$$V = 2\pi a/\lambda \, (n_1^2 - n_2^2)^{\frac{1}{2}} \qquad 4.2.2$$

$$b_{km} = (\beta_{km}^2 - \beta_{cl}^2) \, / \, (\beta_c^2 - \beta_{cl}^2) \qquad 4.2.3$$

The equations governing the modes can be solved numerically, fig 4.2.2 shows the normalised propagation constant as a function of the normalised frequency. The mode cut-off wavelength, λ_0, corresponds to the value of V for which the mode is no longer confined. For the fundamental mode LP_{01}, propagation constant β_{01}, (with l=0,the field profile is radially symmetric), the cut-off is given by V_{co}=0. Therefore, the LP_{01} mode has no cut-off wavelength. The next value of V_{co} is 2.405, the LP_{11} mode. If the normalised input frequency, V,is lower than 2.405, the light will be guided only in the LP_{01} mode, hence the fibre will be single mode at this frequency. The LP_{01} mode consisting of two orthogonal polarisation modes, is degenerate in propagation constant and mode profile. To make a fibre single mode at a particular wavelength, requires choosing suitable values of, ρ, the core radius and $(n_1^2-n_2^2)^{\frac{1}{2}}$ such that V < 2.405 at the wavelength required.

The expression obtained for the electric and magnetic field can be used to find an expression for the Poynting vector and the power flow in the core and cladding. A full derivation can be found in Yariv. Fig 4.2.3 shows the fractional power contained in the cladding as a function of the frequency parameter V. It is clear that at cut-off, the mode spreads into the cladding, away from cut-off the mode is confined to the core. The fundamental LP_{01} mode is the best confined mode. If the light is propagating close to cut-off, then more power will be in the cladding, making the loss due to bending greater.

FIG 4.2.1 THE GEOMETRY OF A STEP INDEX FIBRE

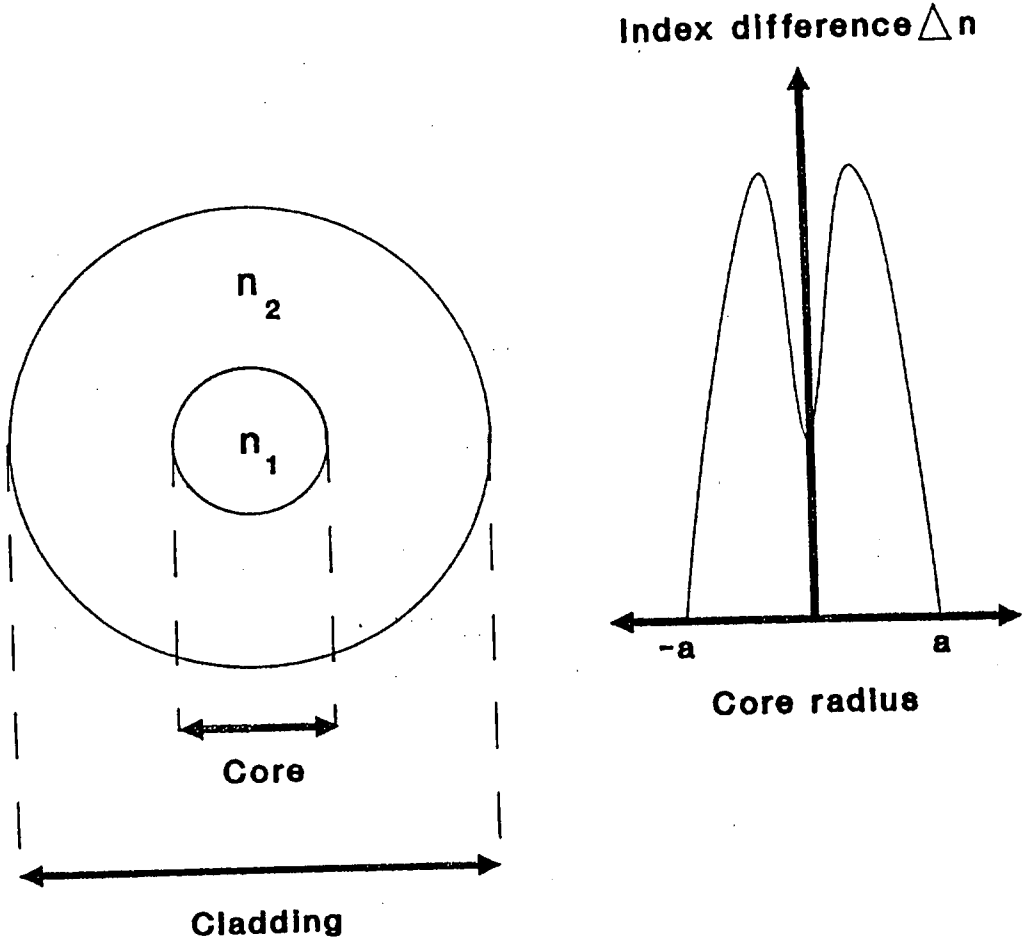

FIG 4.2.2
THE NORMALISED PROPAGATION CONSTANT AGAINST THE NORMALISED FREQUENCY

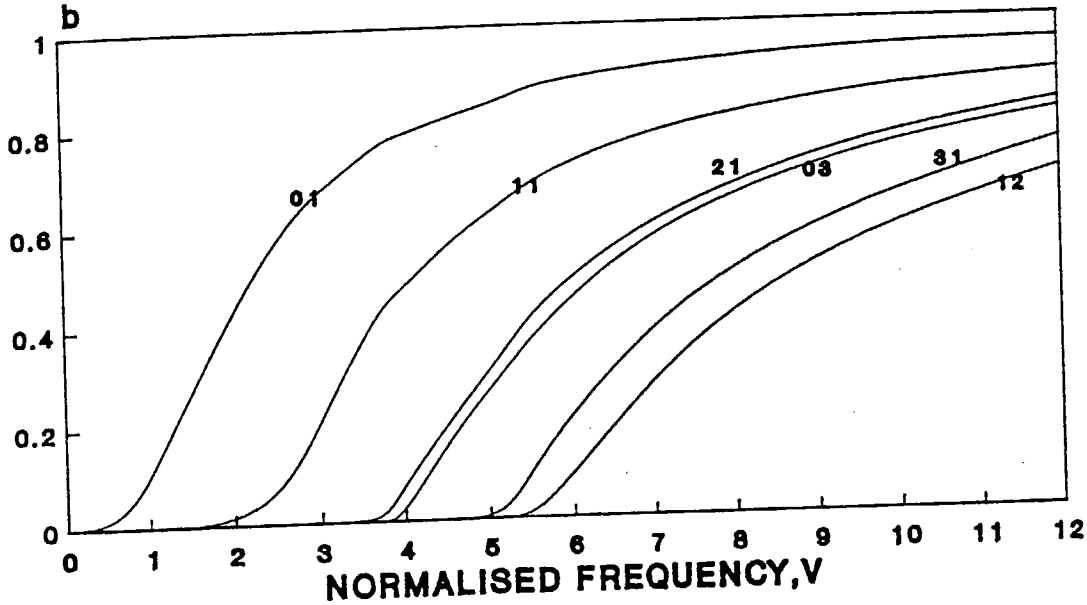

FIG 4.2.3
FRACTIONAL POWER IN THE CLADDING AGAINST FREQUENCY

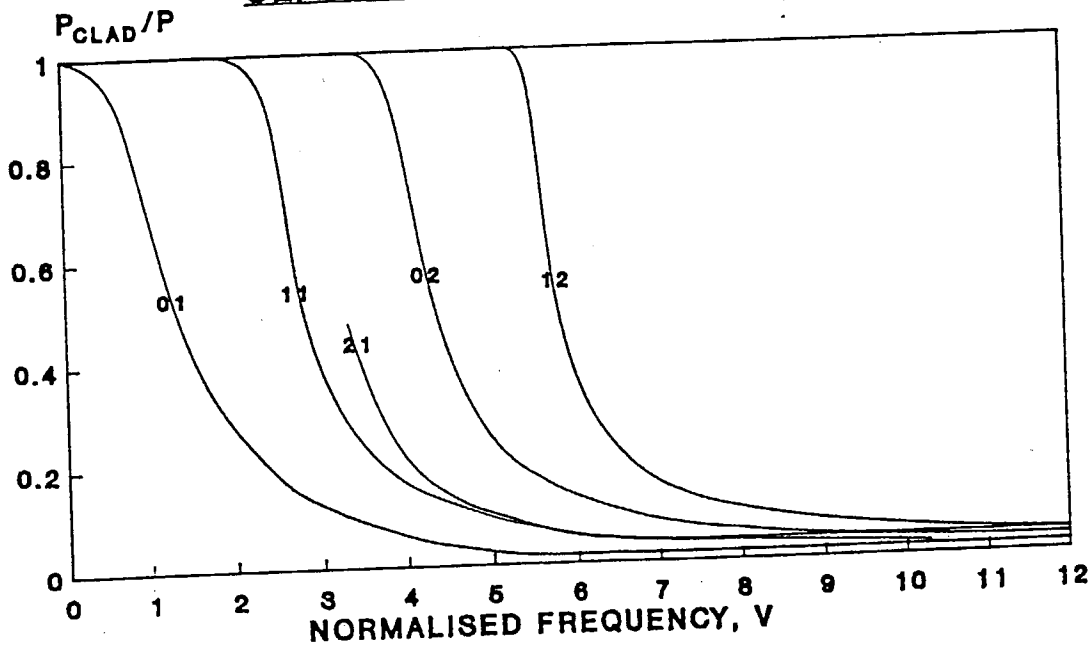

Section 4.3 Dispersion in optical fibres

The velocity at which the mode energy in a light pulse travels down a waveguide is called the group velocity and is characterised by the expression

$$v_g = d\omega/d\beta \tag{4.3.1}$$

The propagation constant for a guided LP_{km} mode is defined by

$$\beta_{km} = n_{km}k_0 = n_{km}(n_1, n_2, \omega)\omega/c \tag{4.3.2}$$

Equation 4.3.2 shows that the propagation constant is a function of the effective material index n_{km}, which is itself a function of frequency. This frequency dependence of the propagation constant leads to different group velocities for different frequencies, this effect is described as dispersion. The dispersion in a waveguide causes pulses to broaden which ultimately puts a limit on high bit rate communication systems which use optical fibre. The dispersion parameter, D, is described by the variation of the group velocity with frequency and is defined by

$$D = 2\pi c/\lambda^2 \, (d^2\beta/d\omega^2) \tag{4.3.3}$$

The dispersion parameter is generally quoted in terms of ps/nm.km. The group velocity dispersion (GVD) in an optical waveguide has a contribution from the material dispersion and from the waveguide dispersion. For multi-mode fibre the propagation constant varies widely between modes as shown in fig 4.2.2, this is the dominant factor for dispersion in multi-mode fibre. In single mode optical fibre dispersion is determined by the material dispersion and that of the intra-mode dispersion.

The dispersion of the LP_{01} mode in a single mode optical fibre can be calculated by consideration of the GVD. The group velocity can be written as

$$1/v_g = d\beta/d\omega$$

$$= \left(\frac{\delta n}{\delta n_1} \frac{\delta n_1}{\delta \omega} + \frac{\delta n}{\delta n_2} \frac{\delta n_2}{\delta \omega} + \frac{\delta n}{\delta \omega} \right) \frac{\omega}{c} + \frac{n}{c} \tag{4.3.4}$$

The first two terms refer to the material dispersion and the third term refers to the waveguide dispersion. For the weakly guiding case $n_1 \approx n_2$ so that

$$\delta n_1/\delta\omega \approx \delta n_2/\delta\omega \approx (dn/d\omega)_m \tag{4.3.5}$$

which means that the group velocity can be written as, using $\omega = 2\pi c/\lambda$,

FIG 4.3.1
THE WAVEGUIDE DISPERSION PARAMETER

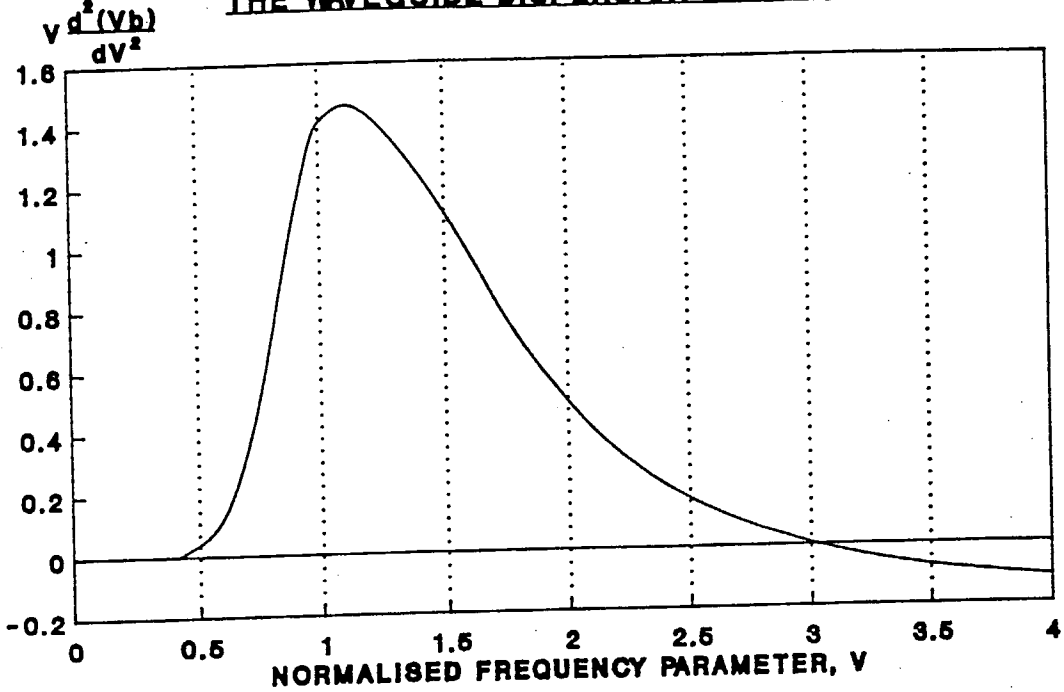

FIG 4.3.2
DISPERSION IN A TYPICAL SINGLE MODE OPTICAL FIBRE

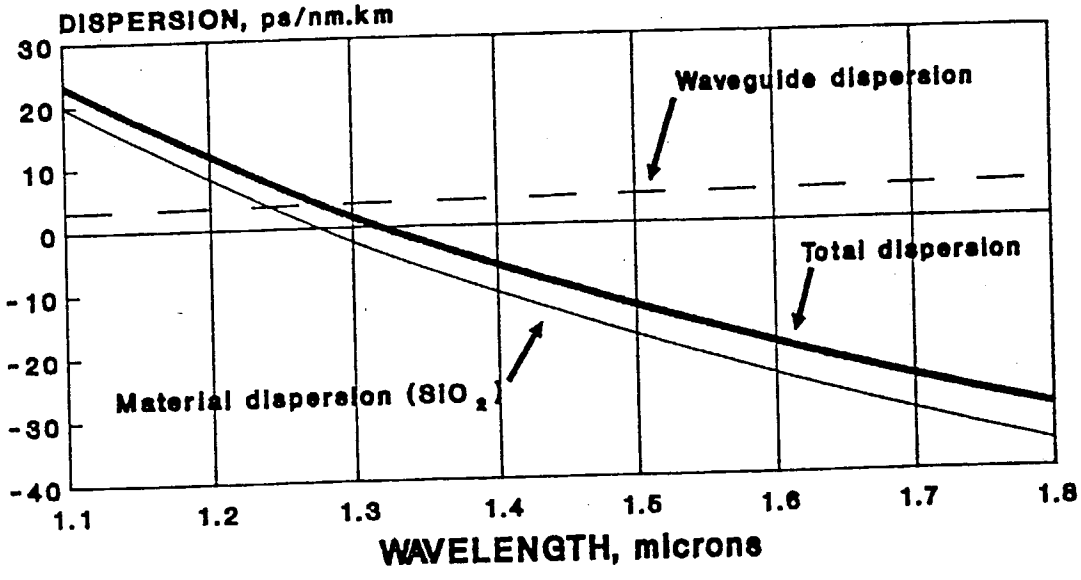

$$\frac{1}{v_g} = \frac{d\beta}{d\omega} = -\frac{\lambda}{c}\left[\left(\frac{\delta n}{\delta\lambda}\right)_m + \left(\frac{\delta n}{\delta\lambda}\right)_w\right] + \frac{n}{c} \qquad 4.3.6$$

This definition of the group velocity can now be used to calculate the group velocity dispersion D, of Eqn 4.3.3. This is given by

$$D = \frac{\lambda}{c}\left[\left(\frac{\delta^2 n}{\delta\lambda^2}\right)_m + \left(\frac{\delta^2 n}{\delta\lambda^2}\right)_w\right] \qquad 4.3.7$$

This can be rewritten in terms of the dispersion parameter given in equation 4.3.8

$$Y_{m,w} = \lambda^2(d^2n/d\lambda^2)_{m,w} \qquad 4.3.8$$

The group velocity dispersion is now given by

$$D = 1/\lambda c \; |Y_m + Y_w| \qquad 4.3.9$$

Equation 4.3.9 shows that the group velocity dispersion is the sum of the material and the waveguide dispersion. In pure silica, the zero dispersion wavelength is at 1.27 μm, the adding of GeO_2 dopants tends to push the zero dispersion to longer wavelengths. At wavelengths longer than the point of zero dispersion, the material dispersion is negative, whilst the waveguide dispersion always remains positive. The net effect is for the point of zero dispersion to shift to longer wavelengths, thus allowing the zero GVD point to be controlled by choice of the fibre parameters. The waveguide dispersion parameter has been calculated by Gower [Gower: 1984] and is given by

$$Y_w = (\Delta N^2/n).Vd^2(Vb)/dV^2 \qquad 4.3.10$$

where $N = c/v_g$ and $\Delta = n_1^2 - n_2^2/2n_2^2$.

For a step index fibre, the waveguide dispersion is dependent upon the core radius, a, and the effective refractive index difference Δ. The parameter $Vd^2(Vb)/dV^2$ is plotted in fig 4.3.1, which allows the waveguide dispersion parameter to be calculated for a particular frequency and fibre parameters. In fig 4.3.2 typical values for the waveguide and material dispersion parameters are plotted along with the overall dispersion parameter. For standard step index fibres, to increase the point of zero dispersion requires increasing Δ and decreasing a. In doing this, loss tends to increase due to an increase in infra-red absorption and Raleigh scattering, due to a larger Δ, and an increase in microbending losses due to decreasing V. By the use of novel fibre structures, the point of zero GVD

can be shifted to 1.5 μm, the point of lowest loss in silica based fibre, and the dispersion made flat over a wide range of wavelength [Ainslie et al: 1986].

Section 4.4 Stimulated Raman Scattering

In this section a description of stimulated Raman scattering (SRS) will be made. In fig 4.4.1 a schematic diagram is shown of the process of SRS. An incident photon from the pump laser, ω_p, interacts with the material, resulting in the incident photons annihilation and the creation of a photon at a lower frequency ω_s. Due to energy conservation, energy is imparted in the material in the form of molecular vibration, of frequency ω_v such that,

$$\hbar (\omega_p - \omega_s) = \hbar \omega_v \qquad 4.4.1$$

The resultant photon at frequency ω_s, will have been stimulated by the incident photon at the same frequency and will be identicle in phase. Spontaneous Raman emission provides the noise to initiate the process.

The gain that is present due to SRS can be calculated by applying Maxwell's equations [Hanna et al: 1979] to the propagation of the applied electric field $\underline{E}$. The resultant electric polarisation, $\underline{P}$, is given by,

$$\underline{P} = \epsilon_0 \chi^{(1)} \underline{E} + \underline{P}^{NL} \qquad 4.4.2$$

where $$\underline{P}^{NL} = \epsilon_0 K^{(2)} \chi^{(2)} \underline{E}^2 + \epsilon_0 K^{(3)} \chi^{(3)} \underline{E}^3 + \ldots.$$

where $\chi^{(n)}$ describes the n^{th} order susceptibility and $K^{(n)}$ is a numerical factor dependent on the non-linear process being considered. Applying Maxwell's equations and by considering plane waves travelling in the +z direction results in the wave equation

$$\frac{\delta^2 E}{\delta z^2} - \left[\frac{1}{c^2}\right]\left[\frac{\delta^2 E}{\delta t^2}\right] = \left[\frac{1}{\epsilon c^2}\right]\left[\frac{\delta^2 P^{NL}}{\delta t^2}\right] \qquad 4.4.3$$

where $c = (\epsilon_0 \mu_0)^{-\frac{1}{2}}$, the phase velocity.

The electric field amplitude at a general frequency ω_j can be written as, assuming slowly varying amplitudes and phases,

$$\underline{E}_{\omega j}(z,t) = (1/2)\{E_j(z) \exp[i(\omega_j t - k_j z)] + c.c\} \qquad 4.4.4$$

and the non-linear polarisation

$$\underline{P}_{\omega j}{}^{NL}(z,t) = (1/2)\{P_j{}^{NL}(z) \exp[i(\omega_j t - k_j)] + c.c\} \qquad 4.4.5$$

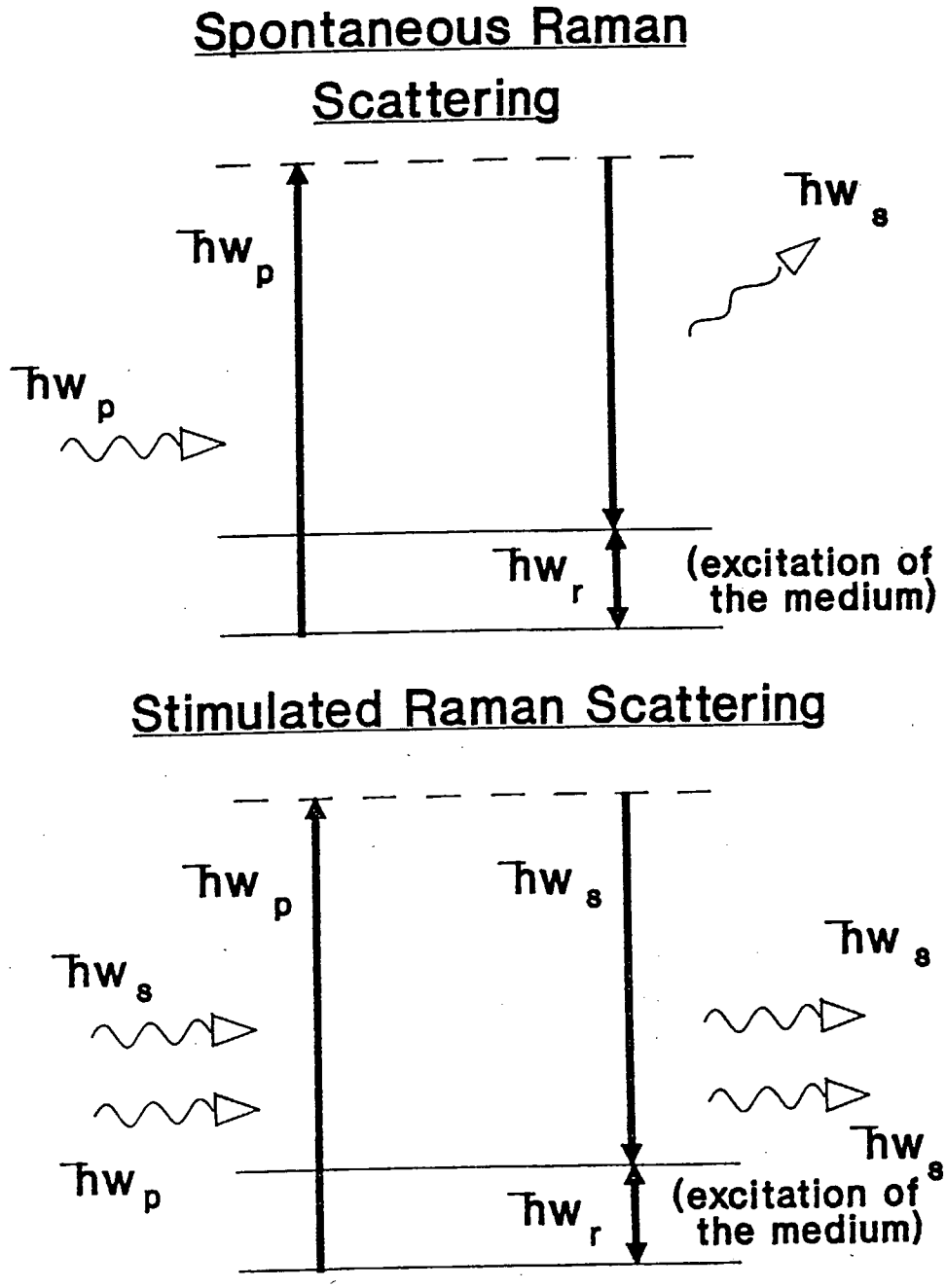

ENERGY LEVEL DIAGRAM OF THE PROCESS OF RAMAN SCATTERING

FIG 4.4.1

This is assuming a zero phase mismatch between $\underline{E}_{\omega j}$ and $\underline{P}_{\omega j}$ (in the Raman process the phases are automatically matched as $\Delta K = K_p - K_p + K_s - K_s$), as is the case for non-parametric processes.

Substituting the expression of equations 4.4.4 and 4.4.5 into equation 4.4.3 and by applying the slowly varying amplitude approximation i.e $\delta^2 E_j/\delta z^2$ is negligible (this implies that the growth of the envelope, in a distance of the order of a wavelength is small) yields;

$$\left[\frac{\delta E_j}{\delta z}\right] = -i\left[\frac{\omega}{2n_j\epsilon_0 c_0}\right] P_j^{NL} \qquad 4.4.6$$

where we have used $k_j = n_j\omega_j/c_0$ and $\epsilon_j = n_j^2 c_0$. The simultaneous action of the fields at the pump wavelength ω_p and Stokes frequency ω_s, produces a polarisation at the Stokes frequency which has a natural resonance when $\omega_p - \omega_s = \omega_r$. The induced polarisation at ω_s is proportional to the electric field at the same frequency, hence the term stimulated arises. This implies that the polarisation has a term dependent on $|E_p|^2 E_s$, so the appropriate non-linear polarisation is

$$P^{NL} = \epsilon_0 K^3 \chi_r |E|_p^2 E_s \qquad 4.4.7$$

χ_r is the Raman susceptibility, $\chi_r = \chi^{(3)}(-\omega_s : \omega_p - \omega_p\omega_s)$. A photon generated at the Stokes frequency results from the absorption of a pump photon with the excess energy, $\hbar(\omega_p - \omega_s)$, absorbed by the material. The imaginary part of χ_r determines the rate at which the pump photons are absorbed, hence it describes the rate at which the Stokes photons are generated [Maier: 1976]. At resonance only the imaginary part of χ_r remains ($\chi_r = \chi_r' + i\chi_r''$) so
using equation 4.4.7 in equation 4.4.6 gives,

$$\frac{\delta E_s(z)}{\delta z} = \frac{3\omega_s}{4cn_s}\chi_r'' |E_p(z)|^2 E_s(z) \qquad 4.4.8$$

In the small signal case $E_p(z) = E_p(0) = E_{p0}$. The Stokes field after a distance L is given by

$$E_s(L) = E_{so} \exp\left(\frac{3\omega_s \chi_r'' I_{po} L}{2\epsilon_0 c^2 n_s n_p}\right) \qquad 4.4.9$$

$$= I_{so} \exp(g_r I_{po} L)$$

where

$$g_r = \frac{-3\omega_s}{\epsilon_0 c^2 n_s n_p} \chi_r''$$

Section 4.5 SRS in optical fibres

The Raman gain present in glass optical fibres is relatively small but due to the high intensities and potentially long interaction lengths with low loss, the threshold of SRS can be low, typically of the order of tens of Watts. The process of SRS has been of great interest as it places an upper limit on the power that can be transmitted through a fibre [Smith: 1972].

Equation 4.4.9 shows that the Raman gain is determined by the intensity, interaction length and Raman gain coefficient. The equation still holds for optical fibres, but some modifications need to be made to allow for the properties of optical fibre.

The Raman amplification is given by [Stolen: Oct 1980]

$$\text{Amplification} \propto \exp G$$

where

$$G = \frac{gLP_{po}}{A} \qquad 4.5.1$$

The area, A, can be approximated for a single mode fibre by using the core size, a. This is a good approximation near cut off, away from cut off the effective area is larger and can be accurately predicted by overlap integral, the approximation is good to a factor of 2.

The interaction length, L, is modified to allow for the linear absorption, α, of the fibre. The interaction length can be replaced by an effective length, L_{eff}, and is defined by Smith [1972],

$$L_{eff} = \frac{1 - e^{-\alpha L}}{\alpha} \qquad 4.5.2$$

The constant, g, is the Raman gain coefficient, fig 4.5.1 shows the Raman gain curve of a silica-core single mode fibre [Stolen et al: 1973] at 526 nm. The Raman gain linewidth in silica glass is noticeably large and is the order of 250 cm^{-1}. The gain can be calculated for other wavelengths, as it scales by $1/\lambda$. The addition of a low percentage of dopants tends not to appreciably affect the gain. The gain curve of fig 4.5.1 was obtained from

polarisation preserving fibre which implies that the pump and Stokes signal will have similar polarisations for the complete length of the fibre. This polarisation does not have to be linear to achieve maximum Raman gain [Stolen: 1979], the Stokes signal will experience maximum gain even if the polarisations are elliptical as long as they are of the same orientation. For non-polarisation preserving fibre the relative polarisations of pump and Stokes become completely random, resulting in a loss of gain. For the Stokes signal polarised perpendicularly to the pump, the gain is an order of magnitude smaller. The effective Raman gain can be approximated by assuming an average value, so the effective Raman gain will be half that of the polarisation preserving case. Using the expression in equation 4.5.1, along with the modifications mentioned it is possible to derive a critical power for the Raman threshold. The Stokes is seeded by spontaneous Raman scattering, which appears all along the fibre length. This noise can be modeled by an effective input signal, $P_{seff}(0)$ [Smith: 1972]. The Stokes output power is given by

$$P_s(L) = P_{seff}(0)\, e^{G} \qquad 4.5.3$$

where

$$P_{seff} = h\nu_s \sqrt{\pi \delta\nu_{FWHM}} G^{-\frac{1}{2}} \qquad 4.5.4$$

where ν_s is the Stokes frequency and $\delta\nu_{FWHM}$ is the half width of the Raman gain spectrum. A critical power has been defined by Smith, at which the pump and Stokes powers are equal. This criterion gives the gain constant a critical value, k, the value being dependent upon several fibre parameters, including length. Applying this constraint to the definition of G gives

$$P_{crit} = \frac{kA}{gL_{eff}} \qquad 4.5.5$$

The value k can be taken as 16 for the cw case [Stolen et al: 1986] and approaches 20 for the pulsed case, when walk-off becomes a problem as will be discussed.

The expression derived for the threshold of SRS in single mode fibre is for the cw case. The physical process becomes much more complicated when the input waveform is pulsed. For input pulses of tens of picoseconds a quasi steady state approximation is valid, as the dephasing time of fused silica is $\approx 10^{-13}$ seconds. The schematic diagram of fig 4.5.2 shows the competing processes when a pulsed source is transmitted through a fibre, MI refers to modulational instability and is discussed in section 4.8. A Stokes signal will grow from spontaneous Raman scattering, if the input pulse has sufficient peak power. The Stokes signal will grow resulting in depletion of the pump, and depending upon the Stokes signal intensity, higher order Stokes signals will be generated. The situation is complicated by GVD, which owing to the large frequency difference between

FIG 4.5.1

THE RAMAN GAIN OF FUSED QUARTZ

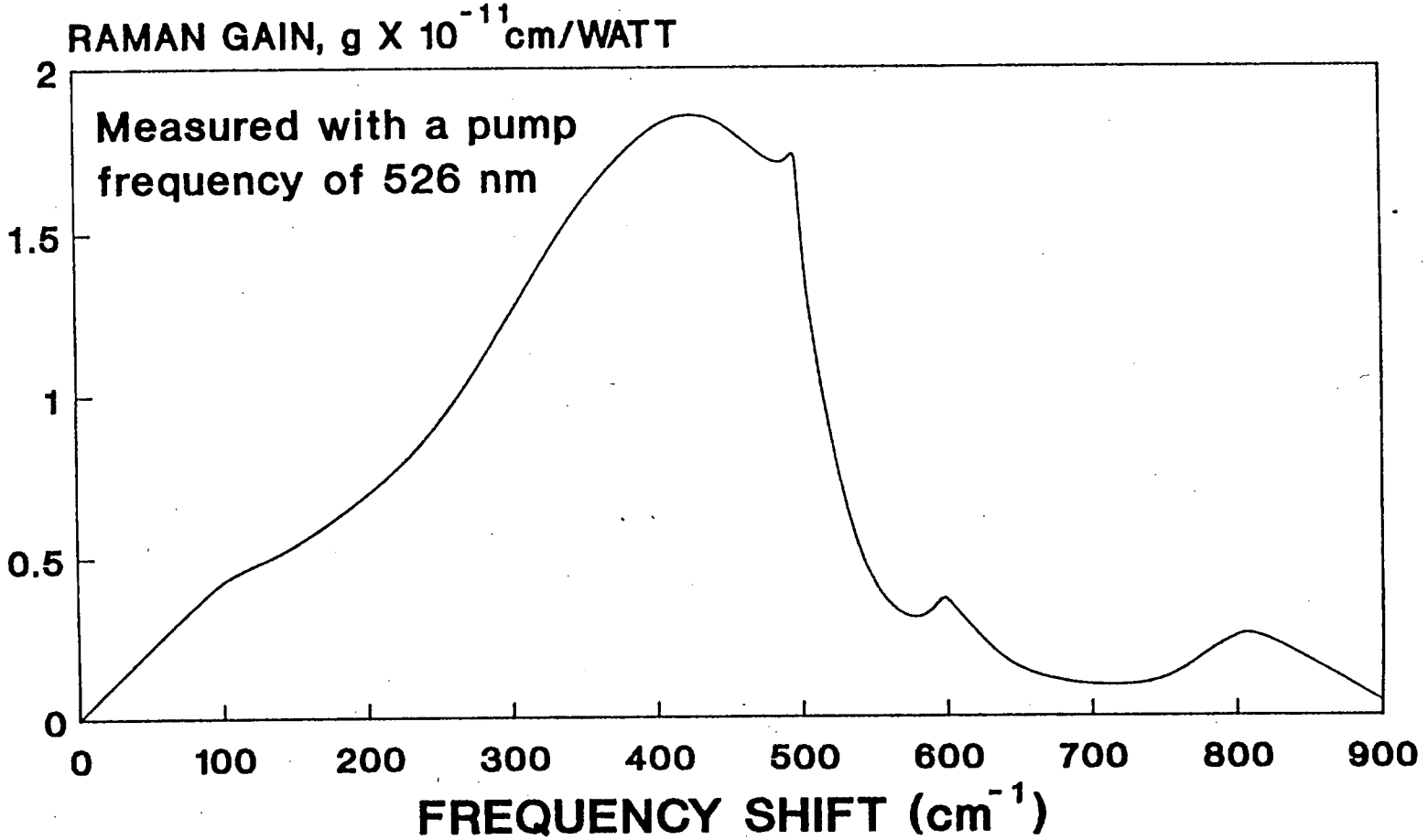

pump and Stokes signal (440 cm^{-1}), causes the Stokes signal to 'walk-off' from the pump, reducing the interaction length. Self phase modulation (SPM) appears in the same order of perturbation theory as SRS and is a competing non-linear process. The SPM tends to chirp the pulses and broaden the spectrum, which along with the process of GVD causes asymmetric intensity profiles and nonsymmetric spectral broadening. The situation is further complicated by cross-phase modulation (XPM)[Islam: 1987] which occurs due to the copropagating pump and Stokes signal. The pump signal induces a non-linear change in refractive index which can spectrally broaden the Stokes signal. It can be seen from the qualitative picture given of pulsed SRS in optical fibre, that it is a difficult task to mathematically model the process. Theoretical work on the subject has attempted to model into the coupled equations, which describe the evolution of pump and Stokes pulses, the effects of GVD, XPM and SPM [Osborne: 1989], [Kuckartz et al: 1987]. These studies have shown the undesirability of generating Stokes radiation when using fibre/grating pulse compression as the SRS tends to de-linearise frequency chirp on the pulse [Schadt et al: 1986]. A recent theoretical study has shown that XPM could cause a reversing of the frequency chirp on the Stokes pulse such that compression in the analomalous dispersion region is not possible [Hook et al: 1989].

The effect of pulse walk-off has been investigated experimentally by Stolen [Stolen et al: 1986]. To account for the effect of GVD a modification can be made to, k, the constant in equation 4.5.3. To account for the GVD of the fibre a simple model can be introduced in which we assume that the Stokes power builds up from a weak injected signal which is equivalent to the spontaneous Raman scattering along the fibre. When the pump wavelength is at 1.3 μm, the generated Stokes radiation will be in the anomalous region of the fibre and will travel slower than the pump. The walk-off distance can be defined as the length l_w in which the Stokes signal passes through one pumpwidth (T)

$$l_w = \frac{v_p v_s T}{v_p - v_s} \qquad 4.5.6$$

where v_s and v_p are the group velocities at the Stokes and pump wavelength respectively. Using the definition of D in section 4.3, equation 4.5.6 can be written as

$$l_w = \frac{T}{D\Delta\lambda} \qquad 4.5.7$$

where D is in units of ps/nm.km for the average wavelength and $\Delta\lambda$ is the spectral separation and is in units of nm. It has been shown experimentally by Stolen that maximum conversion efficiency takes place in $1.5 \rightarrow 2X$ the walk-off distance, for higher powers (when the input power greatly exceeds Raman threshold) conversion is likely to take place within one walk-off distance. A numerical study on combined stimulated

FIG 4.5.2 THE COMPETING NON-LINEAR PROCESSES IN AN OPTICAL FIBRE

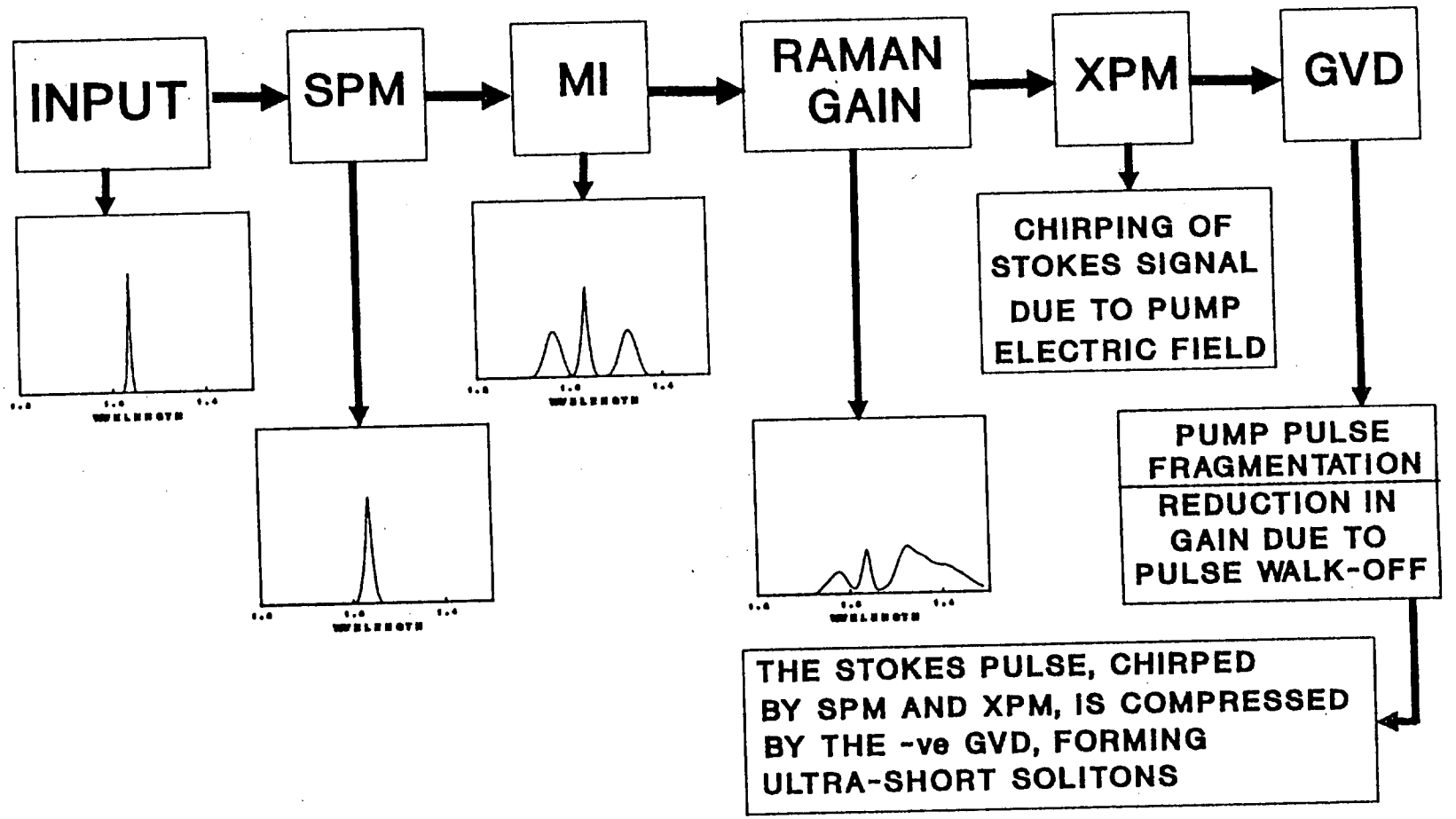

Raman scattering and self-phase modulation in optical fibre [Schadt et al: 1986] has shown that the group velocity of a Stokes pulse, when experiencing the gain from a pump pulse, does not travel at the group velocity of the Stokes frequency. This comes as a result of the difference in gain experienced by the Stokes pulse as the pump pulse is depleted, with the Stokes pulse being pulled towards the region of high gain. Equation 4.5.5 can be modified to obtain an estimate of threshold in the pulse walk-off regime, Stolen has shown that under these conditions a value of k of 20 most accurately predicts the threshold.

Section 4.6: Solitons

It was shown in section 4.3 that pulses propagating through optical fibre tend to spread out in time due to the group velocity dispersion of the fibre, this spreading exists regardless of the sign of the dispersion. Pulse narrowing and the creation of solitons in optical fibre is made possible by the non-linearity that is present in optical fibre, i.e the index of refraction itself is a function of the light intensity

$$n = n_0 + n_2 I \qquad 4.6.1$$

where n_2 is typically 3.2 X 10^{-16} cm^2/W and I is in comparable units.
The effect of the non-linear response on a propagating pulse is to install a frequency chirp on the pulse, broadening the spectrum of the pulse. This process is called self-phase modulation (SPM). The phase of the electric field for a plane wave is given by

$$\theta = \omega_0 t - kz \qquad 4.6.2$$

$$= \omega_0 t - \frac{\omega_0 n_0 z}{c} - \omega_0 n_2 z \frac{I}{c} \qquad 4.6.3$$

The instantaneous frequency is given by

$$\omega_i = \frac{d\theta}{dt} = \omega_0 - \left(\frac{\omega_0 n_2 z}{c} \right) \frac{dI}{dt} \qquad 4.6.4$$

In fig 4.6.1 a pulse is shown with the associated frequency chirp which arises due to its propagation in optical fibre. The diagram shows that in the leading edge of a pulse there will be low frequencies and in the trailing edge high frequencies. For negative GVD high frequencies travel faster than low frequencies resulting in pulse compression. The possibility of soliton like propagation of light through optical fibre was first predicted by Hasagawa [Hasagawa et al: 1973] and experimentally verified by Mollenauer [Mollenauer et al: 1980]. Optical fibres have proven to be an excellent medium for the study of solitons due to their potential low loss and because they can be very accurately characterised. In the following section it will be shown how the propagation of light

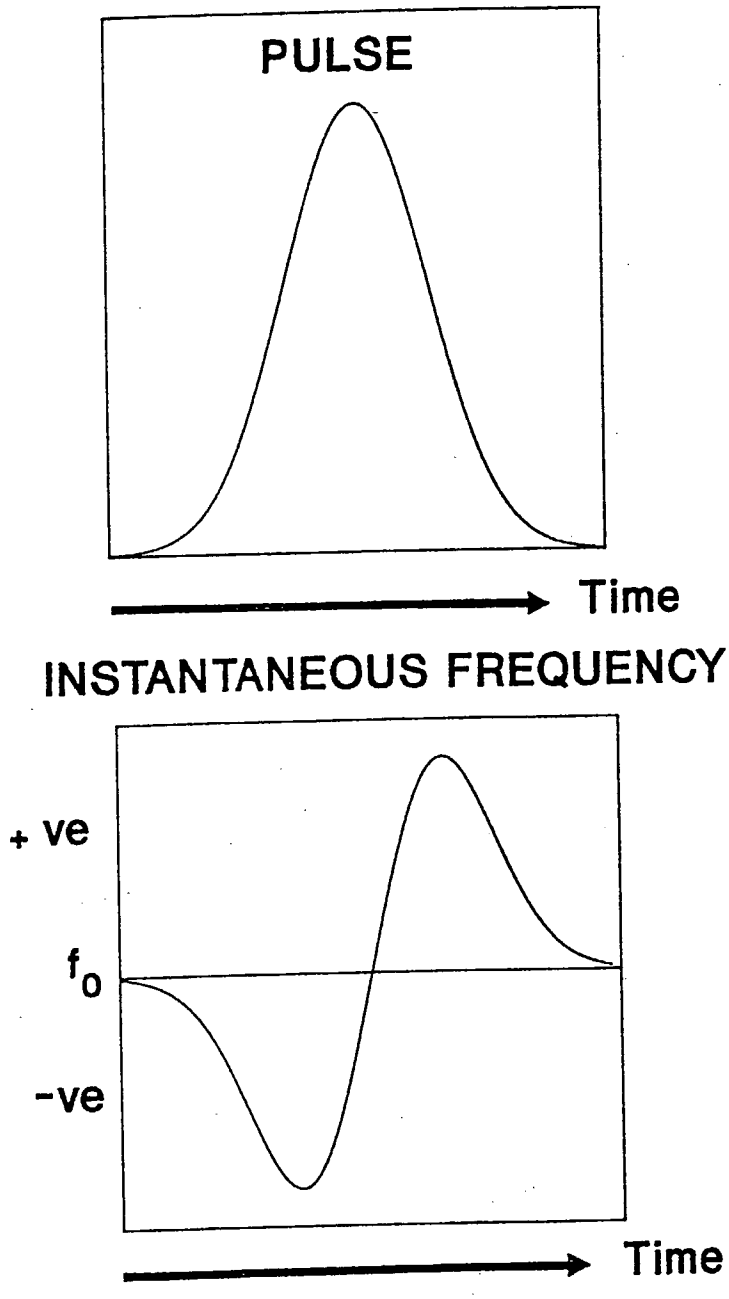

THE FREQUENCY CHIRP IMPARTED ON A PULSE DUE TO SPM

FIG 4.6.1

pulses through optical fibre can be described using the non-linear Schrodinger equation and how this implies soliton like solutions under the correct conditions. It will then be shown how optical solitons can be generated by use of SRS.

The derivation that follows for the wave equation in optical fibre, follows the derivation put forward by Hasagawa [Hasagawa: 1989]. Section 4.6.3 showed that in a dispersive fibre the refractive index and consequently the propagation constant, β, is a function of frequency. For a spectrum that occupies a narrow range of frequencies around ω_0, $\beta(\omega)$ can be expanded such that,

$$\beta - \beta_0 = \frac{\delta\beta}{\delta\omega}\bigg|_{\omega 0}(\omega - \omega_0) + \frac{1}{2}\frac{\delta^2\beta}{\delta\omega^2}\bigg|_{\omega 0}(\omega - \omega_0)^2 \ldots \qquad 4.6.5$$

where higher order terms have been neglected. The wave envelope function, E(x,t) assumed to be a slowly varying function in x and t. This allows the envelope to be fourier transformed, using the variables $\Delta\omega(= \omega-\omega_0)$ and $\Delta\beta(= \beta-\beta_0)$, which represents the small shift of frequency from the carrier frequency and wavenumber respectively. Applying the transforms gives

$$\bar{E}(\Delta\beta,\Delta\omega) = \int_{-\infty}^{\infty}\int_{-\infty}^{\infty} E(x,t)\, e^{i(\Delta\omega t - \Delta\beta x)}\, dx\, dt \qquad 4.6.6$$

The inverse transform is given by

$$E(x,t) = \frac{1}{(2\pi)^2}\int_{-\infty}^{\infty}\int_{-\infty}^{\infty} \bar{E}(\Delta\beta,\Delta\omega)\, e^{-i(\Delta\omega t - \Delta\beta x)}\, d(\Delta\beta)\, d(\Delta\omega) \qquad 4.6.7$$

Differentiating E(x,t) with respect to x and t gives

$$\frac{\delta}{\delta t} = -i\Delta\omega \quad \text{and} \quad \frac{\delta}{\delta x} = i\Delta\beta \qquad 4.6.8$$

Using these definitions on equation 4.6.5 and then operating the resultant expression on the envelope function E(x,t) gives,

$$i\left(\frac{\delta E}{\delta x} + \frac{\delta\beta}{\delta\omega}\frac{\delta E}{\delta t}\right) = \frac{1}{2}\frac{\delta^2\beta}{\delta\omega^2}\frac{\delta^2 E}{\delta t^2} \qquad 4.6.9$$

As shown in section 4.3 the quantity $\delta\omega/\delta\beta$ is the group velocity of a modulated wave, and the quantity $\delta^2\beta/\delta\omega^2$ represents the frequency dependence of the propagation constant i.e the dispersion. The equation describes the propagation of light through a dispersive medium, but excludes any non-linear effects which may occur.

Light propagating through a dielectric medium causes a small perturbation in the refractive index, in proportion to the intensity of the light, as shown in equation 4.6.1. The change in refractive index causes a change in the propagation constant, β, this small change $\delta\beta$ can be added to equation 4.6.5 which describes the effect of the dispersion of the propagation constant on the wave equation. Applying this change to equation 4.6.9 results in

$$i\left(\frac{\delta E}{\delta z} + \frac{1}{v_g}\frac{\delta E}{\delta t}\right) - \frac{1}{2}\frac{\delta^2\beta}{\delta\omega^2}\frac{\delta^2 E}{\delta t^2} - g|E|^2E = 0 \qquad 4.6.11$$

A factor, g, has been introduced which is a correction factor to allow for the variation in light intensity across the cross-section of the fibre. The correction factor has been calculated by Haus [Haus: 1984]. The wave equation can be reduced to a dimensionless form by the transformations given below

$$t' = \frac{(t - z/v_g)}{\tau} \qquad z' = \frac{\delta^2\beta}{\delta\omega^2}\frac{z}{\tau^2} \qquad 4.6.12$$

$$u = \tau g^{\frac{1}{2}} E.(\delta^2\beta/\delta\omega^2)^{-\frac{1}{2}}$$

The wave equation in dimensionless form is given by

$$i\frac{\delta u}{\delta z'} = \frac{\alpha}{2}\frac{\delta^2 u}{\delta t'} + |u|^2 u \qquad 4.6.13$$

where $\alpha = -1$ for positive dispersion and $\alpha = 1$ for negative dispersion. The equation is similar to that of the non-linear Schrodinger equation (NLSE) which describes the trapping of a quasi-particle in a potential V. Equation 4.6.13 is similar except the potential is replaced by $|E|^2$,hence the equation describing the propagation of light in an optical fibre is the non-linear Schrodinger equation. The solutions to equation 4.6.13 are dependent upon whether the light is pulsed or cw and upon the sign of the dispersion. In the region of anomalous dispersion, $\delta^2\beta/\delta\omega^2$ is negative, and the pulse can propagate as a soliton. The non-linear Schrodinger equation has been solved analytically by Zakharov and Shabat [Zakharov et al: 1972] .There are also a number of actual solutions

e.g Satsuma and Yajima [Satsuma: 1974]. The best known and simplest set of solutions take the form,

$$u(\tau,z') = N \text{ sech } (t') \qquad 4.6.14$$

Where $u(\tau,z')$ describes the envelope function in normalised form and N is an integer for soliton solutions. Figure 4.6.2 shows the theoretical propagation of N=1, 2, 3 solitons over one soliton period. The behaviour of the N = 1 soliton can be intuitively understood by considering the frequency chirps imparted by the SPM and the negative GVD. The sense of the chirp due to SPM tends to impart low frequencies in the leading edge of a pulse and high frequencies in the trailing edge as shown in figure 4.6.1. In the region of anomalous dispersion the effect of GVD will be in the opposite sense to that of the SPM and counteract the chirp imparted by SPM. In optical fibres the two effects are of the same order of magnitude, an exact balance is met for an N=1 soliton, resulting in the propagation of an undistorted pulse. The non-linear Schrodinger equation has been solved numerically for N=integer (the pure soliton case) and for an input pulse shape of sech up to N=20 [Mollenauer et al: 1983], although the problem gets more difficult as N increases as there are 2N simultaneous equations to solve which require a lot of computing time on very powerful computers. The N eigenvalues all have a real part of the same value indicating that they have the same velocity and thus form a bound state. As a result there is phase interference between solitons and the superimposed pulse shape oscillates. The solitons have a characteristic period in which this pulse shape reproduces itself given by

$$z_0 = \frac{0.322\pi^2 c\tau^2}{\lambda^2 |D|} \qquad 4.6.15$$

where D is defined in equation 4.3.3 and τ is the FWHM of the input pulse. The peak power of the fundamental soliton is given by

$$P_1 = \frac{0.776\lambda^3}{\pi^2 c n_2} \frac{|D| A_{eff}}{\tau^2} \qquad 4.6.16$$

Where A_{eff} refers to the fibre core area. The peak input powers for higher order solitons are given by the expression

$$P_N = N^2 P_1 \qquad 4.6.17$$

Higher order solitons are generated when the input power is larger than that required for a fundamental soliton for a given pulse width. The phase interference causes the solitons to interact and at particular points along the transmission the pulse width will be

FIG 4.6.2 THE BEHAVIOUR OF N = 1, 2, 3 SOLITONS

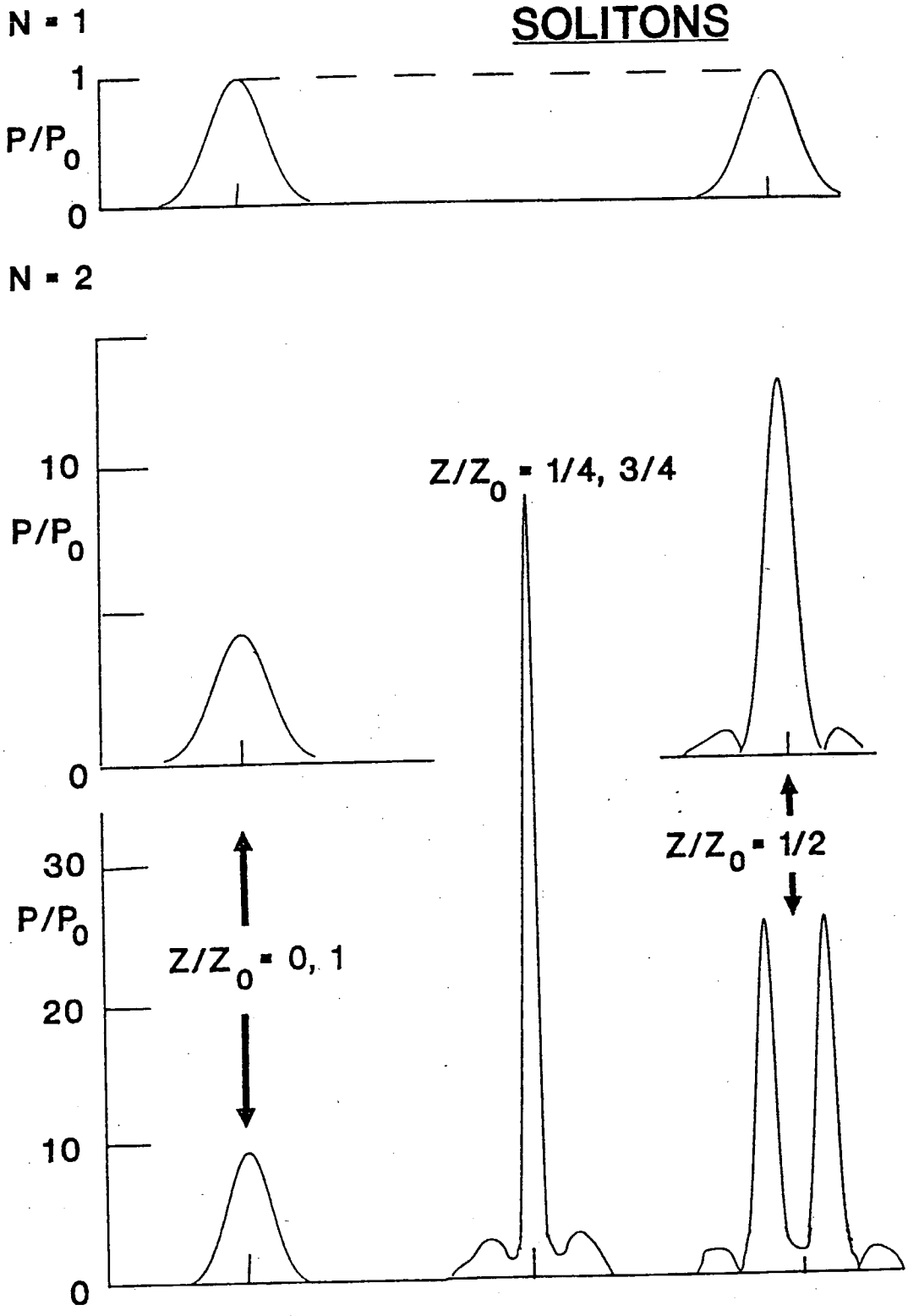

compressed. This property has been exploited to produce extremely short pulses in optical fibre [Mollenauer et al: 1983].

The requirements on the formation of solitons appear to be quite strict, the equations presented require for the input pulse shape to have a prescribed shape and peak power. However, soliton theory predicts and experimental work has shown that any reasonably shaped pulse can form a soliton if it has sufficient power. When the requirements are not exactly met a soliton is formed, with excess energy being deposited in a highly dispersive pedestal.

Section 4.7 The soliton self frequency shift

An important process which modifies the behaviour of sub-picosecond pulses passing through optical fibre is that of the soliton self frequency shift. The effect tends to put a physical limit on the order of the soliton that can be produced. The Fourier transform of an ultra-short pulse will produce a corresponding increase in the bandwidth of that pulse. For instance, the time bandwidth product for a sech pulse is given by $\Delta t \Delta \upsilon \sim .3$, so for a 1 psec pulse the corresponding bandwidth is at least 300 GHz. Section 4.5 showed that the Raman gain in glass optical fibre is very broad and extends from an almost zero frequency to almost 1000 cm^{-1}, with the peak at 440 cm^{-1}. When a solitons pulse duration is less than 1 psec this gain becomes significant. The effect of the Raman gain is to cause a continuous 'channelling' of energy from high frequencies to low frequencies, resulting in N=1 solitons, without pedestals, propagating at longer wavelengths. The effect was first experimentally investigated by Mitschke [Mitschke et al: 1987].

Gordon has produced a theoretical model which accounts for this frequency shift [Gordon: 1986]. The NLSE can be modified to allow for the Raman effect by adjusting the non-linear term to describe a delayed response

$$|u|^2 u \rightarrow u(t) \int f(s) \, |u(t-s)|^2 \, ds \qquad 4.7.1$$

where f(s) is a normalisation factor and tends to zero for sufficiently short delays. Using this expression Gordon has derived an expression for the expected frequency shift in terms of the input pulse duration

$$\frac{dv_0}{dz} = \frac{1.2904 \lambda^2 D H(\tau)}{\tau^4} \text{ (THz/m)} \qquad 4.7.2$$

Where λ, τ and D are measured in cm and ps. $H(\tau)$ is a function of the Raman gain curve and has been numerically computed by Gordon, it is shown in figure 4.7.1. The dependence on τ^{-4} can be understood by the τ^{-2} dependence of the solitons peak power,

FIG 4.7.1

H(τ) FOR SILICA OPTICAL FIBRES

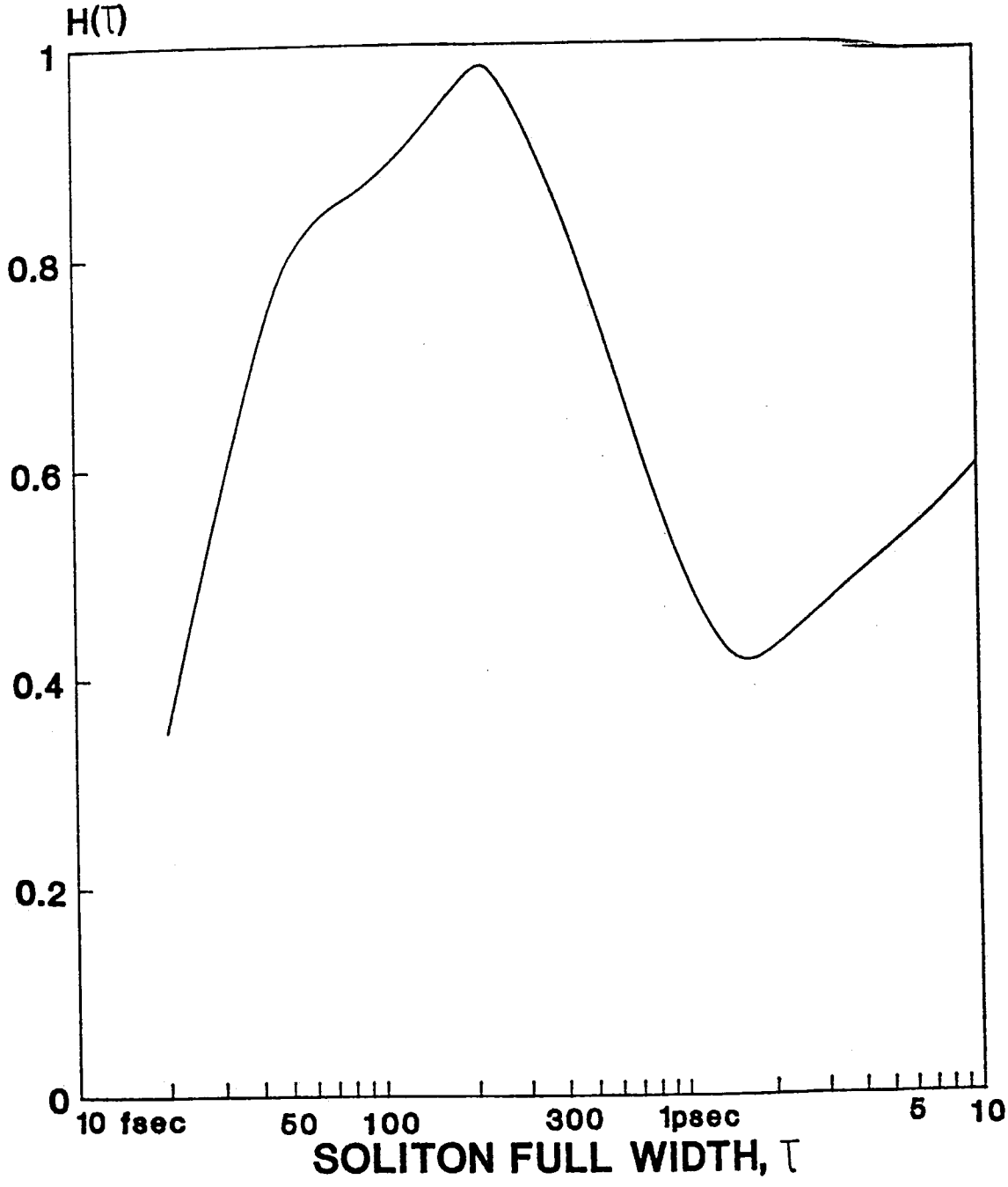

along with the τ^{-1} dependence of its spectral width, which proportionally increases both the effective Raman loss and the resulting frequency displacement.

Section 4.8 Modulational Instability

Modulational instability is a process in which the amplitude and phase modulations of a wave grow as a result of the interplay between non-linearity and anomalous dispersion. The effect has been studied in other areas of physics such as in fluids, plasmas and dielectric media. The possibility of observing modulational instability in optical fibre was first predicted by Hasesgawa [Hasagawa et al: 1980] and was later experimentally verified by Tai et al [Tai et al: Jan 1986]. There has been great interest in the phenomena of modulational instability in optical fibre due to the possibility of using it as a means of very high modulation frequencies (~.3 THz) [Tai et al: Aug 1986]. Continuous-wave-pumped modulational instability has recently been demonstrated [Itoh et al: 1989], with modulation frequencies of up to 130 GHz being observed. In this system it was possible to control the modulation frequency by the tuning of a laser diode. Modulational instability can be induced via XPM. This was first predicted by Agrawal [Agrawal et al: 1987] and was later experimentally verified by Gouveia-Neto et al [Gouveia-Neto et al: Dec 1988]. This process could be detrimental in amplitude modulated multichannel communication systems, giving rise to cross talk between channels. Modulational instability can be observed in optical fibre when the input wavelength falls in the anomalous dispersion region. As a result of the modulational instability exponential gain exists at specific sideband frequencies, these sidebands can rapidly grow from spontaneous amplitude and phase noise. Hasegawa has derived expressions for the modulational instability sideband frequencies and growth rate by consideration of the solutions to the NLSE when a modulated signal is applied [Hasagawa: 1989]. For a detailed derivation of the process of modulational instability the reader is referred to Hasegawa [Hasagawa et al: 1980]. The expressions derived describing the modulation frequency and growth rate are given below

$$f_{max} = \frac{1}{2\pi}\left(\frac{\omega}{c}\left(\frac{n_2}{\beta''}|E|^2\right)\right)^{\frac{1}{2}} \qquad 4.8.1$$

this expression gives the frequency at which the gain is maximum, at this frequency the spatial growth rate is given by

$$\gamma_g = \frac{1}{2} n_2 \frac{\omega}{c} |E|^2 \qquad 482$$

where n_2 is the nonlinear index coefficient (typically $n_2 = 3.2 \times 10^{-16}$ cm^2/W), β'' is the, second order derivative of β relative to ω, E is the electric field amplitude of the pump

wave, ω is the angular frequency of the pump wave and c is the speed of light. By using $\omega/c = 2\pi/n_0\lambda_0$, $|E|^2 = P/S_{ef}(cm^2)$ and $\beta'' = D\lambda_o^2/2\pi c$ where S_{ef} is the effective area of the fibre, and D is the dispersion parameter. The modulation frequency is now given by

$$f_{max} = \left(c \frac{n_2}{n_0} \frac{P}{\lambda^3_0 D S_{ef}} \right)^{\frac{1}{2}} \qquad 4.8.3$$

and the spatial growth rate by

$$\gamma_g = \pi \frac{n_2}{n_0} \frac{P}{S_{ef}\lambda_0} \qquad 4.8.4$$

It has been shown that the formation of modulational instability sidebands at a frequency of ω_m bears a close relationship with the formation of a soliton with amplitude E_o with a pulse duration of ω_m^{-1} [Anderson et al: 1984]. The formation of the sidebands can be thought of as a four wave mixing [Stolen et al: 1974] process where the phase matching between two pump photons and the Stokes and anti-Stokes photons is achieved by the non-linear change in refractive index ($\Delta n = n_2 I$), hence the variation of modulational instability frequency with power.

Section 4.9 A review of soliton Raman generation in optical fibre

The large bandwidth of Raman gain in silica glass has long been of interest due to the possibility of producing a widely tunable source of coherent radiation [Stolen: 1980] . Fibre Raman oscillators have been produced which have been tunable in the green [Stolen et al: 1977], where a modelocked argon ion laser was used as the pump source and in the near infra-red [Lin et al: 1979] from 1.07 μm to 1.32 μm, using a modelocked Nd:YAG laser operating at 1.06 μm. These oscillators produced output pulses in the region of 10-100 psec, due to their operation in the positive dispersion regime and operation with bandwidth limiting devices in the cavities. Kafka and Baer overcame the problem of working in the positive GVD region of the fibre by building a fibre Raman oscillator with a delay line included such that the total round trip dispersion is slightly negative. Using this method they were able to utilize the large Raman gain bandwidth and produce subpicosecond pulses at 1100 nm [Kafka et al: 1986].

The large Raman gain bandwidth in silica glass is theoretically capable of supporting pulses of bandwidth limit of 100 fsec. If the pump wavelength is such that the Stokes wavelength is in the negative dispersion region of the fibre , optical solitons can be formed. The possibility of generating solitons by this method was first suggested by Vysloukh et al [Vysloukh et al: 1983], in which they considered the coupled wave equations describing the Stokes and pump waves. The solution predicts the formation of N=1 solitons at the Stokes wavelength.

A tunable source of radiation, utilizing SRS in optical fibre and operating in the negative dispersion region of the fibre had been produced before this prediction [Lin: 1979]. The cavity included prisms, which were used for tuning the laser, but consequently they limited the bandwidth suppressing the formation of solitons.

The first experimental verification of Vysloukh prediction was made by Dianov et al using a modelocked and Q-switched laser operating at 1.06 μm [Grudinin et al: 1987]. The use of a laser operating at 1.06 μm to study propagation of light pulses beyond the zero dispersion region of a fibre (~ 1.3 μm) was not an ideal choice as high order Stokes bands are required. Nevertheless, a continuum was generated from 1.3 μm to 1.7 μm which contained pulses as short as 70 fsec.

Islam et al first demonstrated the use of a pump laser operating in the normal dispersion regime to produce optical solitons via SRS in the anomalous dispersion region [Islam et al: 1986]. In this experiment they pumped a fibre Raman amplification soliton laser (FRASL), which made use of a dispersion shifted fibre with its zero GVD at 1.536 μm. The laser was synchronously pumped with a color centre laser operating at a wavelength such that the pump and Stokes signal would both travel with the same group velocity, so maximum gain is achieved. The laser produced pulses of a duration of 250 fsec, with 2 mW average power. The initial pulses from the FRASL had a pedestal component associated with their formation which could be removed by the use of two fibres in the ring, one used for gain and one for pulse shaping.

Zysett et al have used a dye laser pumped by a compressed Nd:YAG laser operating around 1.3 μm to investigate soliton formation via Raman effects in single mode fibre [Zysett et al: 1987]. The dye laser was tunable around 1.3 μm and produced 0.83 psec pulses. In a synchronously pumped fibre Raman laser configuration [Zysett et al: 1986] they produced 80 fsec pulses. In a single pass arrangement they observed pulses as short as 70 fsec with a conversion efficiency of 50 %, with a tuning range of 1.36 μm to 1.54 μm. The solitons that they produced were pedestal free and had the characteristics of N=1 solitons. The formation of the solitons were modelled using the NLSE equation including higher order terms and the Raman effect [Beaud et al: 1987], good agreement was found for short length of fibre. The formation of the downshifted solitons is attributed to the break-up of high order solitons formed at the fundamental wavelength via intra-pulse Raman effects i.e the SSFS. The formation is not due to normal SRS, indeed no wavelength shift was observed when the input wavelength was in the normal dispersion region although the peak power was well over the threshold to observe SRS.

The methods discussed so far that have used Raman effects in optical fibre to produce solitons have all been relatively complicated; they have either required 'fine' timing requirements or have involved complex pump lasers. The first authors to report on work which utilised the simplicity of using SRS to produce solitons were Gouveia-Neto et al [Gouveia-Neto et al: Dec 1987]. In their work they used a modelocked Nd:YAG laser operating at 1.3 μm which produced 100 psec pulses. The output from this laser when passed through standard single mode fibre produced solitons with a pulse duration

as short as 100 fsec, with a best conversion efficiency of 10-20 %. The solitons formed were found to be insensitive to the input pump power but were found to have a pedestal associated with their formation. In subsequent work Gomes, Taylor et al have further investigated and exploited this method of producing solitons [Gouveia-Neto et al: Feb 1988]. They have studied the effect of relaunching the solitons such that their input power was below that required to support an N=1 soliton. Using synchronous amplification, again exploiting the Raman effect, it was shown that these solitons could be sustained [Gouveia-Neto et al: April 1988], [Gomes et al: 1988].

Gouveia-Neto et al have used a compressed Nd:YAG laser operating at 1.3 μm to produce tunable solitons from 1.32 μm to 1.5 μm [Gouveia-Neto et al: Oct 1987], [Gouveia-Neto et al: Sept 1988]. This laser has been demonstrated to be a useful source for investigating the transmission of optical solitons in the negative dispersion region of fibre. The laser has been used to investigate the transmission of sub-picosecond pulses at the zero GVD in fibre [Gouveia-Neto et al: Dec 1988] and the suppression of the SSFS by the use of Raman gain [Blow et al: 1988], [Gouveia-Neto et al: 1989].

The threshold for the formation of Raman generation can be reduced by an order of magnitude by synchronsly pumping a fibre Raman oscillator. In this configuration some of the generated SRS is fed back in to the fibre thus reducing threshold. Timing requirements are not as stringent as those found with the FRASL or by Zysett et al [1986] as the oscillators can be pumped with modelocked pulses from a Nd:YAG laser whose pulses are relatively long (~ 100 psec). Kafka and Baer [Kafka et al: 1987] used this technique to produce 160 fsec pulses centred at 1.41 μm with an average power of 20 mW. The fibre Raman soliton laser can be made even simpler by the use of a fibre coupler, eliminating the need for bulk feedback optics, thus making a compact and stable source of sub-picosecond pulses.

The use of feedback can allow more novel means of using SRS. Gouvei-Neto et al have used a fibre Raman ring laser to produce sub-picosecond pulses at 1.5 μm and 1.6 μm by pumping with a Nd:YAG laser operating at 1.3 μm [Gouveia-Neto et al: Nov 1987]. In this experiment they have used dispersion shifted fibre in the oscillator such that the first Stokes band is in the normal dispersion region. Pumping the oscillator sufficiently hard results in higher order Stokes bands being formed which fall in the negative GVD region as form optical solitons. The fibre Raman oscillator has noise advantages over the single pass arrangement as shown in a recent study by Keller et al [Keller et al: 1989]. In this study they investigated in the frequency domain, the noise associated with the formation of solitons via SRS. They found that the solitons formed in a oscillator arrangement had a smaller noise component than in the single pass configuration. In a feedback arrangement, the solitons are formed from an injected signal rather than from spontaneous noise.

SRS has proven to be an important method of producing and investigating the formation of solitons in optical fibre. The relative simplicity and the lack of stringent requirements on the pump laser has made it an attractive alternative for producing sub-

picosecond pulses.

CHAPTER 4: REFERENCES

Agrawal G. P. , 1987, Phys. Rev. Letts. , 59, 880.

Ainslie B. J. and Day C. R. , 1986, J. of Light. Tech., 4, 967.

Anderson D. and Lisak M. , 1984, Opt. Letts. , 19, 468.

Beaud P. , Hodel W. , Zysett B. and Weber H. P. , 1987, IEEE J. Quant. Electron. , QE-23, 1938.

Blow K. J. , Doran N. J. and Wood D. , 1988, J. Opt. Soc. Am. B. , 5, 1301.

Gloge, 1971, Appl. Opt. , 10, 2252.

Gomes A. S. L. , Du Silvuard V. L. , Taylor J. R. , 1988, J. Opt. Soc. Am . B., 5, 373.

Gordon J. P. , 1986, Opt. Lett. , 11, 662.

Gouveia-Neto A. S. , Gomes A. S. L. and Taylor J. R. , Nov 1987, Opt. Lett. , 12, 927.

Gouveia-Neto A. S. , Gomes A. S. L. and Taylor J. R. , Oct 1987, Opt. Comm. , 64, 163.

Gouveia-Neto A. S. , Gomes A. S. L. and Taylor J. R. , Dec 1987, Opt. Lett. , 12, 1035.

Gouveia-Neto A. S. , Gomes A. S. L. and Taylor J. R. , Feb 1988, IEEE J. Quantum. Electron. , 24, 334.

Gouveia-Neto A. S. , Gomes A. S. L. and Taylor J. R. , April 1988, J. Opt. Soc. Am. B. , 5, 799.

Gouveia-Neto A. S. , Sombra A. S. B. and Taylor J. R. , Sept 1988, Opt. Comm. , 68, 139.

Gouveia-Neto A. S. , Falden M. E. and Taylor J. R. , Dec 1988, Opt. Comm. , 69, 173.

Gouveia-Neto A. S. , Gomes A. S. L. and Taylor J. R. , 1989, Opt. Letts. , 14, 514.

Gower J. , 1984, 'Optical Communications Systems', Prentice-Hall International Series in Opto-electronics.

Grudinin A. B. , Dianov E. M. , Korobkin D. V. , Prokohorov A. M. , Serkin V. N. and Khaidarov D. V. , 1987, JETP Lett. , 45, 260.

Hanna D. C. , Yoratich and Cotter, 1979, 'Nonlinear Optics Of Free Atoms And Molecules', Springer Series in Optical Science, Springer Verlag.

Hasegawa A. and Tappert F. , 1973, Appl. Phys. Lett. ,23 , 142.

Hasegawa A. and Brinkman V. F. , 1980, IEEE J. of Quant. Electron. , QE-16, 694.

Hasegawa A. , 1989, 'Optical Solitons in Fibres', Springer Tracts in Modern Physics, Volume 116, Springer Verlag.

Haus H. A. , 1984, 'Waves and Fields in Optoelectronics', Prentice-Hall Series in Solid State Physical Electronics.

Hook A. , Anderson D. and Lisak M. , 1989, J. Opt. Soc. Am. B. , 6, 185.

Islam M. N. , Mollenauer L. F. and Stolen R. H. , 1986, Ultrafast Phenomena V: Springer Series in Chemical Physics, page 46, Springer Verlag, New York.

Islam M. N. , 1987, Opt. Lett. , 12, 625.

Itoh H. , Davis G. M. and Sudo S. , 1989, Opt. Letts. , 14, 1368.

Kafka J. and Baer T. , 1986, Ultrafast Phenomena V. , page 51, Springer Verlag, New York.

Kafka J. and Baer T. , 1987, Opt. Lett. , 12, 181.

Keller U. , Li K. D. , Rodwell M. and Bloom D. M. , 1989, IEEE J. Quant. Electron. , 25, 280.

Kuckartz M. , Schulz R. and Harde H. , 1987, Opt. and Quant. Electron. , 19, 237.

Lin C. and French W. G. , 1979, Appl. Phys. Lett. , 34, 666.

Maier M. , 1976, Appl. Phys. , 11, 209.

Mitschke F. M. and Mollenauer L. F. , 1987, Opt. Lett. , 12, 407.

Mollenauer L. F. , Stolen R. H. and Gordon J. P. , 1980, Phys. Rev. Lett. , 45, 1095.

Mollenauer L. F. , Stolen R. H. and Gordon J. P. , 1983. Opt. Lett. , 8, 289.

Osborne R. , 1989, J. Opt. Soc. Am. B. , 6, 1726.

Satsuma J. and Yajimi N. , 1974, Suppl. of the Prog. Theoret. Phys. , 55, 284.

Schadt D. , Jaskorzynske B. and Osterberg U. , 1986, J. Opt. Soc. Am. B. , 3, 1257.

Smith R. G. , 1972, Appl. Opt. , 11, 2489.

Stolen R. H. and Ippen E. P. , 1973, Appl. Phys. Lett. , 22, 276.

Stolen R. H. , Byorkholm J. E. and Ashkin A. , 1974, Appl. Phys. Letts. , 24, 308.

Stolen R. H. , Lin C. and Jain R. K. , 1977, Appl. Phys. Lett. , 32, 340.

Stolen R. H. , 1979, IEEE J. Quant. Electron. , QE-15, 1157.

Stolen R. H. , Oct 1980, Proc. IEEE. , 68, 1232.

Stolen R. H. , 1980, 'Fibre Raman Lasers', in Fibre and Intergrated Optics Vol 3, 21.

Stolen R.H. and Johnson A. M. , 1986, IEEE J. Quant. Electron. , QE-22, 2154.

Synder A. W. and Love J. D. , 1983, 'Optical Waveguide Theory', Chapman and Hall, London.

Tai K. , Hasegawa A. and Tomita A. , Jan 1986, Phys. Rev. Letts. , 56, 135.

Tai K. , Tomita A. , Jewell J. L. and Hasegawa A. , Aug 1986, Appl. Phys. Letts. , 49, 236.

Vysloukh V. A. and Serkin V. N. , 1983, JETP Lett. , 38, 199.

Yariv, 1985, 'Optical Electronics', Third Edition, Chapter 3, Holt-Saunders International Editions.

Zakharov V. E. and Shabat A. B. , 1972, Sov. Phys. JETP, 34, 62.

Zysett B. , Beaud P. and Hodel W. , 1987, Appl. Phys. Lett. , 50, 1027.

Zysett B. , Beaud P. , Hodel W. and Weber H. P., 1986, Ultrafast Phenomena V, page 54, Springer Verlag, New York.

CHAPTER 5
A STUDY OF SRS IN OPTICAL FIBRE

Section 5.1 Introduction

In this chapter experimental work carried out investigating soliton Raman generation in optical fibre will be presented. The laser used as the pump source for this investigation was the diode pumped modelocked and Q-switched laser as described in chapter 3. The purpose of the experiment was two fold

(i) to generate subpicosecond pulses using an all solid state source

(ii) to investigate the mechanisms which determine the formation of the soliton Raman radiation.

In section 5.3.2 the apparatus necessary to measure the characteristics of the ultra-short pulse is described. This is followed by a description of the experimental results which include investigations of modulational instability, variation of soliton pulse duration with fibre length and the effect of the zero GVD point on the Raman spectrum.

Section 5.2 Experimental Procedure

A schematic diagram of the experimental arrangement is shown in fig 5.2.1 The output from the Nd:YAG laser was launched in to the fibre using a X 20 microscope objective, with a launch efficiency of the order of 50%. An index matching cell was used to prevent feedback in to the laser. The output of the fibre was then either directed in to a monochrometer to measure the spectral content from the fibre or in to an autocorrelator to measure the temporal content of the radiation. A background free autocorrelator was used to measure the pulse durations which incorporated a 1 mm thick $LiIO_3$ crystal with a resolution of better than 20 fsec. The autocorrelator had the facility to scan repeatedly over a predetermined distance about the zero delay. This allowed a large number of autocorrelations to be taken of a soliton, the resultant quoted pulse duration being an average of many autocorrelations. The autocorrelator was constructed using corner cubes for beam steering so as to reduce dispersion in the autocorrelator. The radiation to be autocorrelated covered a large frequency range, as much as 1.2 μm to 1.55 μm, a monochrometer was placed between the frequency doubling crystal and the photomultiplier tube (PMT) to determine the frequency range being autocorrelated. A boxcar integrator was used to extract the signal from the PMT, the boxcar integrator was set to the minimum integration time so as to avoid any distortion in the averaging process. The subsequent autocorrelation represents an average over the entire Q-switched pulse. The output spectrum was measured using a Rank Hilger monochrometer (250 mm), with a resolution of better than 1.5 nm. A Ge photodiode was used to detect the signal from the monochrometer, again the boxcar integrator being used to extract the signal.

In the experiment two different types of fibre were used which had slightly different dispersion characteristics, both fibres being silica based. The characteristics of the two fibres are shown in table 5.2.1. Fibre 1 has its minimum dispersion wavelength

FIG 5.2.1 EXPERIMENTAL ARRANGEMENT

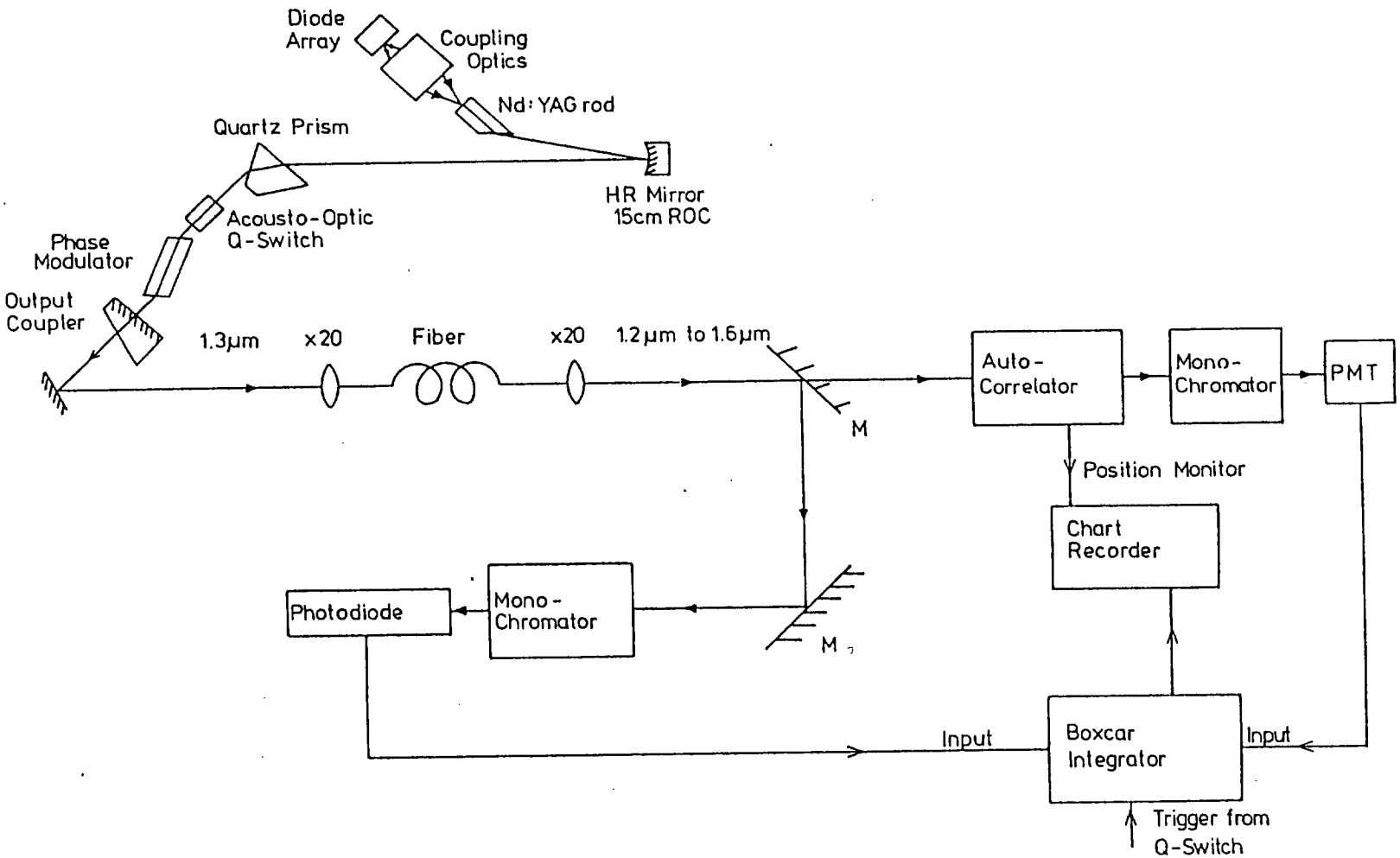

at 1.31 μm, so the input from the laser falls in the anomalous dispersion region, for fibre 2 the zero GVD point is at 1.34 μm, so the input falls in the normal dispersion region.

Table 5.2.1-The fibre characteristics

	Cut off wavelength(λ_o)	Core radius (μm)	Index difference ($n_1 - n_2$)	Zero GVD wavelength	Dispersion slope (normalised)
Fibre 1	1179	4.18 μm	0.004	1.31 μm	$-62.25\lambda + 81.8$
Fibre 2	1240	3.4 μm	0.0067	1.34 μm	$-60\lambda + 80.4$

Loss in the fibres

	Wavelength	
	1.32 μm	1.39 μm
Fibre 1	0.3 dB/km	1 dB/km
Fibre 2	1 dB/km	14 dB/km

(i) Both fibres are non-polarisation preserving.

(ii) The formulae for the GVD are in terms of λ expressed in μm and give, D, expressed in ps/nm.km

The pulse walk off distance can be calculated for both fibres using the dispersion characteristics given in table 5.2.1 and equation 4.5.7. The calculated pulse walk off distance is 150 m for fibre 1 and 300 m for fibre 2. Following the discussion given in section 4.5, the maximum Raman conversion will take place within two pulse walk off distances, which is 300 m and 600 m for fibres 1 and fibres 2 respectively.

Section 5.3.1 Results

The high peak power in the modelocked and Q-switched envelope resulted in large pump depletion in the pump pulse, this was observed after only 60 m of fibre 1. In fig 5.3.1 a photograph is shown of the depleted fundamental pulse when viewed on a fast photodiode (Plessey). The picture of the pump depletion has an estimated X 10 gain in comparison to the picture of the fundamental, so the depletion is much more severe than shown. Estimates of the conversion efficiency were made by measuring the drop in average power at the fundamental wavelength with and without modelocking present (the change in average power between these two states was measured to be negligible). The spoiling of the launch efficiency reduced the average power in the fibre, with the effect that the pump depletion was reduced. To measure threshold the launch efficiency was reduced until the onset of pump depletion. An estimate of the threshold power could be

THE PUMP PULSE

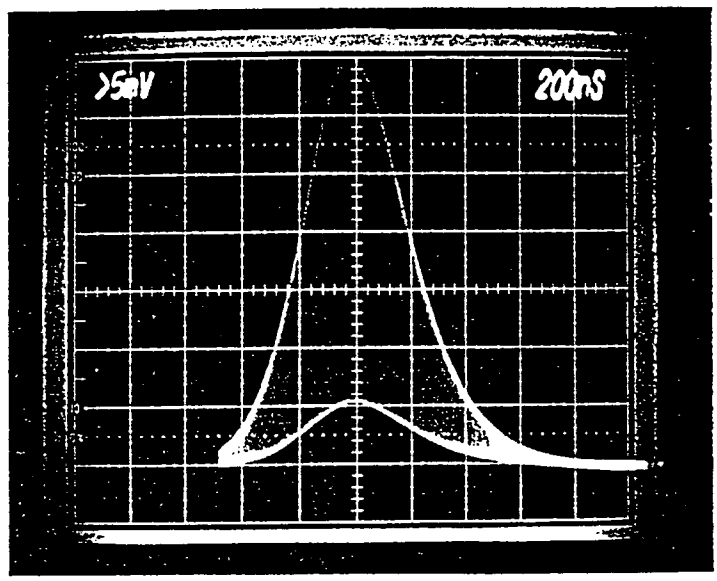

THE DEPLETED PUMP PULSE AFTER 300m OF FIBRE

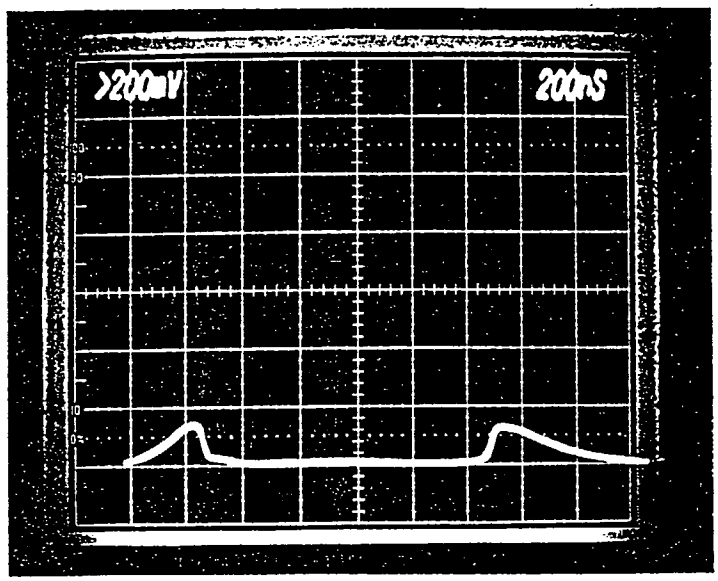

FIG 5.3.1 PUMP PULSE DEPLETION DUE TO SRS

made by measuring the launch efficiency at the onset of depletion and then working out the peak power that would be present in the fibre.

Fig 5.3.2 shows a graph of the threshold against fibre length for fibres 1 and 2, in fig 5.3.2(b) a log graph is plotted for fibre 1. The graphs show that fibre 2 consistently had a higher threshold for Raman generation , approximately 3/2 times the threshold for fibre 1. The log graph shows that in fibre 1 the threshold does not follow the 1/L dependence as predicted by equation 4.5.5 and that after 300m of fibre 1 there is little variation in the threshold power. Fig 5.3.3 shows a graph of the conversion efficiency against fibre length for fibres 1 and 2. This graph shows that in fibre 1 the conversion efficiencies tended to be higher in fibre 1 than in fibre 2. Again it can be seen from this graph that there is little change in the conversion efficiency after 300m of fibre. For fibre 2 it is not until the pulses are passed through 1 km of fibre that the threshold and the conversion efficiency approaches those of fibre 1.

These findings can be compared to the theoretical predictions for SRS as discussed in section 4.5. In table 5.3.1 the theoretical threshold predicted by using equation 4.5.5 are listed for various lengths of fibres 1 and 2. To calculate these values equation 4.5.2 was used to calculate the effective length of the fibre, given the loss at 1.32 μm, as given in table 5.2.1. The effective area of the fibre in equation 4.5.5 is given exactly by an overlap integral but for single mode fibres, A, is close to the actual fibre core area [Stegman et al: 1989]. The core areas are 55 ± 2 μm for fibre 1 and 36 ± 2 μm for fibre 2. A value of g = 3.75 X 10^{-14} was used for the Raman gain coefficient, this has been halved to allow for the reduction in gain in using non-polarisation fibre.

Table 5.3.1

Theoretical thresholds

	Fibre 1	Fibre 2
Length		
100m	293 ± 20 W	194 ± 20 W
300m	98 ± 5 W	66 ± 7 W
1km	----------	30 ± 2 W

Contrary to the experimental results the theory predicts that fibre 2 should have the lower thresholds. The thresholds predicted for fibre 2 are in reasonable agreement with the experimental results but those for fibre 1 are at least 2X to high. The reason for this discrepancy is that in fibre 1 the formation of the Raman radiation is being seeded by the modulational instability (MI) effect discussed in section 4.8 and of which a more detailed experimental description is made in section 5.3.2. The thresholds for the formation of MI sidebands are described by eqn 4.8.4 and predicts much lower thresholds than for SRS. Sidebands generated by MI are acting as a seed for the SRS process hence they lower the threshold for SRS. The generation of MI sidebands is not possible in fibre 2 so the formation of the Stokes radiation is governed solely by the Raman gain.

FIG 5.3.2 (a)
THRESHOLD AGAINST FIBRE LENGTH

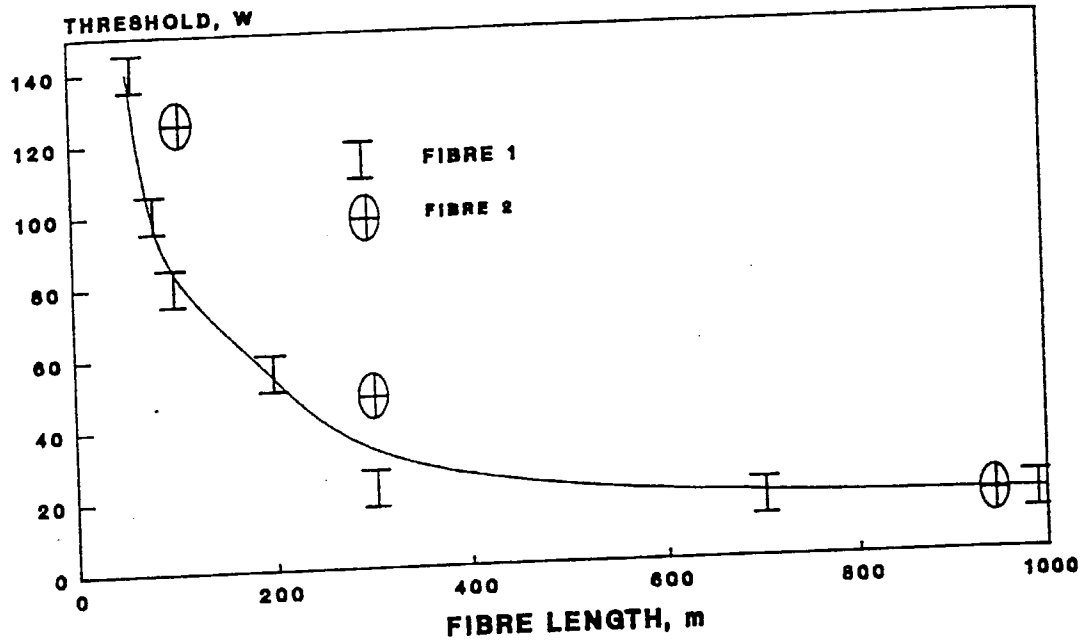

FIG 5.3.2 (b)

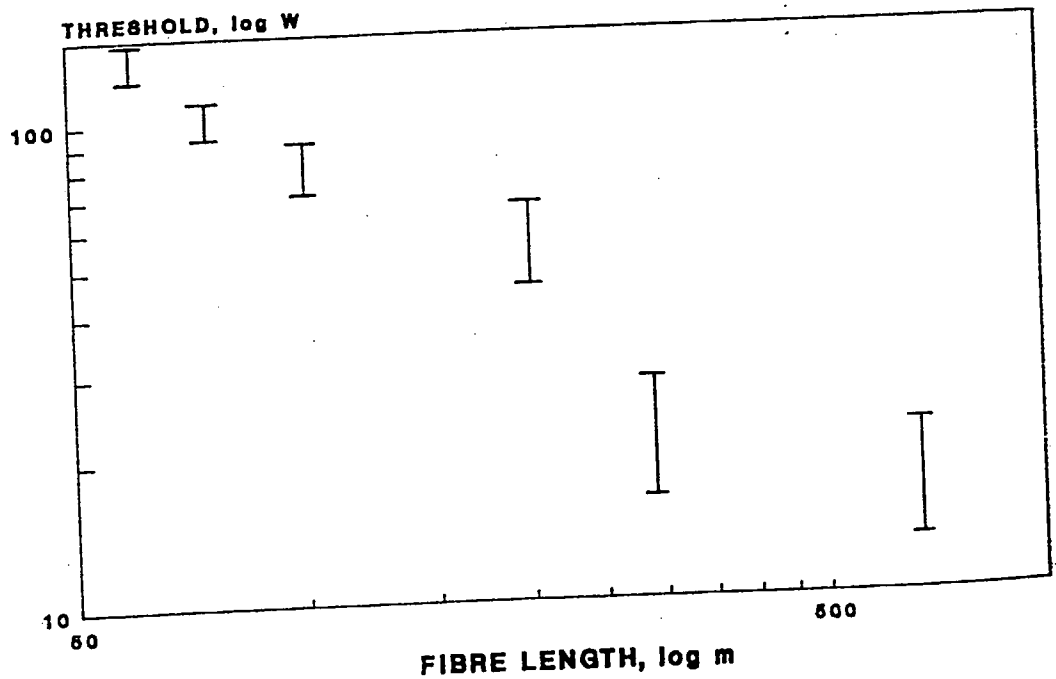

FIG 5.3.3
CONVERSION EFFICIENCY AGAINST FIBRE LENGTH

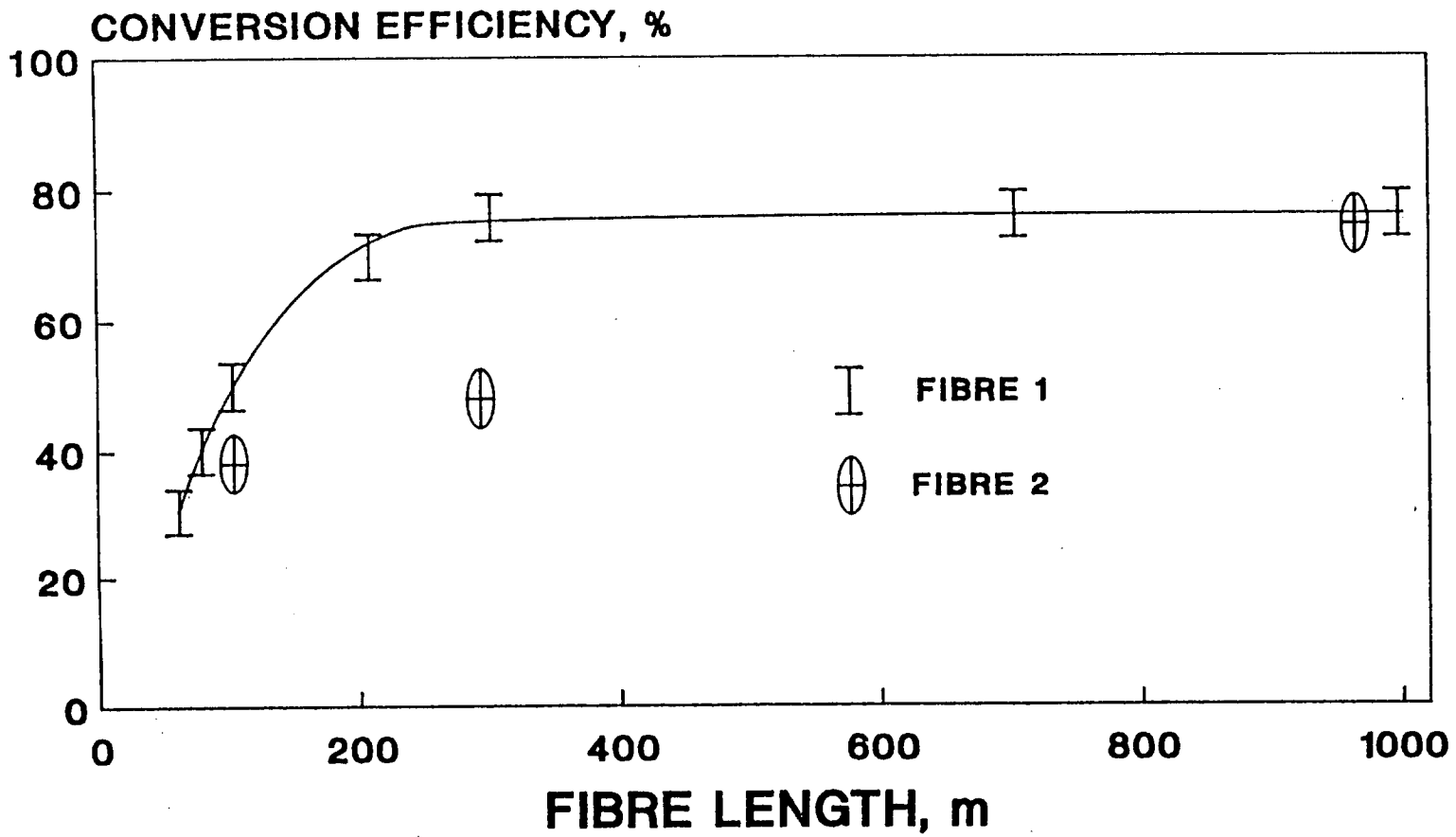

In table 5.3.1 the threshold powers have not been calculated for more than 300m of fibre 1 because after this distance according to theory the Stokes pulse will have passed through the pump pulse due to pulse walk-off. The property that the Stokes pulse is walking through the pump pulse is confirmed by the experimental results which showed that there was little change in the threshold and conversion efficiencies after 300m of fibre.

5.3.2 Modulational Instability

In fig 5.3.4 the spectra obtained in 60m and 1km of fibre are shown, these are typical of all the spectra taken for fibre 1, for both these spectra the laser produced pulses of a peak power greater than 700 W. The spectra show that as well as there being a large Stokes component, a significant anti-Stokes component is formed which is more prevalent in shorter lengths of fibre. Autocorrelations were taken of the sidebands, a typical autocorrelation obtained in 60 m of fibre is shown in fig 5.3.5. The autocorrelated modulation period is 115 fsec which corresponds to a frequency of 8.7 THz. This modulation frequency is in close agreement with the spectrally measured modulation frequency of 8.94 THz. The modulation can be attributed to modulational instability as described in section 4.8. For 60 m of fibre 1 the threshold for the production of Stokes radiation was very close to the peak power from the laser, implying that only the most intense of the modelocked pulses in the Q-switched pulse were taking part in the formation of the Stokes radiation. The $1/\gamma_g$ distance predicted by equation 4.8.4 for an input power of 350 W is 3 m, so 60 m of fibre is adequate to observe modulational instability. The modulation frequency can be estimated by making use of equation 4.8.3. Again the peak power in the fibre is taken to be 350 W, the dispersion at 1.318 μm as - 0.2 ± 0.1 ps / nm.km and the effective area as $S_{ef} = 5.5 \times 10^{-7}$ cm^2, $n_2 = 3.2 \times 10^{-16}$ cm^2/W and $n_0 = 1.5$. the equation predicts a modulation frequency of 9 ± 2 THz which is in reasonable agreement with that measured. The error arises due to uncertainty in the peak power causing the modulational instability and the large error in estimating the dispersion when it is so close to the zero GVD point.

It can be seen from the spectra of fig 5.3.4 that as the fibre length is increased there is a tendency for the modulational instability sidebands to move towards the pump. As the fibre length increases the threshold for Raman generation will decrease, as will that for the modulational instability. The effect of this means that

(i) lower powers will be causing the modulational instability

(ii) the higher powers will deplete due to SRS which tends to pull energy away from the formation of modulational instability.

Equation 4.8.3 shows that the modulational instability sideband frequency is proportional to $\sqrt{P}$, if lower powers are creating the modulational instability then it would be expected that the modulation frequency lowers. Fig 5.3.6 shows a graph of the modulation frequency against fibre length, the graph shows that the modulation frequency is inversely proportional to the square of the fibre length. The variation of the modulation

FIG 5.3.4 SPECTRA OF FIBRE 1

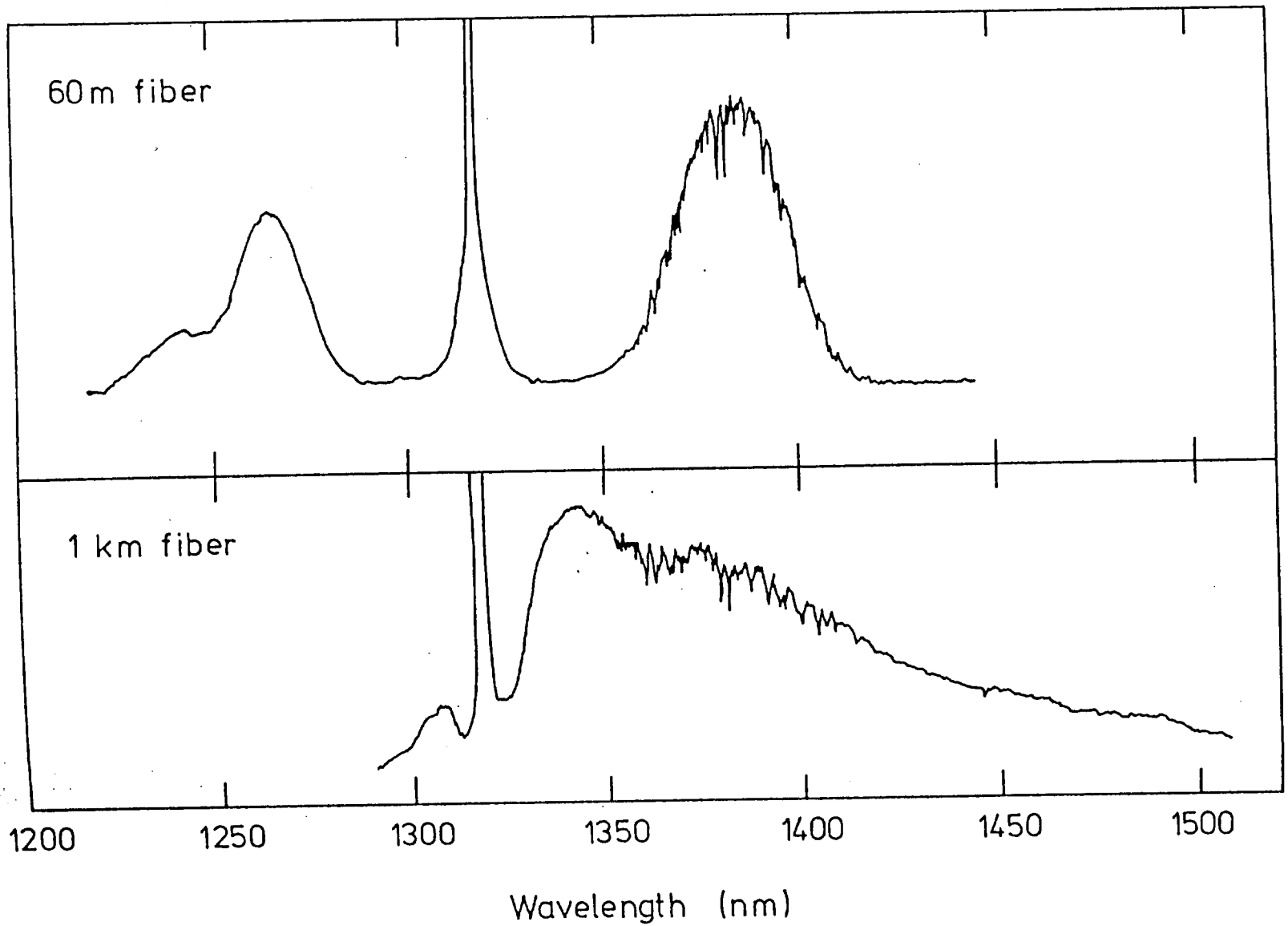

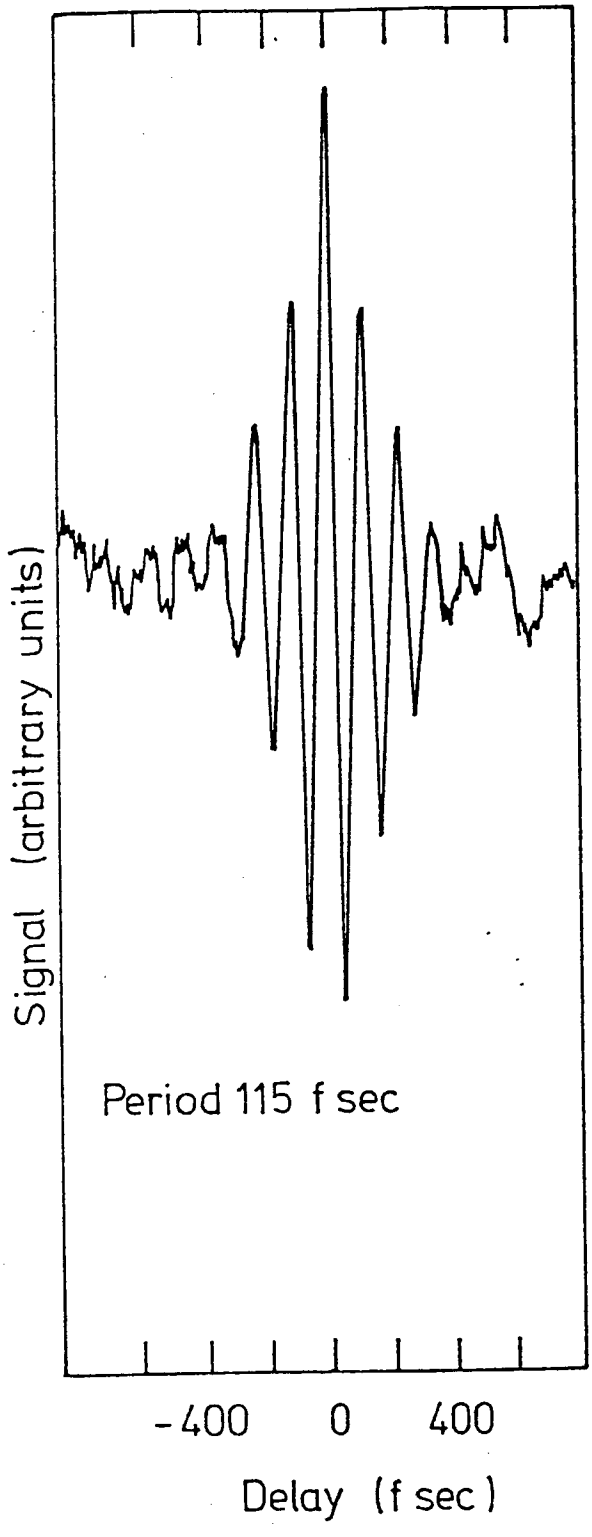

FIG 5.3.5 A TYPICAL AUTOCORRELATION OF MODULATIONAL INSTABILITY

frequency is a complex interplay between the Raman and modulational instability gain, with the Raman gain depleting the pump signal and causing the modulational instability sidebands to move to lower frequencies owing to the lower intensities causing their formation.

The formation of modulational instability sidebands should be independent of the input pulse duration. This was confirmed when just a Q-switched pulse was passed through the fibre. The Q-switched pulse produced a peak power of ~ 10 W, so about 5 W was in the fibre. The 1/e folding distance for this power from equation 4.8.4 is 200 m, implying that only in fibres longer than this will modulational instability be observed. This was confirmed when sidebands were only seen in lengths of fibre over 300 m. The spectra shown in fig 5.3.7 are those obtained when just a Q-switched pulse of 400 nsec duration, 4 mW average power was passed through fibre 1 of lengths 700 m and 2.2 km. Modulational instability sidebands were also observed in 300m and 1km of fibre 1, table 5.3.2 show the frequency of these sidebands.

Table 5.3.2

Fibre length	Modulation frequency
300m	3.5 THz
700m	2.9 THz
1km	2.5 THz
2.2km	1.6 THz

The modulation frequencies obtained can be compared with those predicted by eqn 4.8.3. For an input power of 5W the equation predicts a modulation frequency of 1.1 ± .3 THz. There is a discrepency between theory and experiment, the most likely cause of this error is in the calculation of the dispersion as has been mentioned and in estimating the power causing the MI. The table confirms the results obtained with the Q-switched/modelocked pulse envelope that the MI tends to act as a seed for the SRS process and due to the formation of Raman radiation the MI sidebands are reduced in frequency due to the lower intensity causing the effect. It can be seen in both spectra that the gain due to SRS is broadening the Stokes signal and causing it to move closer to the pump wavelength. In the absence of MI the predicted fibre length for Raman radiation to be formed for 5W pump power in the fibre is 6km. This demonstrates dramatically how the presence of modulational instability can lower the threshold for the SRS process.

The presence of modulational instability plays an important part in shaping the Stokes spectrum. The Raman gain shown in fig 4.5.1 for silica glass shows that the maximum gain is at a frequency of 440 cm^{-1} which corresponds to 1.40 μm for an input wavelength of 1.32 μm. This is the wavelength at which one would expect the Stokes signal to form under normal circumstances. The presence of modulational instability acting as a seed for the Raman gain appears to modify the expected signal. Due to the

FIG 5.3.6(a)
MODULATIONAL FREQUENCY AGAINST FIBRE LENGTH

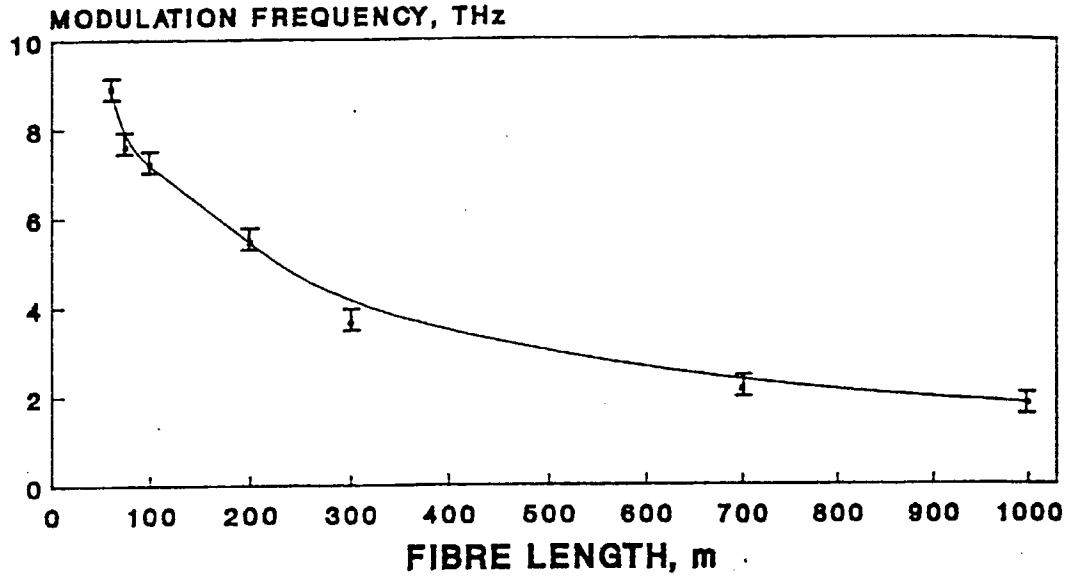

FIG 5.3.6(b)
MODULATIONAL FREQUENCY AGAINST FIBRE LENGTH

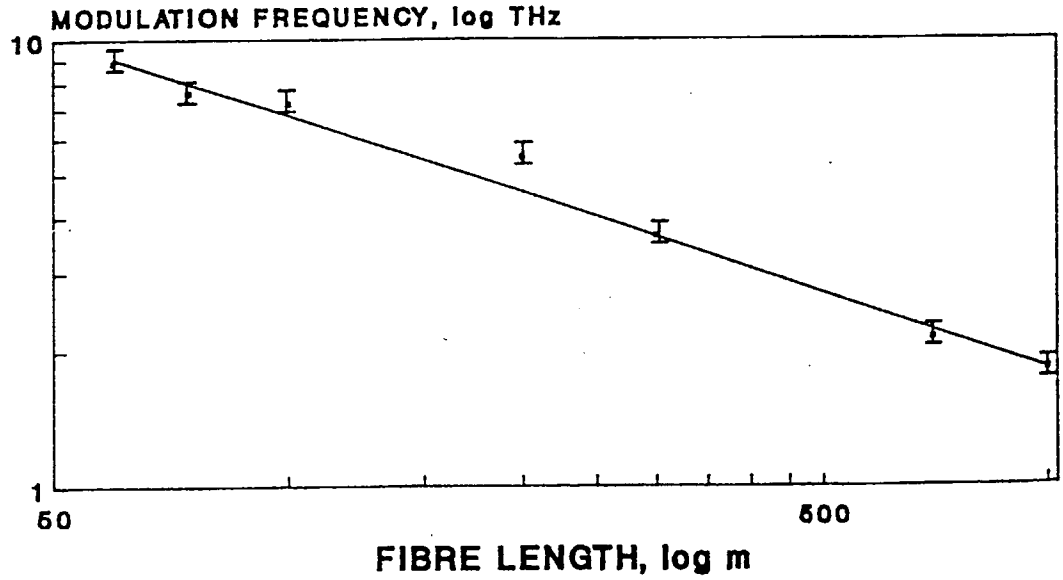

FIG 5.3.7 (a)

SPECTRA OBTAINED WITH A Q-SWITCHED SOURCE

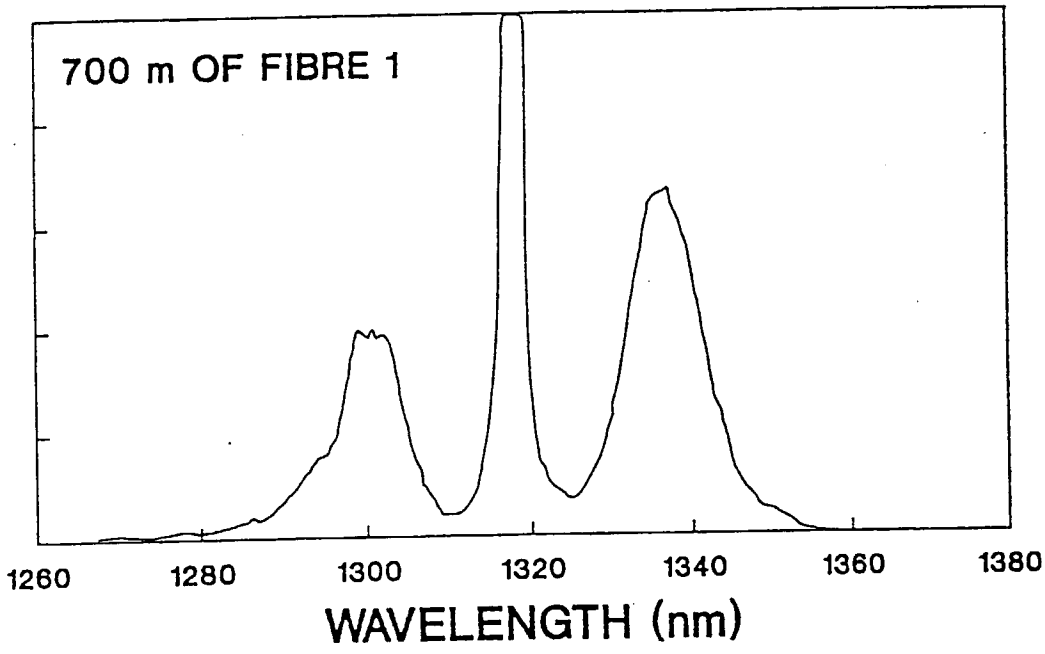

FIG 5.3.7 (b)

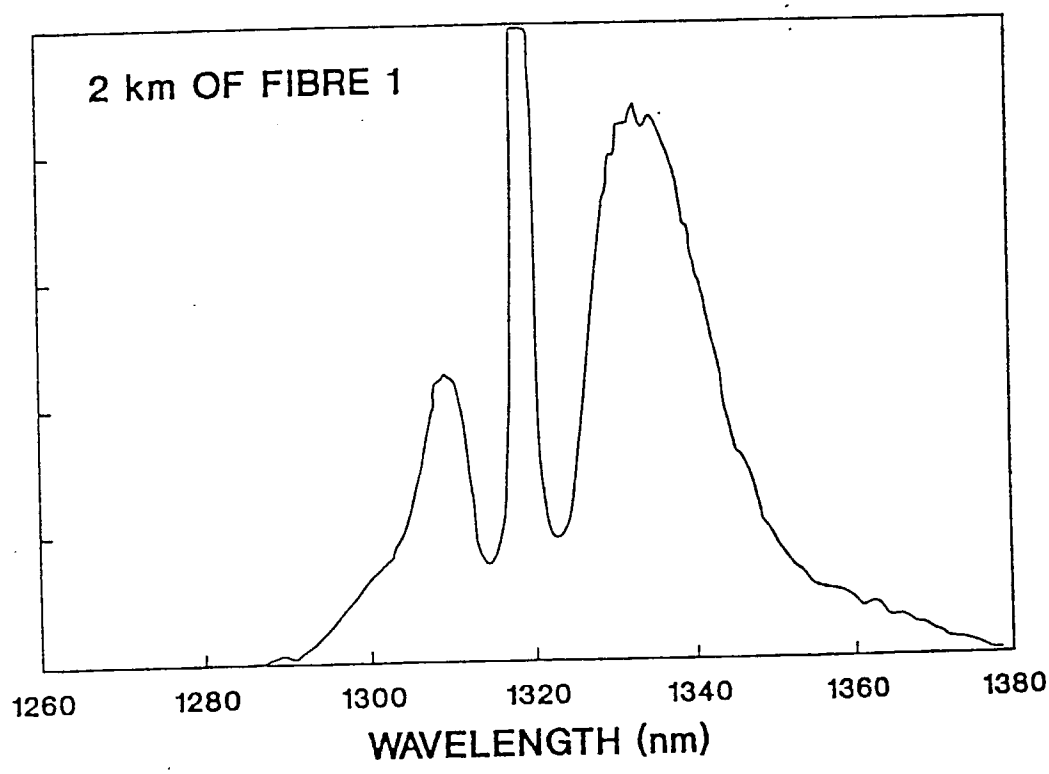

wide bandwidth of the Raman gain (250 cm^{-1}) which extends all the way down to a frequency shift approaching zero, radiation generated by modulational instability will be broadened and amplified by the Raman gain. The spectra of fig 5.3.4 clearly show this effect, where there is a definite frequency shift towards the fundamental wavelength. The modulational instability tends to shift towards the fundamental as the fibre length is increased, the effect that this has on the Stokes spectrum is to also shift it towards the fundamental wavelength. Consequently for 1 km of fibre the tuning range extends down to 1.34 μm, the modulational instability sideband for this fibre length is 20 nm away from the fundamental, hence this is seeding the short wavelength band of the Stokes radiation.

5.3.3 The SRS process in the absence of MI

The zero dispersion wavelength of fibre 2 is 1.34 μm so the pump radiation falls in the normal dispersion region of the fibre, so it cannot form modulational instability sidebands. Fig 5.3.8 shows the spectra obtained in 100m and 1km of fibre 2 when the Q-switched modelocked laser was used as the pump source. Clearly, as expected, there were no modulational instability sidebands formed. In the absence of MI the shape of the spectra appears to be determined solely by the Raman gain. The Stokes radiation generated in fibre 2 was always centred on 1.4 μm, the peak of the Raman gain and showed no variation with either input power or fibre length. This is in contrast to fibre 1 where the bandwidth obtained was highly dependent upon the intensity of the input signal and fibre length. In the absence of MI the experimental thresholds were in reasonable agreement with theoretical predictions. It can be seen that the radiation extends from 1.4 μm to 1.55 μm in 1km of fibre 2. This indicates that the second order Stokes band is being excited which for a pump wavelength at 1.32 μm is at 1.48 μm.

Section 5.4 The evolution of soliton Raman pulses

It was described in chapter 4 that through SRS optical solitons could be produced if the Stokes radiation was generated in the anomalous dispersion region of the fibre. In this section the evolution of the solitons with fibre length, pump power and the effect of the soliton self frequency shift will be discussed. In fig 5.4.1 a graph is shown of the evolution of the solitons formed at 1.36 μm in fibre 1 and at 1.4 μm in fibre 2 with fibre length. It can be seen that the minimum pulse duration occurred in a fibre length of 100 m, this was the case for both fibres 1 and 2. The pulse durations of the solitons in 100 m of fibre in fibres 1 and 2 were measured to be 98 fsec and 88 fsec respectively assuming a sech pulse profile. Typical autocorrelations of the pulses are shown in fig 5.4.2(a&b). The mechanism for the formation of these solitons is a complicated one, being an interplay between SRS, the loss of the fibre and the fundamental power required to support an N=1 soliton. In fibre 1 modulational instability is seeding the soliton formation, solitons form in the anomalous dispersion region when there is sufficient power in the modulational instability sidebands to sustain an N=1 soliton. Evidence for this comes from the modulational instability sidebands shown in fig 5.3.5 for 60 m of

FIG 5.3.8 SPECTRA OF FIBRE 2

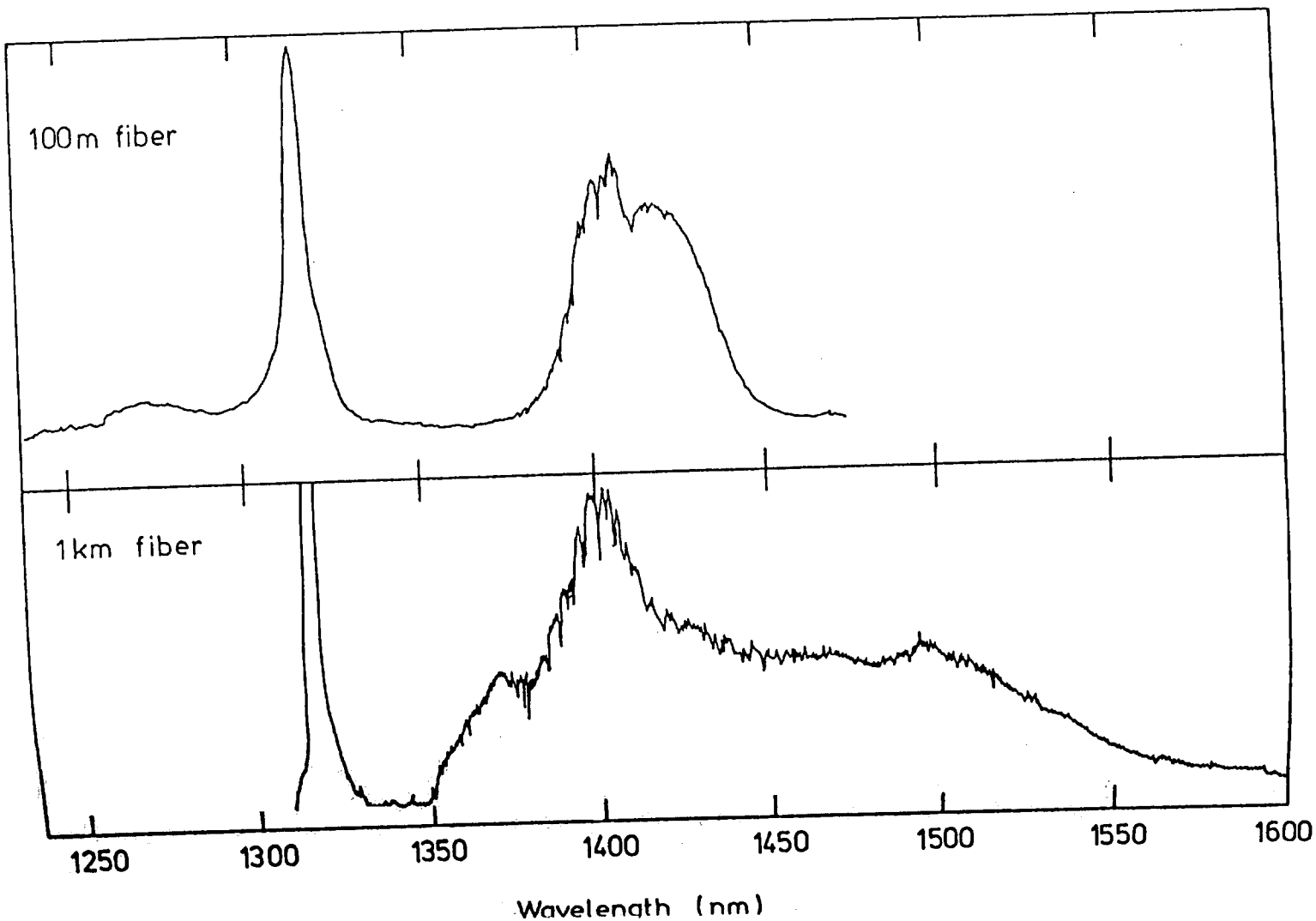

fibre which have evolved in to solitons in 100 m of fibre. In fibre 2 the soliton is forming from spontaneous noise. In both fibres the pulse duration of the soliton formed increased with increasing fibre length after 100m of fibre. The soliton in propagating through the fibre looses energy through absorption, so the pulse broadens so that there is still sufficient power to sustain an N=1 soliton. The effect was more pronounced in fibre 2 where the loss was greater, the soliton pulse duration broadening from 88 fsec in 100 m of fibre to 280 fsec in 1 km. Associated with the formation of these solitons were highly dispersive pedestal components. The pedestal component was more pronounced in fibre 1; in 100 m of fibre the ratio of soliton to pedestal autocorrelated intensity was 2.6 to 1 in comparison to 4.1 to 1 for fibre 2. There are two main factors which determine the size of the pedestal component

(i) the Stokes radiation has a frequency chirp

(ii) the power at the Stokes wavelength is in excess of that required to produce an N=1 soliton.

If the Stokes radiation is chirped energy will be deposited in to a highly dispersive pedestal [Blow et al: 1986]. The fundamental input was 2X bandwidth limited for a sech pulse profile, this in combination with the property that radiation generated via SRS tends to have a frequency chirp several times larger than the fundamental means that the Stokes radiation will be generated with a significant frequency chirp which is shed in to the pedestal. The bandwidth of the Stokes radiation in fibre 1 was 45 nm which supported a 98 fsec soliton which gives a time bandwidth product of 0.66, this is 2X bandwidth limited for a sech pulse. In fibre 2 the 88 fsec pulse was 2X bandwidth limited.

The fundamental power needed to sustain an N = 1 soliton in fibres 1 and 2 can be calculated using eqn 4.6.16. In using this equation a pulse of a duration of 100 fsec has been assumed and the dispersion was calculated using the fibre properties given in table 5.2.1. The powers were calculated for a wavelength of 1.36 μm for fibre 1 and 1.4 μm for fibre 2. The effective areas were the same as those described in calculating the threshold in section 5.3.2. The fundamental power that is required to support an N = 1 soliton is 300 W for fibre 1 and 310 W for fibre 2. These are the minimum values and do not take into account the fibre loss which will tend to push the fundamental power higher. The loss in fibre 2 is greater which will further increase the power necessary to generate a soliton in comparison to fibre 1. Excess energy in the formation of a soliton is shed in to the highly dispersive pedestal, so it would be expected that the pedestal in fibre 2 would be smaller than that in fibre 1.

The formation of the soliton with a large pedestal component means that a large proportion of the energy at that wavelength will be carried in the pedestal. The ratio of the energy in the soliton to that in the pedestal can be estimated by the intensities and pulse durations obtained in the second order autocorrelations. Allowing for the cross correlation between soliton and pedestal gives

FIG 5.4.1
PULSE DURATION AGAINST FIBRE LENGTH

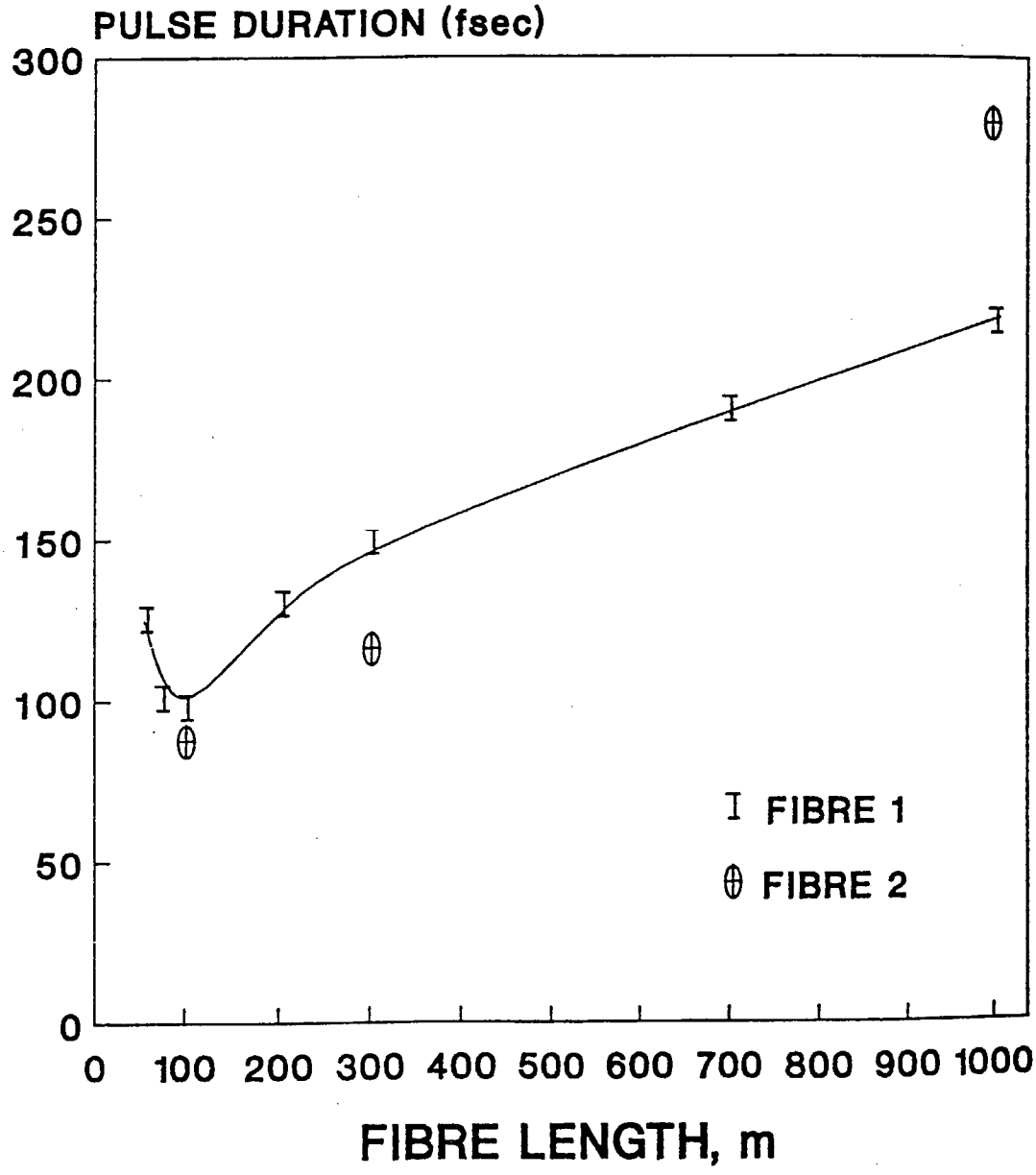

$$\text{Energy in Pedestal} \approx \left[1 + \frac{I_{AP}\tau_p}{2I_{AS}\tau_s} \right] \text{Energy in soliton}$$

5.4.1

where I_{AP}/I_{AS} is the ratio of the second harmonic autocorrelation intensities of pedestal and soliton. The quantities τ_p and τ_s refer to the pulse duration of the pedestal and soliton respectively. For instance, in 100 m of fibre 2 the pedestal had a duration of the input pulse, ~ 30 ps and the soliton had a duration of 88 fsec. The ratio of the soliton to pedestal was 4 to 1. This gives an average energy of 2% in the soliton component, this corresponds to approximately 1 kW peak power in the soliton.

A reduction of the average power by reducing the launch efficiency resulted in little change in the soliton pulse duration but had a significant effect on the pedestal component. For instance, in 2km of fibre 1 at 1.4 μm a reduction in the launch efficiency by 20% resulted in a reduction of the pedestal component by the same amount, the ratio of the intensities being 55 to 1 for a soliton with a pulse duration of 500 fsec. A further reduction in the pedestal component can be achieved by making use of intensity dependent polarisation in fibres due to the Kerr effect [Stolen et al: 1982]. The higher intensity solitons experience a higher degree of polarization change than the less intense background, which in combination with waveplates and polarisers allows separation of the two pulses. Gouveia-Neto [Gouveia-Neto et al: Feb 1988] have used this method to reduce a pedestal from 25 to 1 to better than 200 to 1.

For shorter lengths of fibre (< 100 m) it was found that the generated solitons were sensitive to any stress induced birefrigence in the fibre. Stress applied to the fibre resulted in a rotation of the polarisation of the Stokes radiation relative to the fundamental, hence reducing the gain. Experiments on short lengths of fibre required particular care to avoid stress in the fibre, making positioning of the fibre critical.

In both fibres with increasing fibre length the Raman spectrum tended to broaden. The broadening of the spectra can be accounted for by two processes

(i) in longer lengths of fibre the threshold is reached to excite more of the Raman gain profile and second order Stokes band.

(ii) the generation of ultra-short pulses means that the soliton self frequency shift becomes a significant effect, with the spectrum broadening due to intra-pulse Raman scattering.

The soliton self frequency shift for a 100 fsec pulse in 100 m of fibre can be using equation 4.7.2. The equation predicts that for a 100 fsec pulse the predicted change in bandwidth will be of the order of one pulse bandwidth(~50 nm). Clearly in both fibres 1 and 2 this magnitude of frequency shift does not occur. This observation agrees with a theoretical model by Blow [Blow et al: 1988] and a recent experimental study Gouveia-Neto et al [Gouveia-Neto et al: 1989] which has shown that the competing Raman gain

FIG 5.4.2

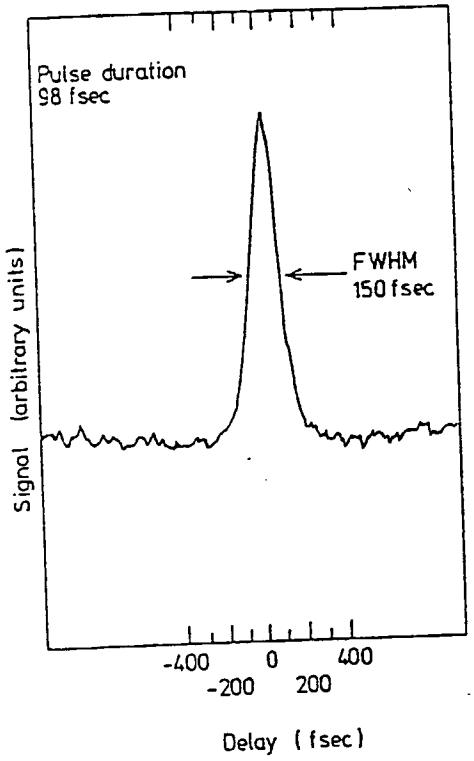

AN AUTOCORRELATION OF A PULSE IN 100m OF FIBRE 1

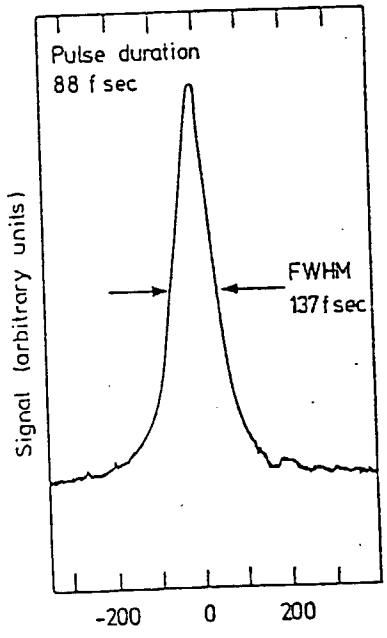

AN AUTOCORRELATION OF A PULSE IN 100m OF FIBRE 2

FIG 5.4.3
A TYPICAL AUTOCORRELATION OF A SOLITON AT 1480 nm

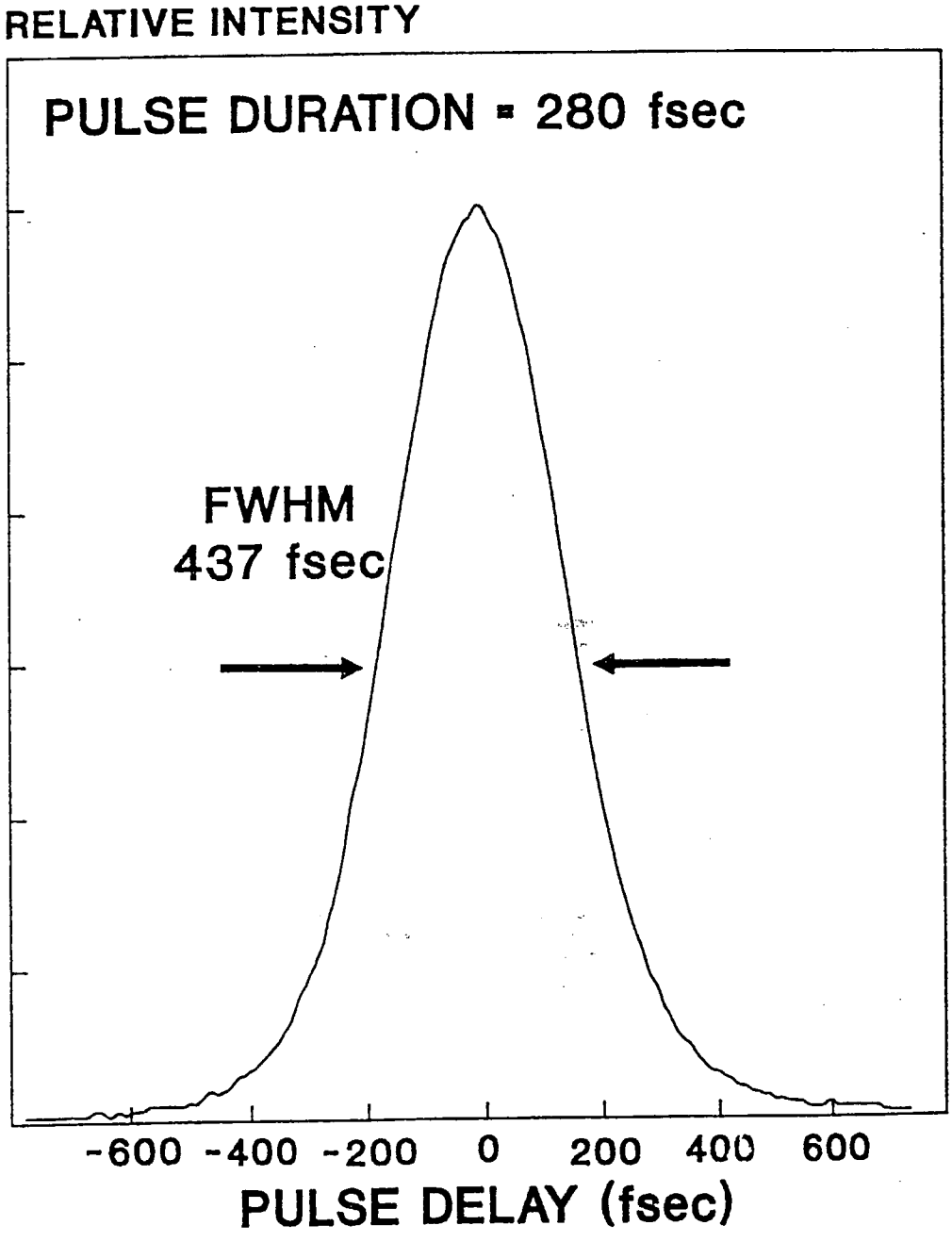

from the pulse and from the fundamental pump cause a clamping of the wavelength to a fixed value, suppressing the soliton self frequency shift. In those experiments the Raman gain of the pump was essentially constant, whereas in this experiment the pump pulse in propagating through the fibre is heavily depleted. This means that the Raman gain experienced by the soliton is not constant throughout the fibre length so the soliton self frequency shift will still be playing a part in the broadening of the spectrum but not to such an extent as theory predicts.

A large tuning range is obtained in 1 km of both fibres, in fibre 1 the radiation has a bandwidth from 1.34 μm to 1.45 μm. In fibre 2 the bandwidth spreads from 1.4 μm to 1.55 μm. By adjusting the phase matching angle of the $LiIO_3$ crystal and by adjustment of the monochrometer between the second harmonic crystal and the PMT, these wavelengths could be autocorrelated. It was found that solitons existed at all these wavelengths. The trend in both fibres with increasing wavelength was for the pulse duration to increase and for the pedestal component to decrease. In both fibres after ~ 1.44 μm the solitons were formed with a soliton to pedestal intensity ratio of better than 30:1. For instance, in 1 km of fibre 2 at 1.48 μm the 280 fsec pulse was formed with a pedestal component of better than 30 to 1. Fig 5.4.3 shows a typical autocorrelation at this wavelength, a curve fitting routine was used on this data and the pulse shape was found to best match that of a hyperbolic secant pulse shape. The radiation formed after ~1.44 μm is due to the soliton self-frequency shift of the solitons formed around 1.4 μm, these solitons should be formed pedestal free. Excess energy can be given to these solitons due to second order Raman gain which is centred at 1.48 μm. This excess energy would explain the small pedestal component that was observed in the solitons formed after 1.44 μm. The suppression of the soliton self-frequency shift is reduced in 1km of fibre 2 as by this stage the pump pulse is heavily depleted.

A cross correlation measurement was carried out on the radiation emitted at 1.4 μm. The resultant autocorrelation failed to resolve the sub-picosecond pulses formed, suggesting that timing jitter and the formation of Raman radiation from spontaneous noise caused excessive noise in the generated solitons.

Section 5.5 Conclusion

In this chapter it was shown how a laser diode pumped Nd:YAG laser, modelocked and Q-switched, could be used to generate tunable sub-picosecond pulses in optical fibre by the use of SRS. The system developed produced pulses as short as 88 fsec and radiation from 1.34 μm to 1.45 μm and 1.4 μm to 1.55 μm, the tuning range being dependent upon the particular fibres characteristics. In the investigation the importance of modulational instability on the formation of the Stokes radiation was investigated, with sideband frequencies as high as 8.94 THz being observed.

The experimental work has shown that the process of modulational instability plays an important role in determing the threshold for the generation of Raman radiation and consequently the conversion efficiencies obtained. Neglecting the effect of

modulational instability, theory predicts that fibre 2 should have lower thresholds than fibre 1, but the experimental work showed that due to the seeding of the Raman process by modulational instability, fibre 1 had the lower thresholds and higher conversion efficiencies. As a consequence of this effect solitons were formed in shorter lengths of fibre 1 than fibre 2, the solitons forming from the modulational instability sidebands when there was sufficient power to support an N = 1 soliton.

The solitons formed by SRS were found to have large pedestals associated with their formation with typically less than 2% of the energy in the soliton. In fibre 2, where modulational instability was not present, the pedestal component was smaller. This can be attributed to the lower conversion efficiencies in fibre 2 and the higher power needed to sustain an N = 1 soliton both of which contributed to there being less excess energy to be deposited in the pedestal in comparison to fibre 1. To generate solitons with small pedestal components it was found that it was preferable to use fibre 2 where modulational instability was not acting as a seed for the process.

Modulational instability was shown to influence the wavelength range that was created in the fibre, modulational instability tended to pull the spectrum to shorter wavelengths. The tuning range in fibre 1 was 1.34 μm to 1.45 μm and in fibre 2, 1.4 μm to 1.55 μm. For both fibres the solitons formed after ~1.44 μm had soliton to pedestal ratios of better than 30:1. This meant that fibre 2 had the greater tuning range of near pedestal free solitons. The process of modulational instability has been shown to be beneficial in lowering the threshold and highering the conversion efficiencies due to SRS but due to the frequency pull of the process the solitons formed when it is present tend to be formed with a much larger pedestal component.

REFERENCES: CHAPTER 5

Blow K. J. and Wood D. , 1986, Opt. Comm. , 58, 349.

Blow K. J. , Doran N. J. and Wood D. , 1988, J. Opt. Soc. Am. B. , 5, 1301.

Gouveia-Neto A. S. , Gomes A. S. L. and Taylor J. R. , Feb 1988, IEEE J. Quant. Electron. , 24, 332.

Gouveia-Neto A. S. , Falden M. E. , Sambra A. S. B. , Wigley P. G. J. and Taylor J. R. , 1989, Opt. Letts. , 13, 901.

Stegman G. I. and Stolen R. H. , 1989, J. Opt. Soc. Am. B., 6, 652.

Stolen R. H. , Botineau J. and Ashkin A. , 1982, Opt. Letts. , 7, 512.

CHAPTER 6
CONCLUSION AND FUTURE WORK

Section 6.1 Introduction

In this chapter the main achievements and findings of the experiments described in this thesis are summarised. In section 6.3 future work in this area will be discussed with the aim of producing an all solid state source of cw sub-picosecond pulses.

Section 6.2 A summary of the achievements of this thesis.

The main achievement described in this thesis is the development of an all solid state source of sub-picosecond pulses. To acheive this a diode laser pumped Nd:YAG laser operating at 1.3 μm was developed. In chapter 2 the use of diode lasers as pump sources for solid state lasers is discussed. In this chapter the focusing optics necessary to efficiently longitudinally pump a Nd:YAG laser are described. The output from the diode laser in this experiment was of poor optical quality; the output was non-diffraction limited in one plane, astigmatic and highly divergent. To utilise this output special focusing optics were required which corrected for these imperfections without a great loss in the available pump power. The optics described in chapter 2 were able to focus the output from the diode laser so that the waist was small enough to allow efficient longitudinal pumping of a solid state laser.

The solid state material used was Nd:YAG utilising the transition at 1.3 μm, the transition has a gain cross section 1/4 that of the more commonly used transition at 1.06 μm but efficient lasing action at 1.3 μm was obtained through careful design of the laser cavity and components. The design of a Nd:YAG laser cavity suitable for diode pumping and the insertion of intra-cavity modulators is described in chapter 3.

The laser was modelocked so as to achieve high output powers and ultra-short pulses. Both amplitude and frequency modulation techniques were used to actively modelock the laser. In the case of AM modelocking the stability of the modelocked pulses were found to be very dependent upon the diffraction efficiency of the modulator. Stable modelocking was achieved with a modulator operating at 120 MHz. Near bandwidth limited Guassian pulses were observed of a duration of 46 psec and a peak power of 0.46 W.

FM modelocking was achieved by the use of a $LiNbO_3$ phase modulator which could be operated over a frequency range of 100-400 MHz by the changing of the resonance frequency of the LC circuit built around the crystal. The modelocked pulses from this laser were highly stable and insensitive to the amount of phase retardation from the modulator. Pulses of a duration of 19 psec were measured, which were 2X bandwidth limited for the sech pulse shape. The peak power in a modelocked pulse was 4.6 W. It was found that the FM modelocking technique was a much more stable and versatile method of modelocking the laser than that of AM modelocking.

The stability and ease of characterisation of the diode laser pumped system made it an ideal system to test the theories for homogeneously broadened modelocked lasers. The pulse durations from the modelocked laser were compared to those predicted by the self-consistent theory of Kuizenga and Siegman. The pulse durations, given the parameters of the systems, in both the AM and FM cases agreed well with theory. In the case of FM modelocking the pulses were two times bandwidth limited. This could be explained by the unusually large bandwidth when the laser was free running, which was due to spatial hole burning, which meant that the phase modulator had little effect on the observed lasing bandwidth.

The peak powers from the FM modelocked laser were insufficient to excite the non-linear effects in optical fibre that we wished to study. An increase in the peak power from the laser was achieved by simultaneously modelocking and Q-switching the Nd:YAG laser. An acousto-optic modulator was used to spoil the cavity. The Q-switch was run at 1 kHz with a small amount of pre-lase which was found necessary for stable FM modelocking to occur. It was found that the average pulse duration in the Q-switch envelope was 30 psec. The Q-switch envelope had a duration of 400 nsec with an energy of 4 μJ. This corresponds to a peak power in excess of 1kW in the peak of the modelocked Q-switched envelope.

The high peaked powered pulses at 1.3 μm were intense enough to stimulate non-linear effects in optical fibre. The wavelength of 1.3 μm is of particular use for studying these effects as it falls at one of the transmission windows of silica optical fibre, the wavelength is around the point of zero dispersion and the first Stokes band generated by stimulated Raman scattering falls in the anomalous dispersion region of the fibre. These last two properties allow efficient conversion of the pump wavelength to the first Stokes band as pulse walk off is minimised and allows the Stokes band to form ultra-short pulses with soliton like properties. In the study of soliton generation in optical fibre via SRS two types of fibre were used with slightly different dispersion characteristics such that the pump wavelength at 1.318 μm was in the normal dispersion region for one fibre and in the anomalous region for the other. Launching of the 1.3 μm Q-switched/modelocked pulse train through fibre lengths of 60- 2km resulted in conversion efficiencies to longer wavelengths of better than 30% in both fibres. The broad bandwidth of the radiation generated by SRS in the anomalous dispersion region supported pulses as short as 88 fsec. The shortest pulses for both fibres were observed in 100 m of fibre. Subsequent lengthening of the fibre length resulted in the broadening of the Stokes spectra and second order Stokes bands being excited. The solitons pulse durations increased with increasing fibre length. In these investigations there was a noticeable difference in the thresholds and the spectra obtained from the two fibres. For instance in 1km of fibre when the pump wavelength fell in the anomalous dispersion region the Stokes signal had a spectral range of 1.34 to 1.45 μm. When the pump wavelength was in the normal dispersion region the Stokes signal had a spectral range of 1.4 to 1.55 μm. The reason for this difference was the formation of modulational sidebands around the pump wavelength

through a non-linear process called modulational instability (chapter 4.8). This process has a lower threshold than SRS and can only occur when the pump wavelength is in the anomalous dispersion region of the fibre. The sidebands tended to act as a seed for the SRS with the effect of lowering the threshold and pulling the spectrum towards the sideband wavelength. Due to the high peak powers that were used in this experiment modulational instability sidebands of a frequency as high as 8.9 THz were observed.

The measurements made of the characteristics of the pulses generated by SRS were averages over the entire Q-switched pulse envelope. The experiment could be improved by the use of a fast boxcar integrator such that its integration time was over a few modelocked pulses which for this experiment would require an integration time of about 10 nsec. The integration 'window' then could pick out modelocked pulses of roughly the same intensity. The peak power in these modelocked pulses are described by the Q-switched envelope, by scanning the window across the envelope information could be obtained of how the generated Stokes pulses vary with intensity.

The advantage of using the SRS process in optical fibre to produce sub-picosecond pulses is in the simplicity of the experimental arrangement and the conditions required and in the large bandwidth that can be generated which supports ultra-short pulses. The method does have some drawbacks. As described in these experiments the solitons tend to be formed with a large pedestal component, caused by the power present in the Stokes radiation being larger than that required to support an N=1 soliton and the Stokes radiation being generated with a large frequency chirp. Both these conditions result in the formation of a highly dispersive pedestal. These pedestals can be removed by making use of intensity dependent polarisation effects in optical fibre but this means that a large proportion of the Stokes energy is being discarded. The stability of the ultra-short pulses are degraded by the presence of this pedestal as shown by Keller [Keller et al: 1989]. This instability limits the use of the pulses in applications such as electro-optic sampling. The experiments described in chapter 5 showed that solitons with small pedestals tended to be produced in the fibre where modulational instability was not observed, in this fibre solitons with a soliton to pedestal component of better than 30:1 were observed over a wavelength range of 1.44 to 1.55 μm. The stability of the solitons can be improved by the use of a fibre Raman oscillator as described in section 6.3.3. In this arrangement the Stokes radiation is not formed from spontaneous noise but from a Stokes signal which is fed back in synchronisation with the pump.

The system developed is a compact source of sub-picosecond pulses from 1.34 to 1.55 μm. The generation of ultra-short subpicosecond pulses in this wavelength region are of importance for applications in time resolved spectroscopy and in telecommunications.

Section 6.3.1 Future work

The use of stimulated Raman scattering in optical fibres to produce an all solid state source of tunable sub-picosecond pulses has been demonstrated in this thesis. To produce these non-linear effects in the optical fibre the solid state laser needed to be

simultaneously Q-switched and modelocked. The simultaneous Q-switching of the laser tends to limit the usefulness of the short pulses from the fibre as they are in a pulsed form which makes the pulses very difficult to synchronise to another experiment. This problem can be overcome by operating the system in a cw modelocked mode. The diode laser pumped Nd:YAG lasers peak output power needs to be increased for cw SRS thresholds to be reached. Although entirely new diode pumped systems could be developed to achieve this, such as the side pumped arrangements described in chapter 2.3, the necessary powers to generate cw subpicosecond pulses via SRS could be achieved by polarisation coupling two 1W diodes of the type described in this thesis. This would bring a two fold increase in the pump power without the need to drastically change the Nd:YAG cavity design and only a small addition to the pump optics would be required. Extrapolating the known characteristics of the laser described in chapter 3 for this increase in pump power predicts that a maximum cw power of about 270 mW could be obtained. When FM modelocked this should produce peak powers of the order of 40 W.

6.3.2 CW sub-picosecond pulse generation via SRS

The peak power predicted in section 6.3.1 could be used to generate SRS in optical fibre by various methods. The most simple of these is to pass the output through a fibre in a single pass arrangement. If the fibre labelled as fibre 1 in chapter 5 was used, about 400m or more of fibre 1 would be needed to generate efficiently Stokes radiation in such an arrangement, with this order of input power.

The experimental work described in chapter 5 showed how the threshold for SRS is reduced when modulational instability acts as a seed for the process. The property that the threshold for SRS can be lowered by use of a seed has been exploited by Greer et al [Greer et al: 1990]. They have used a cw diode laser with an output power of ~ 1mW and tunable around 1.36 μm to preferentially seed SRS in optical fibre. This method lowers the threshold for soliton formation via SRS and allows a certain degree of tunability in the output wavelength by control of the diode laser. In this experiment modulational instability is a competing process against the seeding and needs to be avoided. This requires that the zero dispersion point should be between the pump wavelength and the seed wavelength of the diode laser. This system could produce an all solid state source of tunable cw subpicosecond pulses in the 1.34 to 1.4 μm region.

The threshold and stability of the solitons produced by SRS can be improved by the use of feedback, thus forming a fibre Raman oscillator. The fibre Raman oscillator is synchronously pumped such that a percentage of the Stokes signal generated by a single pass is fed back in synchronisation with a pump pulse entering the fibre. This acts as a seed for the SRS and lowers the threshold of the system. To make the system compact and to reduce the number of optical components needed to make the resonator, a fibre coupler could be used to form the resonator, a possible resonator is shown in fig 6.1. The requirements of the coupler is to transmit as much of the 1.3 μm pump in to the fibre loop and to couple out around 50% of the Stokes signal around 1.4 μm. The splices that

are necessary to form the loop can be made with only a loss of about 0.2 dB. Due to pulse walk-off the experiments have shown that a fibre of around 300m would be optimum to form the resonator loop, if fibre 1 was used and the pump laser supplied 19 psec pulses.

The mode spacing of the fibre Raman oscillator needs to be an integral number of the mode spacing of the pump laser to achieve synchronous pumping. This can be easily achieved when using the FM modelocked laser as the resonant circuit driving the phase modulator has a low Q, with a bandwidth of about 3 MHz at 295 MHz resonance. Changing of the modelocking frequency is equivalent to changing the fibre length, for instance at a frequency of 295 MHz a change of 1 kHz is equivalent to changing a 300m resonator by ~ 1mm. Assuming a 60% loss in the fibre Raman resonator and a gain of exp G where G is defined in equation 4.5.1, the threshold is predicted to be 40 mW for a 300m long resonator.

The use of a fibre Raman oscillator offers the advantage of reduced threshold and stable soliton production as the Stokes signal is formed from the seeding pulse rather than from spontaneous Raman scattering. The reduced threshold from these systems also opens the possibility of exciting the second Stokes band implying sub-picosecond pulses will be present to a wavelength of 1.5 μm.

6.3.3 The generation of tunable sub-picosecond pulses by the use of additive pulse modelocking.

Recent studies have shown that the use of a nonlinear external cavity can enhance the pulse shortening in actively modelocked color-center lasers and in Ti:Al_2O_3 [Blow et al: 1988], [French et al: 1989]. The technique has been shown to be self-starting (i.e the modelocking process is passive without the need of active components) in Ti:Al_2O_3 [Goodberlet et al: 1989], in a flashlamp pumped Nd:YAG laser [Liu et al: 1990] and a diode pumped Nd:YAG laser [Goodberlet et al: 1990]. Using this method of modelocking in Nd:YAG pulses as short as 1.7 psec have been obtained. The technique is called additive pulse modelocking (APM) because the pulse shaping mechanism depends on the coherent addition of pulses that are feedback from the external cavity to pulses in the main laser cavity. The two APM modelocked Nd:YAG lasers mentioned have used a fibre in the external cavity to provide the necessary non-linearity. The external cavity needs to be matched to the main laser cavity such that the time of flight of a pulse in the external cavity is an integral number of that in the main cavity so as to achieve pulse overlap. The combination of the output coupler of the main laser and the non-linear external cavity could be thought of as forming a non-linear Fabry-Perot resonator which effectively means that the mirror reflectivity experienced by the laser is intensity dependent. The experiments have shown that for optimum modelocking the external cavity should only be a few integral numbers of the main laser cavity length (typically ~ 1m). In this case around 100 mW was needed in the external cavity to obtain stable self-starting modelocking.

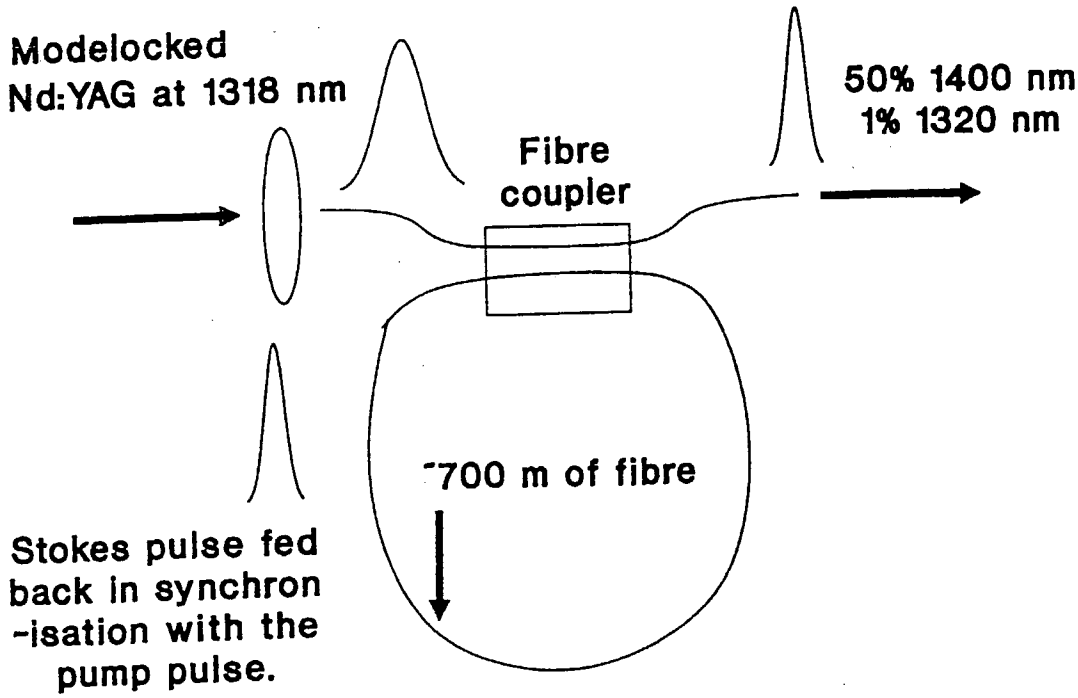

FIG 6.1 A FIBRE RAMAN OSCILLATOR

FIG 6.2 ADDITIVE PULSE MODELOCKING

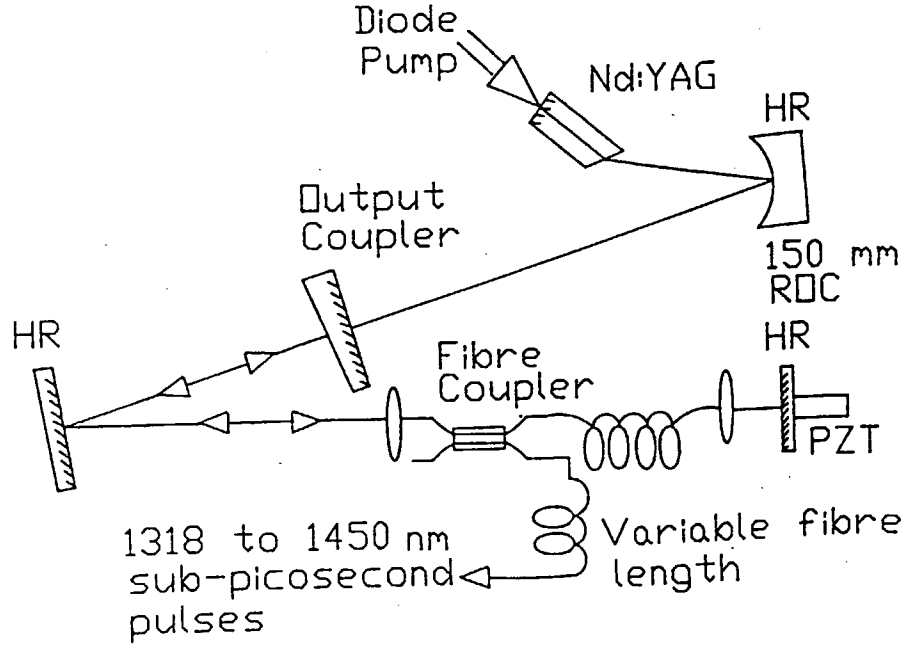

The application of this technique to a diode laser pumped Nd:YAG laser operating at 1.3 μm would be of great interest in itself and as a possible pump source for the generation of SRS in optical fibre. The development of a Nd:YAG laser operating at 1.3 μm which uses self-starting APM has possible advantages over a 1.06 μm system. One factor which acts as a limit to the minimum pulse duration obtainable from this system is dispersion in the fibre, this is at a minimum at 1.3 μm in silica optical fibre, combine this with the property that the 1.3 μm transition has a larger gain bandwidth, then you would expect a 1.3 μm to generate shorter pulses than the 1.06 μm system. Theoretical considerations of APM have shown that the threshold for self-starting is proportional to the gain cross section, which at 1.3 μm is a quarter that of the 1.06 μm transition so lower thresholds should be obtained.

Sufficient powers to achieve self-starting APM could be obtained by the use of two polarisation coupled 1W diode lasers as pump sources for a Nd:YAG laser operating at 1.3 μm, as was described in section 6.2. Good modelocking via APM requires the use of a large output coupling, which may be away from the ideal and so a drop in power from the maximum obtainable may be suffered. Even so, a power of 200 mW should be obtainable from such a laser of which about 1/2 would be required to initiate the APM. This would mean that 100 mW of modelocked power should be obtainable with a pulse duration of ~ 1.5 psec. This implies that a peak power of ~ 0.5 kW could be obtained.

The high peak power available from such a system is well over the threshold for the generation of Stokes radiation in optical fibre. The most compact and efficient way of utilising this output would be by the use of a fibre coupler in the non-linear arm of the external cavity, the system envisaged is shown in fig 6.2. A fibre coupler that has a 50% coupling ratio should allow both processes to be initiated. The passage of the modelocked pulses through the fibre would then require no launching optics. Generation of Stokes radiation could then be formed by the passing of the high intensity pulses through 100's of meters of single mode fibre. If this fibre has a dispersion minimum at a shorter wavelength than the pump wavelength, then the 1.5 psec pulses will form high order solitons which will break up due to the Raman gain and SSFS to form Stokes radiation at longer wavelengths [Gouveia-Neto et al: 1988]. The solitons formed have the property that they are pedestal free and their wavelength can be controlled by the input power to the fibre and the fibre length. The system envisaged would be a relatively simple and compact source of picosecond and sub-picosecond pulses from 1.3 to 1.5 μm.

REFERENCES: CHAPTER 6

Blow K. J. and Nelson D. P. , 1988, Opt. Letts. , **13**, 1026.

French P. M. W. , Williams J. A. R. and Taylor J. R. , 1989, Opt. Letts. , **14**, 686.

Goodberlet J. , Wang J. , Fujimoto J. G. and Schulz P. A. , 1989, Opt. Letts. , **14**, 1125.

Goodberlet J. , Jacobson J. and Fujimoto F. G. , 1990, Opt. Letts. , **15**, 504.

Greer E. J. , Patrick D. M. , Wigley P. G. J. , Vukusic J. I. and Taylor J. R. , 1990, Opt. Letts. , **15**, 133.

Gouveia-Neto A. S. , Sombra A. S. B. and Taylor J. R. , 1988, Opt. Comm. , **68**, 139.

Keller U. , Li K. D. , Rodwell M. and Bloom D. M. , 1989, IEEE J. Quant. Electron. , **25**, 280.

Liu L. Y. , Huxley J. M. , Ippen E. P. and Haus H. A. , 1990, Opt. Letts. , **15**, 553.

APPENDIX-PAPERS PUBLISHED

Mode-locked and Q-switched operation of a diode laser pumped Nd:YAG laser operating at 1.064 μm

G. T. Maker, S. J. Keen, and A. I. Ferguson
Department of Physics, University of Southampton, Southampton SO9 5NH, United Kingdom

(Received 17 June 1988; accepted for publication 22 August 1988)

We describe the performance of a mode-locked and Q-switched Nd:YAG laser operating at 1.064 μm, optically pumped by a 500 mW diode laser. The cw mode-locked system provides bandwidth-limited pulses of 55 ps duration, with a corresponding peak power of 3.3 W. When Q-switched the energy within the 100 ns pulse envelope is 10 μJ giving a peak power in the largest pulse of 7 kW. Preliminary results for operation at 1.32 μm are also reported.

In recent years the diode laser pumped Nd:YAG laser has been shown to be an efficient and reliable method of converting the relatively limited coherence of the diode laser to high quality single mode oscillation in the Nd:YAG material.[1] In this letter we report on mode-locked and Q-switched operation of a diode laser pumped Nd:YAG laser at 1.064 μm. This provides a compact all solid-state source of short laser pulses in a TEM_{00} mode with high efficiency and reliability. This makes an ideal source as a master oscillator for a high-power laser at wavelengths of importance for a wide range of technologies including medicine and communications.

Flashlamp-pumped continuous-wave mode-locked and Q-switched Nd:YAG lasers have become accepted for a wide range of applications. However, the efficiency of these systems is in the region of 0.1% and as a consequence large power supplies and cooling water systems are required. Furthermore, typical mode-locked pulse durations are in excess of 70 ps. The diode pumped laser reported here has an overall efficiency in excess of 3% and pulse durations of 55 ps. The design has not been fully optimized and simple improvements to the system will enable higher efficiencies and shorter pulses to be obtained.

The theory of active mode locking of a homogeneously broadened gain medium has been extensively studied. The diode pumped Nd:YAG laser system is ideal for making comparisons between theory and experiment because of the simplicity and cleanliness of the system.

In the self-consistent field theory of Kuizenga[2] for the evolution of a mode-locked pulse in an actively mode-locked homogeneously broadened laser, the steady-state pulse duration (full width at half-maximum) is given by

$$\tau_p \simeq \frac{(2\ln 2)^{1/2}}{\pi}\frac{1}{\theta_m^{1/2}}\frac{1}{f_m^{1/2}}\frac{1}{\Delta f^{1/2}}g^{1/4},$$

where Δf is the bandwidth (FWHM) of the laser transition, f_m is the drive frequency applied to the modulator, half the repetition rate of the laser, g is the round trip gain coefficient for the electric field amplitude, and θ_m depends on the active modulator transmission characteristic for the electric field given by

$$m(t) = \cos(\theta_m \sin 2\pi f_m t).$$

If the above pulse is assumed to be Gaussian, the bandwidth-limited bandwidth (FWHM) is expected to be given by

$$\Delta\nu = (2\ln 2/\pi)(1/\tau_p).$$

The Kuizenga theory is also capable of predicting the number of round trips required for the pulse to evolve from initial random noise to this bandwidth-limited pulse shows that the duration will be reduced to within 5% of steady-state value after M round trips, where M is given:

$$M = (0.38/g^{1/2}\theta_m)(\Delta f/f_m).$$

This parameter is important in designing a prelase switched mode-locked pulse train where steady-state (lase) mode locking has to be established before the Q-sw is opened.

A schematic diagram of the mode-locked and switched diode pumped Nd:YAG laser is shown in Fi The pump source was a 500 mW GaAlAs diode laser (S 2432), temperature controlled for operation at 807 nm. output from this 10×1 phased array diode was collected lens of 6.5 mm focal length and numerical aperture of 0. (Melles Griot 06 GLC001/D). The beam was then pa through a prism pair set up as an anamorphic beam expa er (Melles Griot 06 GPU 001). The optimum expans ratio was found to be approximately 3.5×. Finally, a 25 focal length lens was used to focus the pump beam onto end of the Nd:YAG rod producing a spot size smaller t the 45 μm spot size of the lasing mode on the Nd:YAG surface.

It was found that in order to even approach the theor cal limit of the pulse duration from the actively mode-loc system it was necessary to eliminate any source of intra vity étalon effects. With this in mind we found that the m satisfactory cavity arrangement was a three-mirror as

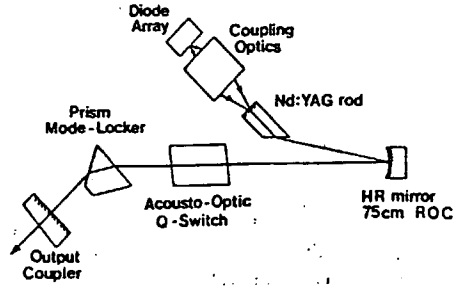

FIG. 1. Schematic diagram of the mode-locked and Q-switched cavity, showing the pump optics configuration. The largest cavity dimens shown is about 60 cm.

 0003-6951/88/441675-03$01.00

matically compensated cavity similar to that developed and commonly used for dye lasers. This cavity has the advantage of providing a strong intracavity focus and a long collimated arm suitable for the insertion of a mode locker. In addition no intracavity surfaces are close to normal incidence to the lasing mode except one end of the rod and the output mirror. We found that the output mirror has to have the outer surface wedged at an angle of at least 2° to prevent feedback.

The Nd:YAG rod was 10 mm in length and 4 mm in diameter with a 1% doping level of Nd^{3+} ions. The pump face of the rod was dielectrically coated to be of high transmission at the pump wavelength of 807 nm and high reflection at the lasing wavelength of 1.064 μm. The other face of the rod was cut at Brewster's angle. This provided both a low intracavity loss with no possibility of forming an intracavity étalon, and allowed easy accessibility of the laser diode focusing optics. An intracavity folding mirror of 15 cm radius of curvature produced an intracavity focus and could be angled to compensate for astigmatism introduced by focusing into the Brewster angle rod. The optimum angle of incidence on the mirror was found to be 12° for 1.064 μm in close agreement with the analysis of Hanna.[3] The laser output was taken from a plane output coupler of 10% transmission with a 10° wedged rear surface. The output spot size was approximately 600 μm.

With this cavity the pump threshold was found to be 77 mW and cw power was 45 mW at a pump power of 250 mW. This corresponds to a slope efficiency of 23% and a conversion efficiency of pump light reaching the Nd:YAG rod surface to cw mode-locked 1.064 μm radiation emitted of 18%.

Mode locking was accomplished using a high-Q prism mode locker commonly used in ion lasers (Crystal Technology) and was driven at a frequency of 114 MHz by a frequency synthesizer and power amplifier (Marconi 2022A and Wessex Electronics RC601-5) at a power level of up to 1 W. This is at a frequency close to the third harmonic of the design frequency of 38 MHz for this modulator. The average power diffracted from the zero order at 1.064 μm was measured to be 7.6%. This is considerably lower than the diffraction efficiency at the design frequency but added convenience of operating at a cavity length of 65 cm made operation at third harmonic the better choice.

The mode-locked system was optimized by use of a fast photodiode and sampling oscilloscope and the pulse duration was measured using a background-free autocorrelation. The bandwidth of the pulses was measured using a plane-plane Fabry–Perot étalon which was optically isolated from the laser to prevent feedback.

Figure 2 shows a typical autocorrelation trace of pulses at 1.064 μm. The best pulse durations measured from traces like this were 55 ps FWHM. It was found necessary to include an étalon of 225 GHz free-spectral range and a finesse of 2 into the cavity to limit the bandwidth and give clean autocorrelations. The measured bandwidth was 7.2 GHz giving a time-bandwidth product of 0.40 very close to that expected for a bandwidth-limited Gaussian pulse. The peak power in the pulse trains is thus calculated to be 3.3 W with an energy of 200 pJ per pulse.

The performance of the mode-locked laser can be com-

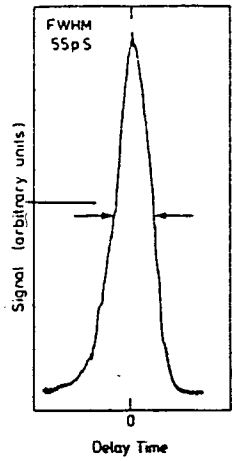

FIG. 2. Background-free autocorrelation trace of a typical 1064 nm mc locked pulse.

pared with the theory of Kuizenga using Eq. (1). The sa rated power gain coefficient in both lasers is that needed sustain oscillation against the estimated losses of 14% round trip. This corresponds to a round trip voltage g coefficient of 0.07. The bandwidth at 1.064 μm may be ta to 150 GHz. The depth of modulation θ_m can be determi experimentally by measuring the time-averaged single p power diffraction efficiency ϵ, and by calculating the aver diffracted power over one cycle, which gives the relations

$$\epsilon = \tfrac{1}{2}[1 - J_0(2\theta_m)],$$

where $J_0(x)$ is the zero-order Bessel function of x. For t laser system the deduced θ_m was 0.397 at 1.064 μm. Ins ing this and the other parameters into Eq. (1) gives a p dicted pulse duration of 54.6 ps. It can also be seen from (1) that the loss of diffraction efficiency at the third harm ic is compensated by the increased modulation frequen Clearly a mode locker specifically designed for higher mo lation frequency would be capable of better diffraction e ciency and should therefore produce shorter pulses. shortness of the pulse duration reported is probably du part to operation at a higher frequency and to the fact t the diode pumped system is cleaner and better behaved t a flashlamp-pumped system.

The mode-locked diode pumped Nd:YAG system readily be operated in a mode-locked and Q-switched mo We have studied this system using an acousto-optic Q-swi operated at a frequency of 80 MHz (Gooch and Hous A0II01/2 1163). At a drive power of 1.5 W the diffract efficiency was 20% which was sufficient to hold off la oscillation. The laser was operated in a prelase mode which the power to the acousto-optic Q-switch was adjus such that the laser operated just above threshold. This abled the mode locking to take place between Q-switch pulses and enabled a steady-state pulse to evolve. He when the Q-switch was opened short pulses were alre established in the cavity. The repetition rate of the syst was set at about 1 kHz. The Q-switched pulse envelope v

FWHM and the energy in the train was 10 μJ. The energy of the largest pulse in the Q-switched envelope was corresponding to a peak power of 7 kW. The peak to amplitude stability was better than 2%.

The diode pumped mode-locked and Q-switched AG laser is an efficient, reliable, compact, and stable source of short light pulses that requires no water cooling. Replacing the 1.064 μm optics and adjusting the dog-leg angle the cw mode-locked laser cavity can be made to operate at 1.3 μm. Preliminary results for this system are an average cw mode-locked power of 9 mW with pulse durations of less than 50 ps. A mechanical chopper placed into the cavity gave a Q-switch pulse duration of 100 ns and a mode-locked, Q-switched peak power of approximately 800 W.

The 1.064 μm system will find a wide range of applications as a source for nonlinear optics, as a master oscillator for large Nd:YAG systems,[4] and for time-resolved studies. The system operating at 1.3 μm should prove useful in optical communication research. Both the 1.064 and 1.3 μm lasers should have sufficient power to further shorten pulses via a fiber-grating pulse compressor[5] or the soliton like propagation of a stimulated Raman pulse,[6] respectively.

The authors are grateful to SERC (Science and Engineering Research Council) for financial support of this work in the form of a research grant and research studentships to GTM and SJK.

[1] D. L. Sipes, Appl. Phys. Lett. 47, 74 (1985).
[2] D. J. Kuizenga and A. E. Siegman, IEEE J. Quantum Electron. QE-6, (1970).
[3] D. C. Hanna, IEEE J. Quantum Electron. QE-5, 483 (1969).
[4] P. Esherick and A. Owyong, J. Opt. Soc. Am. B 4, 41 (1987).
[5] J. D. Kafka, B. H. Kolner, T. Baer, and D. M. Bloom, Opt. Lett. 9, (1984).
[6] A. S. Gouvela-Neto, A. S. L. Gomes, and J. R. Taylor, Opt. Lett. 12, (1987).

MODE-LOCKING OF DIODE LASER-PUMPED Nd : YAG LASER AT 1·3 μm

Indexing terms: Semiconductor lasers, Optical communications

We report on the development of a mode-locked AlGaAs diode laser pumped Nd : YAG laser operating at 1·3 μm. The laser produces pulses of 47 ps duration with a time-bandwidth product of 0·42, which is close to the limit for Gaussian pulses.

Introduction: There are many applications in optical communications where a powerful source of short light pulses at 1·3 μm is needed. Although diode lasers are capable of producing substantial average powers at this wavelength they have proved not to be capable of short-pulse, high-peak power operation owing to facet damage. As a result of this, optical communications studies have been undertaken using flashlamp-pumped mode-locked Nd : YAG lasers operating on the 1·3 μm transition. These lasers are cumbersome, requiring cooling water and large power supplies. We have developed a diode laser pumped mode-locked Nd : YAG laser operating at 1·3 μm. The system is compact, efficient and reliable and requires no water cooling which makes the system transportable. The laser produces pulses of 47 ps, close to the bandwidth limit with average powers in excess of 5·5 mW when pumped with a 1 W diode. We have established that system is capable of producing considerably more average power by use of an optimum output coupler. We estimate that 30 mW is available. Furthermore, the peak power can be increased greater than a thousand fold by use of Q switch In this case peak powers in excess of 4 kW are available.

System: A schematic diagram of the laser cavity is show Fig. 1. The pump source was a 1 W, 20-element phased a AlGaAs diode laser (SDL 2462) which was temperature-tu into the maximum absorption of the Nd : YAG rod at 807 The output from the diode was collected using a 6·5 mm f length lens with a numerical aperture of 0·615 (Melles G 06GLC 001/D). The beam was then made approximately cular by passing it through an anamorphic beam expar (Melles Griot 06GPU001) and then focused using a len 25 mm focal length.

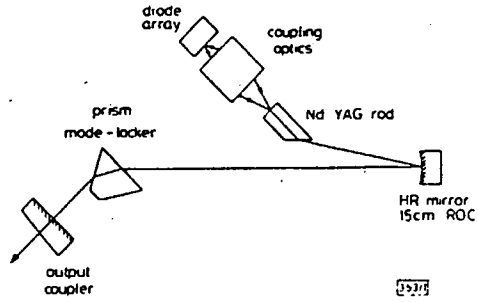

Fig. 1 *Schematic diagram of mode-locked laser cavity*
Overall cavity length is approximately 60 cm

The Nd : YAG laser cavity was set up in a three-mirror astigmatically compensated configuration. The rod was 4 mm in diameter and 10 mm in length and was doped with 1% Nd^{3+} ions. One end of the rod was dielectrically coated to be a high reflector at 1·3 μm and high transmission at the pump wavelength of 807 nm. The other end of the rod was cut at the Brewster angle. The cavity was completed by a 150 mm radius of curvature mirror and a plane output coupler. The focusing mirror was set at an angle of incidence of 13° and provided compensation for the astigmatism caused by focusing into the Brewster-angled rod.[1] The output coupler reflectivity was 93% at 1·3 μm and the rear surface was wedged at an angle of 10° to suppress feedback.

Mode-locking was achieved by use of an acousto-optic amplitude modulator placed close to the output coupler. The modulator was in the form of a fused silica Brewster-angled prism and offered wavelength selection between the 1·318 μm and 1·338 μm transitions. The fundamental resonance of the modulator was 120 MHz and the diffraction efficiency when driven with 2 W of RF power was 8%.

Results: The output power of the laser, when pumped with a 1 W laser diode, was 5·5 mW and the threshold was found to be 680 mW incident on the Nd : YAG rod, corresponding to a slope efficiency of 4·3%. The laser always operated in the TEM_{00} mode on the 1·318 μm line. The output power of the laser was far from being optimised. The optimum output coupling was estimated by making the output mirror a high reflector and by inserting a thin plate into the cavity. Measurement of the power reflected from the plate as a function of angle enabled the power coupled out to be maximised. We found that the maximum useful power was 30 mW and corresponded to 2% output coupling. The 7% output coupler that we had available therefore was far too large and increased threshold excessively.

The pulses from the laser were optimised by using a sampling oscilloscope and fast photodiode, the exact pulse duration then being measured using a background free autocorrelator. The laser linewidth was simultaneously measured using a plane-plane Fabry–Perot interferometer. A typical autocorrelation trace is shown in Fig. 2. The autocorrelation trace full width at half-maximum (FWHM) was measured to be 66 ps. The autocorrelation closely approximated that of a Gaussian pulse with a duration of 47 ps. The corresponding bandwidth was measured to be 9 GHz giving a time-bandwidth product of 0·42. This is close to the bandwidth limit for Gaussian pulses of 0·44.

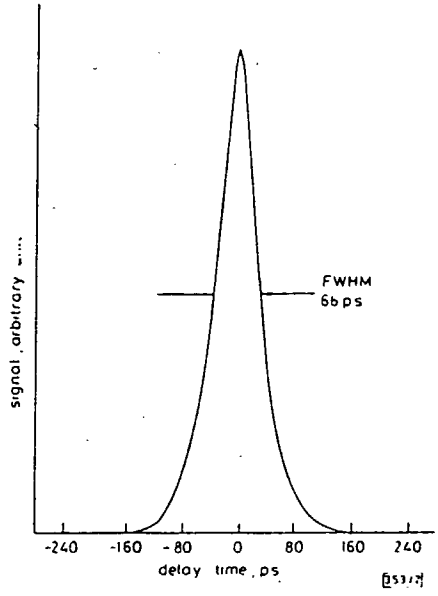

Fig. 2 *Typical second-order autocorrelation trace of mode-locked pulse at 1·318 μm*

Pulse duration = 47 ps

The pulses can be compared with the predictions of the Kuizenga and Siegman theory of mode-locking of a homogeneously broadened laser.[2] In this theory a Gaussian pulse evolves within the cavity until a steady state is reached between the narrowing caused by the modulator and the broadening by the gain medium. For the parameters appropriate to our laser system the Kuizenga and Siegman theory predicts a pulse duration of τ_p = 54 ps. This is in fair agreement with our experimental observation.

The pulse duration of this laser compares very well with that of continuous-wave flashlamp-pumped lasers which are typically in the 100 ps region. The pulse duration is slightly smaller than that obtained with a similar laser diode-pumped Nd : YAG laser operating at 1·06 μm[3] mainly owing to the larger bandwidth of the 1·3 μm transition.

Conclusion: We have developed a very stable, compact and reliable source of bandwidth-limited pulses of less than 50 ps duration at 1·318 μm. The system is far from optimum in terms of available average output power.

There are many applications for this source in optical communications systems and fibre-optic sensors, the performance of the system comparing favourably with flashlamp-pumped systems, being more compact and stable. It will be possible to use nonlinear optical techniques for further pulse compression and these will be reported on in a future publication.

Acknowledgment: We are grateful to SERC for financial support of this work in the form of a research grant and research studentships for Maker and Keen.

S. J. KEEN
G. T. MAKER
A. I. FERGUSON*

Department of Physics
University of Southampton
Southampton SO9 5NH, United Kingdom

* Present address: Department of Physics & Applied Physics, University of Strathclyde, Glasgow G1 1XQ, United Kingdom

6th February 19

References

1 HANNA, D. C.: 'Astigmatic Gaussian beams produced by axially asymmetric laser cavities', *IEEE J. Quantum Electron.*, 1969, QE-5, pp. 483–488

2 KUIZENGA, D. J., and SIEGMAN, A. E.: 'FM and AM mode-locking of the homogeneous laser—Part I: Theory', *IEEE J. Quantum Electron.*, 1970, QE-6, pp. 694–708

3 MAKER, G. T., KEEN, S. J., and FERGUSON, A. I.: 'Mode-locked and Q-switched operation of a diode laser pumped Nd : YAG laser operating at 1·064 μm', *Appl. Phys. Lett.*, 1988, 53, pp. 1675–167

Subpicosecond pulse generation from an all solid-state laser

S. J. Keen and A. I. Ferguson[a)]
Department of Physics, University of Southampton, Southampton SO9 5NH, United Kingdom

(Received 14 June 1989; accepted for publication 18 September 1989)

We describe an all solid-state (holosteric) laser source which produces subpicosecond pulses at 1.4 μm. The system consists of a diode laser pumped Nd:YAG laser which is frequency modulated (FM) mode locked and Q switched at 1.32 μm. In continuous wave operation the laser produces pulses of 19 ps while simultaneous Q switching and mode locking result in 30 ps pulses being contained in a Q-switched envelope of energy 2.1 μJ. The output of the laser, when passed through a 1 km single-mode optical fiber, produces a spectrally broad Raman signal with its peak at 1.4 μm and the overall conversion efficiency at 12%. The pulse duration at 1.4 μm has been measured to be 280 fs. We believe this is the first time that subpicosecond light pulses have been generated by an all solid-state laser system.

The diode laser pumped Nd:YAG laser is an important new laser source since it has been shown to be a very efficient method of converting electrical energy into optical energy. The all solid-state (holosteric) nature of these devices ensures that they are compact and reliable, requiring no cooling water, high voltage power supplies, and all the other services that conventional lasers require. The diode pumped Nd:YAG laser operating at 1.3 μm is of particular interest for studies of propagation phenomena in silica optical fibers since the laser wavelength is centered on one of the transmission windows of communications fiber, and is at the point of zero dispersion.

In this letter we report on a diode laser pumped Nd:YAG laser operating at 1.32 μm which has been mode locked using the frequency modulation (FM) technique. The FM technique has proved to be very reliable and convenient to use since it allows a free choice of operating frequency and a low drop in output power when mode locked.[1] The FM mode locking of the laser resulted in pulses of duration 19 ps, with an energy of 44 pJ. The peak output power of the laser can be enhanced by three orders of magnitude by simultaneously Q switching and mode locking, increasing the output power to greater than 700 W. In this mode of operation the laser is an ideal source for the study of nonlinear effects in optical fibers.

It has been demonstrated[2,3] that by passing a laser of high peak power at 1.3 μm through a single-mode optical fiber, ultrashort soliton-like pulses can be generated via stimulated Raman scattering (SRS). Due to the high intensities and long interaction lengths obtainable with optical fibers, the conversion to longer wavelengths can be very efficient with thresholds typically of the order of 10 W for a 1 km fiber. The peak of the broad Raman gain is at 1.4 μm in the negatively dispersive region of the fiber; and if the pulses have sufficient energy, they exhibit soliton-like behavior. Using the laser we have observed soliton-like pulses of duration 280 fs at 1.4 μm. We believe that this is the first time that a holosteric laser has been used in the generation of subpicosecond light pulses, making this the first subpicosecond holosteric laser system.

A schematic diagram of the laser system is shown in F 1. The pump source was 1 W phased-array gallium alu num arsenide (GaAlAs) diode laser (Spectra Diode L 2462) which was temperature tuned to the maximum of Nd:YAG absorption at 807 nm. The output from the la was focused onto the end of the Nd:YAG rod using h numerical aperture lenses and a prism beam expander as been described before.[4] The Nd:YAG laser was in the fo of a three-mirror astigmatically compensated arrangem The rod was 4 mm in diameter and 10 mm long. One en the rod was coated to be a high reflector at 1.3 μm and hig transmitted at the pump wavelength. The other end of rod was cut at Brewster's angle. A quartz prism was inc ed in the cavity to discriminate between the two lasing tra tions centered at 1.3 μm. The cavity was completed b concave mirror of 150 mm radius of curvature set at an an of incidence of 13° for astigmatic compensation and a pl output coupler of 99.5% reflectivity which was mounted a translation stage.

Mode locking was accomplished by driving a ph modulator at the cavity mode spacing of 295 MHz. modulator consisted of a $LiNbO_3$ crystal set at Brewst angle with the electric field applied along the z axis to m use of the r_{13} electro-optic coefficient. The radio freque power was inductively coupled and produced about 1 rad of phase retardation for 1 W of applied power.

Q switching was provided by an acousto-optic mod tor made of lead molybdate (Isle Optics) which was ant flection coated at 1.3 μm. The modulator was driven a MHz at a power level of 1 W and gave an estimated diffr tion efficiency of 26%.

The laser was found to lase with a threshold of 328 m incident onto the Nd:YAG rod with a maximum continu wave (cw) output of 15 mW, corresponding to a slope ciency of 3.2%. These results were obtained using an ou coupler which was far from optimum. We estimate that the optimum output coupling, a power of ~40 mW wa available from the system. The insertion loss of the LiN phase modulator is estimated to be 3%, while inserting t switch in the cavity the output power is reduced to 14 m

When optimally FM mode locked, the output po dropped to 1.5 mW. The pulse duration of the mode-loc pulse was measured using a second-order background

[a)] Present address: Department of Physics & Applied Physics, University of Strathclyde, Glasgow G4 0NG, United Kingdom

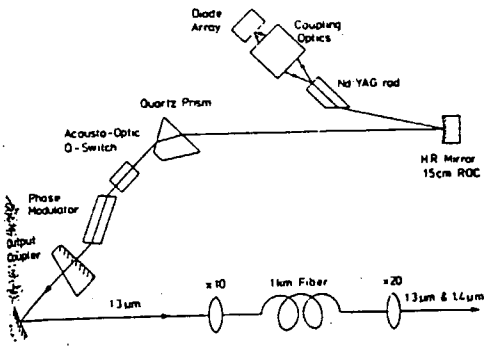

FIG. 1. Schematic diagram of the mode-locked and Q-switched laser cavity. The overall cavity length is ~ 50 cm.

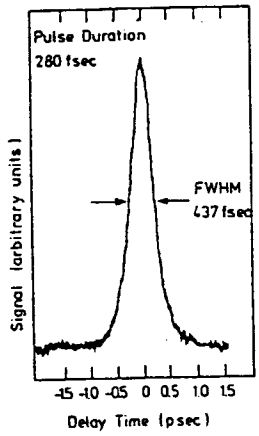

FIG. 3. Typical second-order autocorrelation trace of the generated Ram signal at 1.4 μm.

autocorrelator. A typical autocorrelation is shown in Fig. 2. The best fit to the autocorrelation was found to be a sech^2 pulse of 19 ps duration. The peak power in a mode-locked pulse is estimated to be 2.2 W. The bandwidth of the laser was simultaneously measured using a plane-plane Fabry–Perot interferometer. When optimally mode locked, the laser had a bandwidth of 35 GHz corresponding to a time-bandwidth product for the laser of 0.66 which is 2× bandwidth limited for sech^2 pulses. The pulse duration of 19 ps fits well with the 22 ps pulse duration predicted by the Kuizenga–Sigman theory[5] for homogeneously broadened lasers using our system parameters. Mode locking was found to be very stable and insensitive to both alignment of the phase modulator and the rf power applied. To further increase the peak power available from the system, the laser was simultaneously Q switched and mode locked. Stable simultaneous Q switching and mode locking was achieved by adjusting the hold-off of the Q switch such that the laser was just above threshold between Q-switch pulses. This small amount of prelase allows the mode locking to be in a steady state when the Q switch is opened. The Q-switch envelope had a duration of 350 ns and an energy of 2.1 μJ. The average pul duration of a mode-locked pulse in the Q-switch envelo was found to be 30 ps again, a sech^2 shape best fitting t autocorrelation. This corresponds to the peak power of t largest pulse in the train having a peak power in excess 700 W.

We have used the output of this laser to generate sub cosecond pulses centered around 1.4 μm in a 1 km sing mode optical fiber by SRS. The experimental arrangemen shown in Fig. 1; the 1.3 μm is launched with an efficiency 40%, the peak power in the fiber in excess of 280 W. T generated Raman radiation was found to be centered at μm but wavelengths as far as 1.6 μm were observed. Th radiation accounted for 30% of the average energy out of t fiber; the Raman radiation was generated with an over efficiency of 12%.

The generated Raman signal was autocorrelated usin 1-mm-thick $LiIO_3$ crystal; the 1.4 μm signal was picked o by the use of a monochromator between the doubling crys and the photomultiplier tube. The subsequent autocorre tion is shown in Fig. 3; the autocorrelation was found to b fit a sech^2 pulse of 280 fs duration. The pulse is on top o broad pedestal of 50 ps duration. The autocorrelated pu duration was insensitive to the launch efficiency and t length of the Q-switch pulse.

It has been shown[6] that the generated Raman solit exhibits a significant time and frequency jitter. A cross-c relation measurement of a Raman soliton pulse with its ne est neighbor failed to resolve the 280 fs pulse formed, su gesting that the combination of the instability in t formation of the Raman radiation from spontaneous no and jitter in the mode locking due to Q switching is caus instability in the Raman pulses.

We have developed a laser diode pumped FM mo locked Nd:YAG laser capable of producing 19 ps pulses cw operation and 30 ps pulses contained in a 2.1 μJ switched envelope. The technique of FM mode locking proved to be an attractive way of mode locking a laser, of ing versatility in mode-locking frequency and pulse du

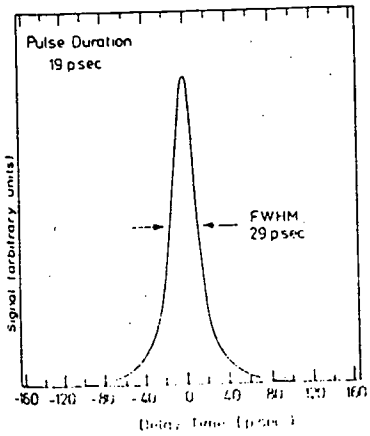

FIG. 2. Typical second-order autocorrelation trace of a mode-locked pulse at 1.318 μm.

tions which are far shorter than typical commercial amplitude-modulated mode-locked Nd:YAG lasers.

When the laser was simultaneously mode locked and Q switched the peak mode-locked pulse had a peak power in excess of 700 W. This makes the laser an ideal source for the study of nonlinear effects in optical fiber.

We have demonstrated this by passing the output of the laser through 1 km of single-mode optical fiber, producing pulses of 280 fs duration at 1.4 μm. We believe this is the first time a holosteric laser has been used to generate subpicosecond light pulses.

Further experiments using this laser to study nonlinear effects in optical fiber will be reported in future letters. The FM mode-locked Nd:YAG laser developed has potential use as a pump source for a synchronously pumped fiber Raman laser. This system would promise an all solid-state source of cw subpicosecond pulses.

The authors are grateful to the Science and Engineeri: Research Council (United Kingdom) (SERC) for financ: support for this work in the form of a research grant ar research studentship for SJK.

[1]G. T. Maker and A. I. Ferguson, Opt. Lett. 14, 788 (1989).
[2]A. S. Gouvei-Neto, A. S. L. Gomes, and J. R. Taylor, Opt. Lett. 12, 1((1988).
[3]P. Beaud, W. Hodel, B. Zysset, and H. P. Weber, IEEE J. Quantum El tron. QE-23, 1938 (1987).
[4]G. T. Maker, S. J. Keen, and A. I. Ferguson, Appl. Phys. Lett. 53, 1((1988).
[5]D. J. Kuizenga and A. E. Siegman, IEEE J. Quantum Electron. QE-6, ((1970).
[6]U. Keller, K. D. Li, M. Rodwell, and D. M. Bloom, IEEE J. Quant Electron. QE-25, 280 (1989).